(2)

'ATION PAGE

1 AGENCY USE ONLY (Leave blank)	2 REPORT DATE	3 REPORT TYPE AND DATES COVERED
	15 February 1991	FINAL 15 Sept. 1987-14 Dec. 1990

4 TITLE AND SUBTITLE
Microstructure, Porosity and Mechanical Property Relationships of Calcium-Silicate-Hydrate: A Final Report for the Period 15 Sept. 1987 to 14 Dec. 1990

Grant No. AFOSR-87-0395

5 AUTHORS
Grutzeck, M.W. (PI), S. Hoyle, S. Kwan, J. LaRosa, S. Bozich

7 PERFORMING ORGANIZATION NAME AND ADDRESS
The Pennsylvania State University
Materials Research Laboratory
University Park, PA 16802

PSU-AFOSR-91-1

AFOSR-TR- 91 0257

9 SPONSORING/MONITORING AGENCY NAME AND ADDRESS
Air Force Office of Scientific Research
Bolling Air Force Base, DC 20332

BK1 410

NE

10 SPONSORING/MONITORING AGENCY REPORT NUMBER
2306/A2

11 SUPPLEMENTARY NOTES

12a DISTRIBUTION/AVAILABILITY STATEMENT
Unlimited.

13 ABSTRACT (Maximum 200 words)
The structure of calcium silicate hydrate (C-S-H) formed as a result of solution/sol mixing, and hydration of tricalcium silicate (C_3S) under fixed pH conditions has been studied. MAS NMR and related analytical techniques (x-ray diffraction, SEM/TEM, and TGA) were used to characterize the hydration products.

Two C-S-H phases having distinctly different structures (molecular and micro) and weight loss characteristics exist in the system CaO-SiO_2-H_2O and along the 10 wt. % isoalumina join through the system CaO-Al_2O_3-SiO_2-H_2O. Coexisting phases form somewhere between 10 and 20 wt. % alumina.

C_3S hydrated as a function of pH (11-12) confirmed that at low pHs (<11.5), a C-S-H consisting predominantly of Q_2 silicate chains forms. At pH ≥ 11.5, a second C-S-H formed which consists of a combination of Q_1Q_2 silicate units. This C-S-H is more typical of that normally associated with the hydration of C_3S or portland cement without pH control. The C_3S hydrated at pH 13 contained only silicate dimer (Q_1) and large quantities of crystalline $Ca(OH)_2$. In this instance an entirely different gel (perhaps an alkali aluminosilicate hydrate) might be forming.

In a parallel study, zeolites have been synthesized from synthetic and waste glasses (fly ash) mixed with alkali hydroxide solutions. Linde B_1, chabazite and gobbinsite have been observed under certain conditions (relatively high Ca and alkali content). These data have been used to evaluate the feasibility of producing zeolite-cement composites.

14 SUBJECT TERMS
calcium silicate hydrate (C-S-H) structure, NAS NMR, C_3S, pH, zeolites, aluminosilicate hydrate

17 SECURITY CLASSIFICATION OF REPORT	18 SECURITY CLASSIFICATION OF THIS PAGE	19 SECURITY CLASSIFICATION OF ABSTRACT	20 LIMITATION OF ABSTRACT
Unclassified	Unclassified	Unclassified	None

PSU-AFOSR-91-1

Microstructure, Porosity and Mechanical Property Relationships of Calcium-Silicate-Hydrate

Michael W. Grutzeck
The Pennsylvania State University
Materials Research Laboratory
University Park, PA 16802

15 February 1991

A Final Report for the
Period 15 September 1987–14 December 1990

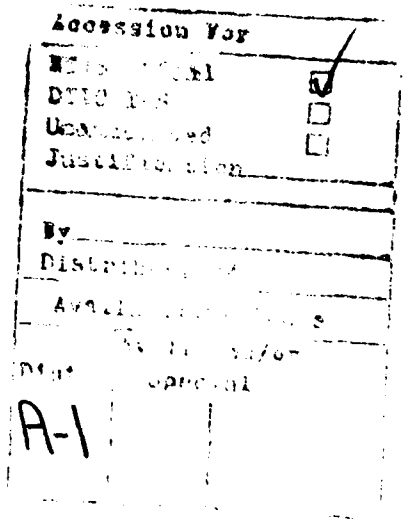

Unlimited Distribution

Prepared for

Air Force Office of Scientific Research
Bolling AFB, DC 20332-6448

Table of Contents

Abstract

The structure of calcium silicate hydrate (C-S-H) formed as a result of solution/sol mixing, and hydration of tricalcium silicate (C_3S) under fixed pH conditions has been studied. MAS NMR and related analytical techniques (x-ray diffraction, SEM/TEM, and TGA) were used to characterize the hydration products.

Two C-S-H phases having distinctly different structures (molecular and micro) and weight loss characteristics exist in the system $CaO\text{-}SiO_2\text{-}H_2O$ and along the 10 wt. % isoalumina join through the system $CaO\text{-}Al_2O_3\text{-}SiO_2\text{-}H_2O$. Coexisting phases form somewhere between 10 and 20 wt. % alumina.

C_3S hydrated as a function of pH (11-12) confirmed that at low pHs (<11.5), a C-S-H consisting predominantly of Q_2 silicate chains forms. At pH ≥ 11.5, a second C-S-H formed which consists of a combination of Q_1Q_2 silicate units. This C-S-H is more typical of that normally associated with the hydration of C_3S or portland cement without pH control. The C_3S hydrated at pH 13 contained only silicate dimer (Q_1) and large quantities of crystalline $Ca(OH)_2$. In this instance an entirely different gel (perhaps an alkali aluminosilicate hydrate) might be forming.

In a parallel study, zeolites have been synthesized from synthetic and waste glasses (fly ash) mixed with alkali hydroxide solutions. Linde B_1, chabazite and gobbinsite have been observed under certain conditions (relatively high Ca and alkali content). These data have been used to evaluate the feasibility of producing zeolite-cement composites.

Microstructure, Porosity and Mechanical Property Relationships of Calcium-Silicate-Hydrate

Introduction

Calcium silicate hydrate (C-S-H) is a poorly crystalline hydrate which is responsible for the majority of the properties commonly associated with portland cement and concrete. Earlier work by Ramachandran and Grutzeck (1,2), suggested that multiple C-S-H phases did exist and that they have distinctly different properties.

Our objective was to continue to investigate the relationship of microstructure and porosity of the C-S-H phases to their intrinsic mechanical properties. We were specifically interested in whether-or-not multiple C-S-H phases existed, and if so, what were their impact on the resulting mechanical properties of cement-based materials.

The work described in the following report builds on, and expands the scope of previous studies. The report consists of three sections, each of which will be published as a paper when the work is completed. The first deals with equilibrium C-S-H structure types that form from mixtures of lime, alumina, silica, and water, both in the presence and absence of sodium hydroxide. The second section deals with the nature of the different C-S-H structure types which develop as tricalcium silicate is hydrated under controlled pH conditions. The final section describes low-temperature synthesis of zeolites from synthetic and waste glasses, and the preliminary development of a self-generating zeolite-cement composite. Although the latter section is not complete, it does serve as an introduction to the concept and feasibility of producing such a composite material.

Part I. Equilibrium Studies

Introduction

Even though cement and concrete have been studied for nearly 100 years, questions still remain as to the nature and interrelationship of the calcium silicate hydrates (C-S-H) which form

during the hydration process. Traditionally, an equilibrium approach has been used to study these fine-grained, x-ray amorphous hydrates. Workers such as Flint and Wells (3), Roller and Ervin (4), and Taylor (5), have mixed solutions or sols containing lime and silica and examined the solid-liquid relationships which developed as a function of time. Solutions were analyzed and data on the nature of the solid phases were inferred using rules of phase equilibrium. Until quite recently, researchers were unable to directly study the structure of C-S-H without first drying it or dissolving it in an acid. Traditional diffraction methods used for structural investigations cannot be used because C-S-H is amorphous. However, with the development of Solid State Nuclear Magnetic Resonance, researchers are now beginning to unravel the structural complexities of gel-like materials such as C-S-H.

Grutzeck et al. (6) used ^{29}Si magic angle spinning NMR to examine precipitates in the system $CaO\text{-}SiO_2\text{-}H_2O$. They reported the existence of two C-S-H structure types. One C-S-H consists predominantly of Q_2 silicate-chains (Ca/Si molar ratio 0.65-1.0) and the other C-S-H consists of a combination of Q_2 chains and Q_1 silicate dimers (Ca/Si molar ratio $\geq$1.1). The work described in the following paragraphs is a description of continuing efforts in this area of solution/sol mixing experiments. However, the scope of the study has been broadened to include colloidal alumina and, on occasion, NaOH.

Experimental Procedures

In order to study the solubility/structural effects of alumina in C-S-H, and identify the aluminosilicate phases which could coexist with C-S-H, progressively larger amounts of alumina were added to the alumina-free system. Because of our earlier work, we were reasonably sure that two C-S-H phases existed in the system $CaO\text{-}SiO_2\text{-}H_2O$. Therefore, it was logical to extend the scope of the study to include similar information for three isoalumina joins through the quaternary system $CaO\text{-}Al_2O_3\text{-}SiO_2\text{-}H_2O$. In total, four planes of constant alumina concentration were

studied: 0,* 10, 20 and 30 wt. %. See Figure 1 for a sketch of the system and the composition of mixtures studied (solid dots). Mixtures were prepared from freshly calcined reagent grade $CaCO_3$, colloidal silica (Cab-O-Sil), colloidal alumina (Rhone Poulenc flash calcined), and freshly boiled deionized water. Typically, two grams of solids were mixed with 100ml of water (w/s=50/1) in a 125ml high density polyethylene bottle. Samples were protected from the effects of carbonation by storing the bottles in a vacuum desiccator. Mixtures were subjected to constant gentle agitation on a shaking table. Samples were allowed to equilibrate at both room temperature and 60°C, the latter were shaken periodically rather than continuously.

Because alumina is often viewed as being relatively insoluble in aqueous solutions, various colloidal alumina and/or aluminum hydroxides were investigated as potential source of alumina. It was found that among gibbsite, γ-alumina and a Rhone Poulenc flash calcined alumina, the Rhone Poulenc alumina had the highest reactivity. Rates of reaction were tracked with x-ray diffraction and TEM. In all cases, the starting material had been consumed by the reaction in one to two months.

pH of mixtures falling along the various fixed alumina joins were monitored regularly, and pH versus composition plots were constructed in order to chart the progress of reaction and the mixture's approach to equilibrium. After a few months, solid samples of C-S-H were also taken for characterization.

The System CaO-SiO_2-H_2O

A series of confirming runs and expanded compositions were studied. No alumina was added to these mixtures (0 wt. % Al_2O_3 join). pH plots and a corresponding phase diagram constructed from the data are given in Figure 2. Labeled circles represent mixtures which were characterized using x-ray diffraction and scanning electron microscopy.

* The 0 wt. % Al_2O_3 join was studied in order to confirm earlier work (6). It is often dangerous to repeat experiments but, in this instance, results were similar.

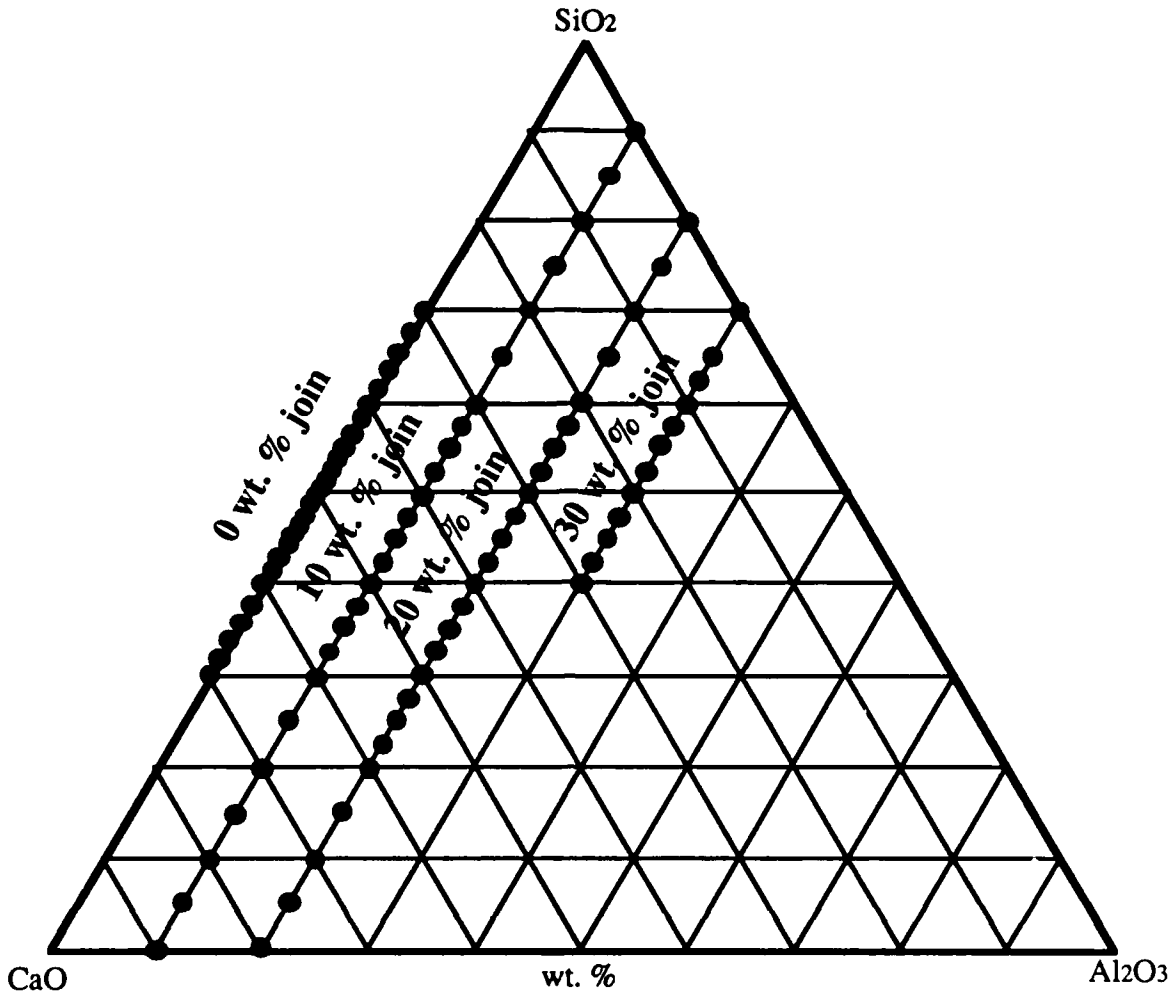

Figure 1. Composition of mixtures studied along the 0, 10, 20 and 30 wt. % Al_2O_3 isocompositional joins. The 0% Al_2O_3 study was used to confirm earlier work in the system $CaO\text{-}SiO_2\text{-}H_2O$. The 10, 20 and 30 % Al_2O_3 studies were new, focusing on the occurrence of C-S-H in the system $CaO\text{-}Al_2O_3\text{-}SiO_2\text{-}H_2O$.

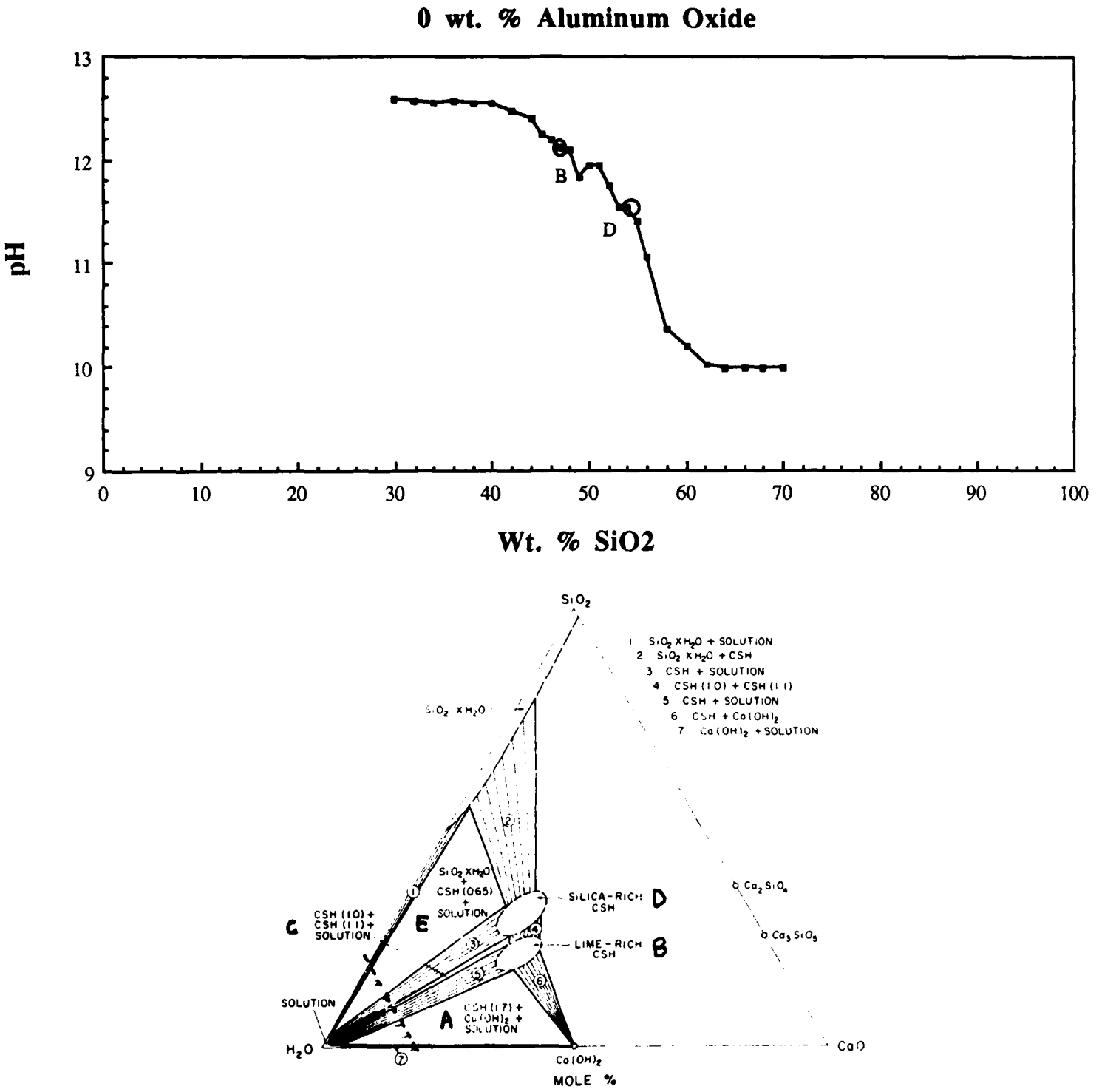

Figure 2. pH-composition plot of mixtures in the system CaO-SiO_2-H_2O (top), and a corresponding ternary phase diagram constructed from these data (bottom). Letters denote various phase assemblages present in the system. Solid circles represent compositions of mixtures discussed in the text. The dashed line near the water apex (lower figure) is a highly exaggerated sketch of the location of the pH-composition plot.

pH-Composition Plots

A pH composition plot for the fully equilibrated system $CaO\text{-}SiO_2\text{-}H_2O$ is given in Figure 2 (top). The horizontal portions of the curve signify the presence of a three-phases invariant triangle in the system. The pH of the solution as well as its composition within an invariant phase assemblage is constant because of the constraints imposed on the system by the phase rule; for example, in a three-component system, such as $CaO\text{-}SiO_2\text{-}H_2O$, the system will be invariant if no degrees of freedom exist. This invariancy can only occur if temperature and pressure are fixed (e.g. room temperature, atmospheric pressure) and three phases coexist simultaneously.

$F=C-P+2$

$F=3-3+2$

$F=2$ (fixed pressure, temperature)

$F=0$

Since the horizontal portions of the curve denote compositional extremes of the 3-phase triangles, it is an easy matter to construct a phase diagram from the data [see Figure 2 (bottom)]. Water contents of the C-S-H's were taken from the literature. The diagram contains three invariant triangles in which two solid phases are in equilibrium with solution (labelled A, C, E in figure). These are separated by two-phase fields (numbered 1-7). Tie lines denote the composition of coexisting solid and liquid phases. The letters B and D denote the compositions of the C-S-H phases discussed in the following sections. Note that mixtures A, C and E each contain two solids [C-S-H + $Ca(OH)_2$, C-S-H + C-S-H, and silica gel + C-S-H, respectively], whereas B and D are phase pure C-S-H.

X-ray Diffraction

In order to confirm the existence of and characterize the two C-S-H phases in the system $CaO\text{-}SiO_2\text{-}H_2O$, routine X-ray diffraction patterns were collected for two representative C-S-H samples (labeled B and D in Figure 2, top). See Figures 3 and 4 for their patterns. The x-ray diffraction pattern of mixture B with composition closer to $Ca(OH)_2$ contained, as expected, peaks

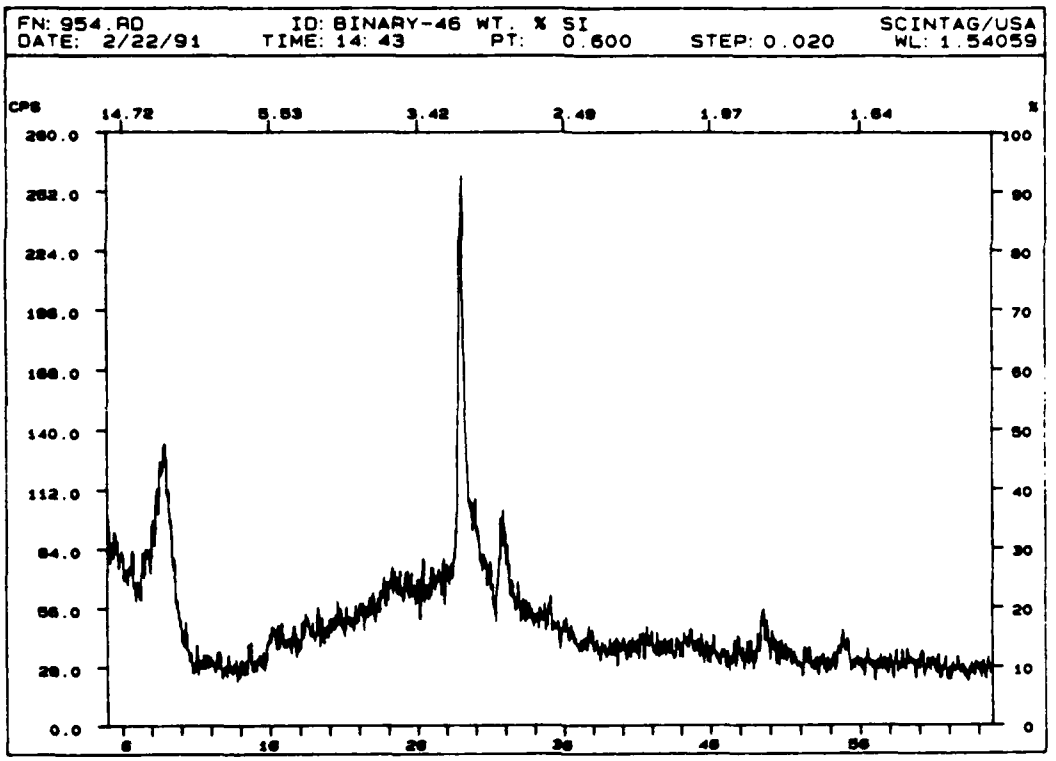

Figure 3. X-ray diffractogram of the Ca-rich C-S-H (B) containing 46 wt. % SiO_2 and 54 wt. % CaO. The nature of the peak at 9°2θ is unknown.

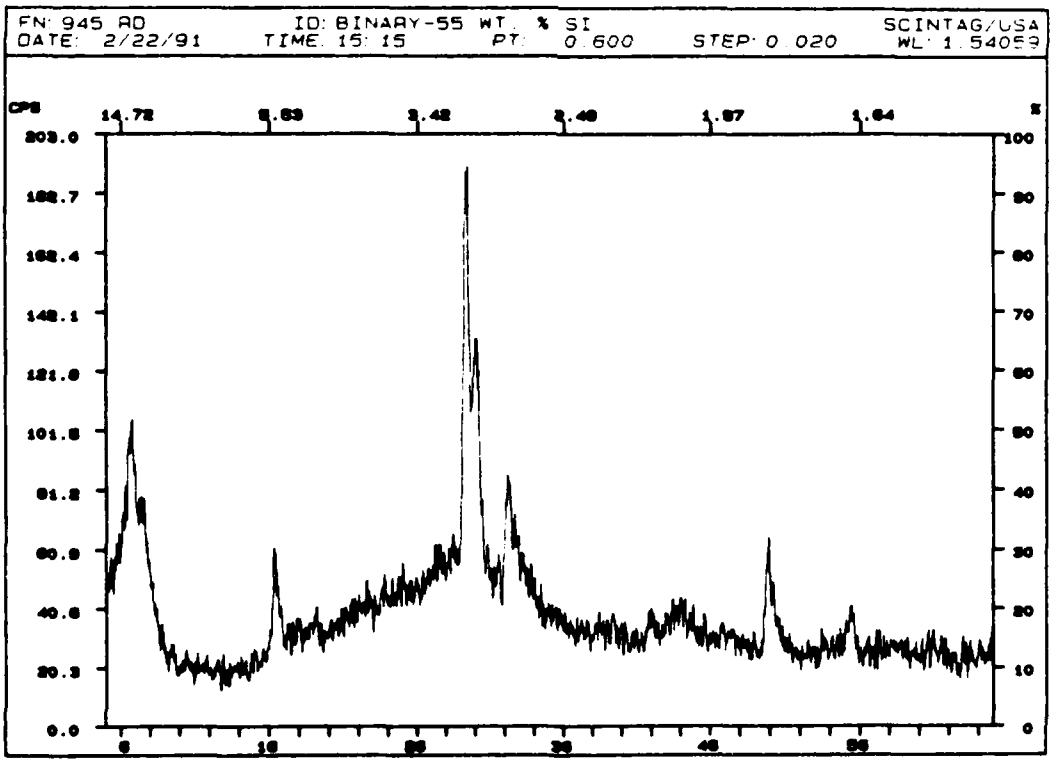

Figure 4. X-ray diffractogram of the silica-rich C-S-H (D). Mixture contains 55 wt. % SiO_2 and 45 wt. % CaO. The nature of the peaks at 7° and 17°2θ are unknown.

from C-S-H, and one unidentified peak at ~9° 2θ. There are also potential peaks at ~50° 2θ and ~55° 2θ. However, their intensities are not very much larger than background noise. As for the C-S-H sample with composition closer to the amorphous silica gel (D), its X-ray pattern showed the characteristic peak at 29° 2θ from C-S-H and a similar unidentified peak now at ~7° 2θ. The two peaks that were very small at ~50 and 55° 2θ are now more pronounced. In addition, there is now a new peak at ~17°2θ. The major peaks closely resemble C-S-H I [JCPDS #33-306].* The fact that the C-S-H patterns (B, D) are similar suggests that their long-range order is very similar even thought their atomic level structure is different.

The System CaO-Al_2O_3-SiO_2-H_2O

In addition to the 0 wt. % join, three additional isoalumina joins through the system CaO-Al_2O_3-SiO_2-H_2O were also studied (see Figure 1). In addition to pH-composition plots, x-ray diffraction, MASNMR, TGA and SEM data were also collected for selected mixtures. The 10, 20 and 30 wt. % alumina mixtures were equilibrated at room temperature. In addition, a second set of 30 wt. % alumina mixtures were also equilibrated at 60°C with and without added NaOH.

pH-Composition Plots

Figure 5 represents pH-composition plots of mixtures falling along the 10 and 20 wt. % isoalumina joins. These plots are nearly identical to those for the system without alumina (Figure 2, top). Once again, the two horizontal portions of the curves suggest the presence of large invariancies in the system. In this instance, the phase diagram consists of a tetrahedron with CaO, Al_2O_3, SiO_2 and H_2O at its corners. Since we are working with four phases, the invariancy is shaped like a pyramid of some sort; the flat portions of 10 and 20 wt% plots suggest that one volume occurs near the CaO corner and another near the SiO_2 corner of the phase diagram. Between these invariances, the pH varies as a function of composition. The system has at least

* Joint Committee on Powder Diffraction Standards, Swarthmore, PA 19081.

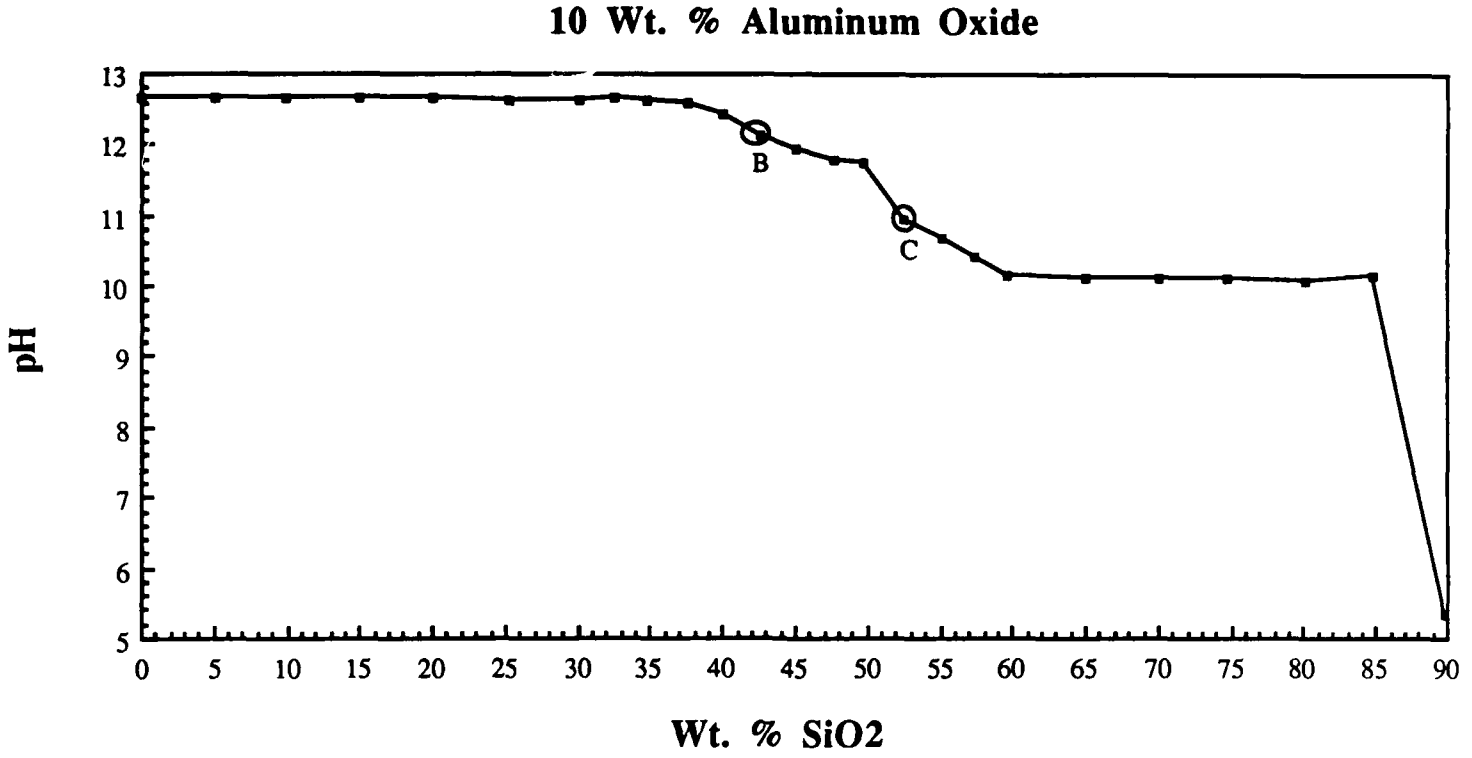

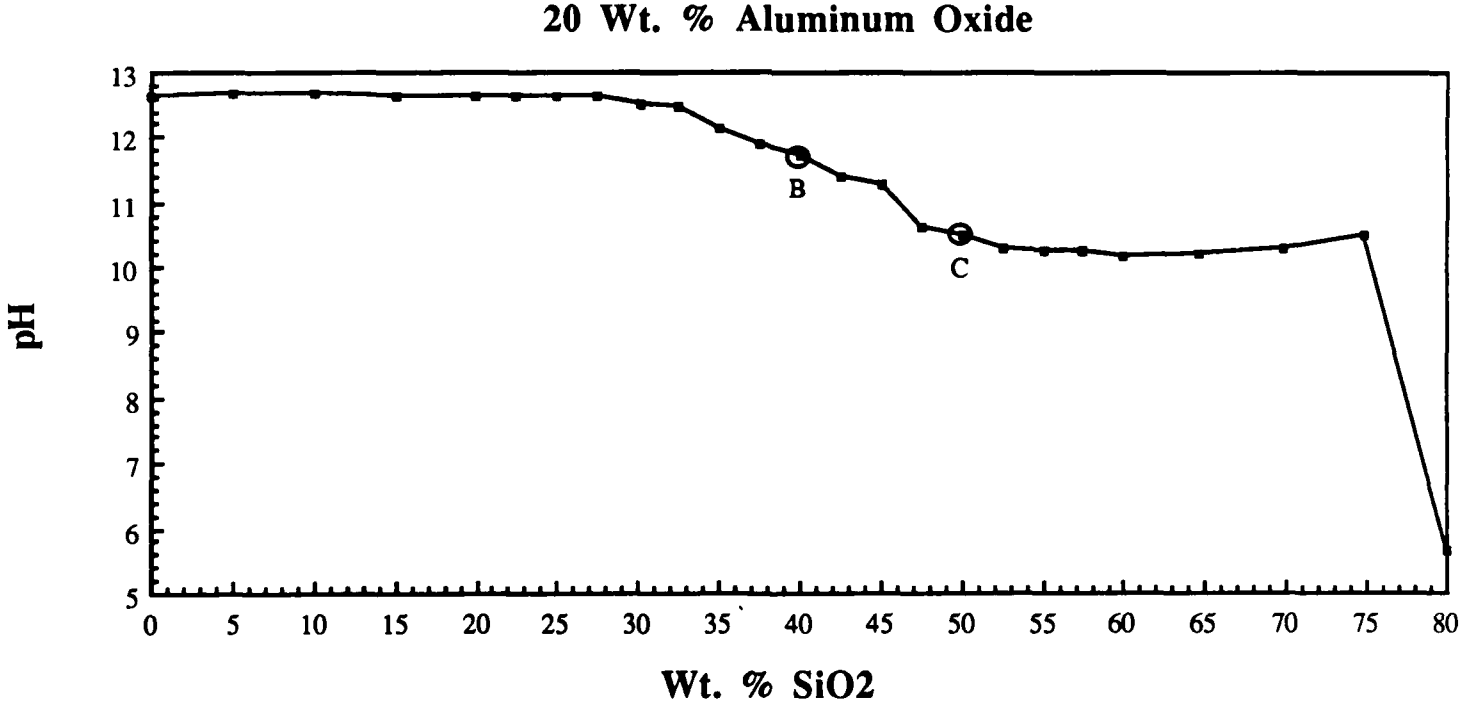

Figure 5. pH-composition plots for mixtures falling along the 10 and 20 wt. % isoalumina joins through the system $CaO\text{-}Al_2O_3\text{-}SiO_2\text{-}H_2O$. Solid circles represent samples which were characterized and/or are discussed in the text.

one degree of freedom. Whether or not the two C-S-H phase fields which fall in this compositional range are also separated by an invariancy as in the CaO-SiO_2-H_2O system (Figure 2) is not as clear. However, there seem to be "flat spots" centered around 47.5 wt. % SiO_2 in the 10 wt. % Al_2O_3 mixtures and 45 wt. % SiO_2 in the 20 wt. % Al_2O_3 mixtures. The existence of these "flat spots" along the various alumina joins suggest that the two C-S-H phases identified earlier, do in fact extend into the quaternary system.

A similar plot of pH versus composition for mixtures containing 30 wt. % Al_2O_3 (hydrated at 60°C) and deionized water is given in Figure 6 (top). The shape of this curve is identical to that obtained from room temperature data. Once again, this plot is similar in appearance to the plots of the 10 and 20 wt. % samples. The system is invariant from ~ 50 to ~ 65 wt. % SiO_2 when deionized water is used as mixing solution however the pH is slightly lower (9.7) compared to the 10 and 20 wt. % sections (10.0).

As an alternative, this set of mixtures was also run with an elevated alkali hydroxide content, substituting 1.5M NaOH solution for the deionized water. The plot obtained in this case is given in Figure 6 (bottom). In this instance, the pH-composition plot is nearly horizontal over the entire range of composition studied (13.2 ± 0.2). This behavior is apparently due to the large excess of NaOH introduced into the system.

Four samples along both the 10 and 20 wt. % isoalumina joins (A-D, Figure 5 top and bottom) were freeze-dried and subjected to x-ray diffraction investigation. In both instances the most lime-rich samples (A) contained peaks attributable to $Ca(OH)_2$, C-S-H (~29° 2θ), hydrogarnet ($3CaO{\cdot}Al_2O_3{\cdot}SiO_2{\cdot}4H_2O$ → 20 wt. % only), and an unidentified peak at ~11° 2θ. Similarly the samples closest to the silica apex (D) contained peaks attributable to C-S-H (~29° 2θ) and an amorphous hump due to silica gel.

Figures 7 and 8 represent x-ray diffraction patterns of the two C-S-H phases along the 10 and 20 wt. % isoalumina joins, respectively. In each figure, the upper plot is of the more Si-rich C-S-H and the lower plot of the more Ca-rich C-S-H (labeled C and B, respectively in Figure 5).

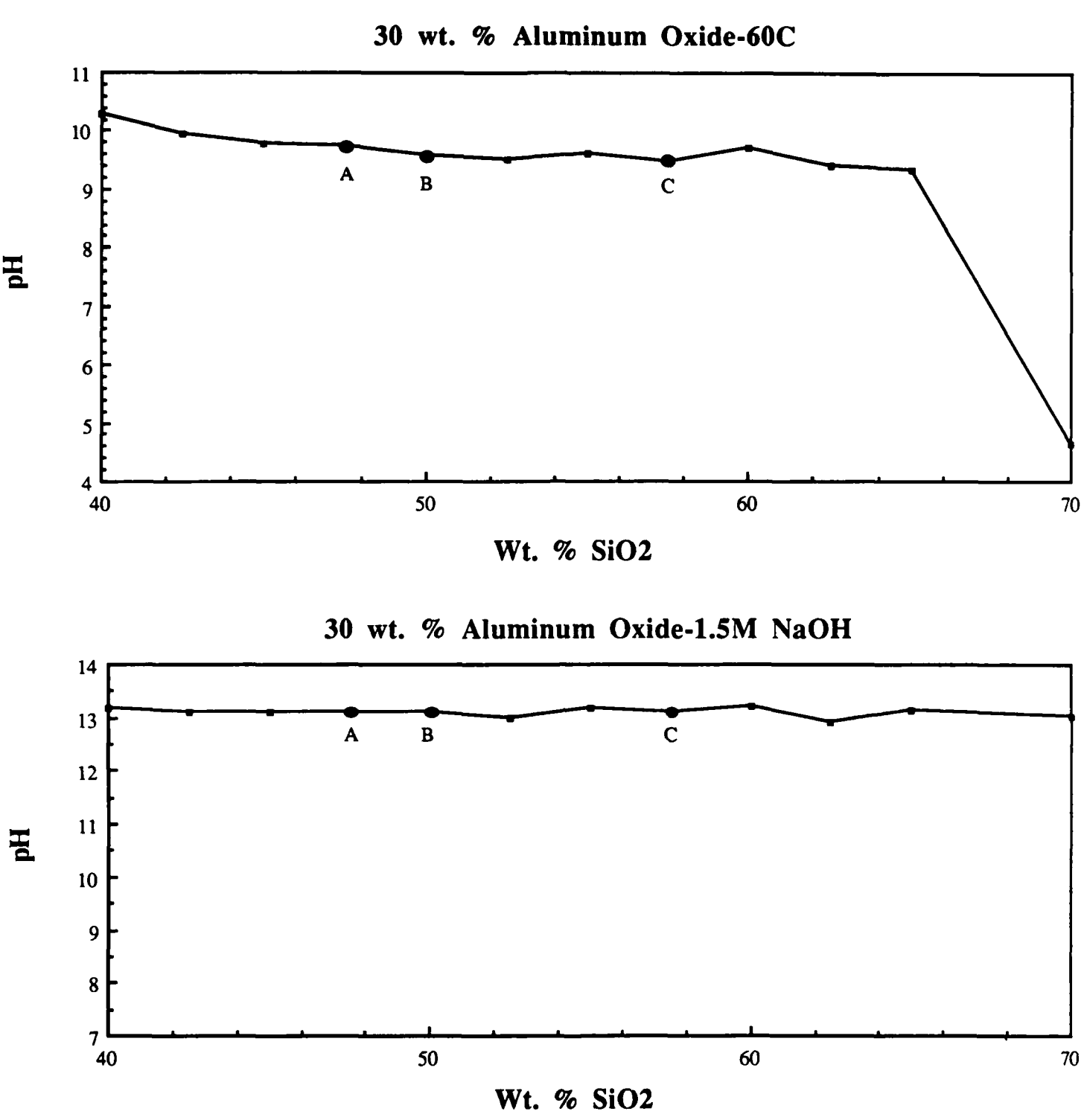

Figure 6. pH-composition plots of mixtures falling along the 30 wt. % isoalumina joins through the system $CaO\text{-}Al_2O_3\text{-}SiO_2\text{-}H_2O$. The curves represent 60°C data. The upper curve is identical in shape to the room temperature plot. The lower curve represents behavior in the systems when the mixing water was replaced by 1.5M NaOH solution. Solid circles (A, B, C) represent samples which were characterized and/or are discussed in the text.

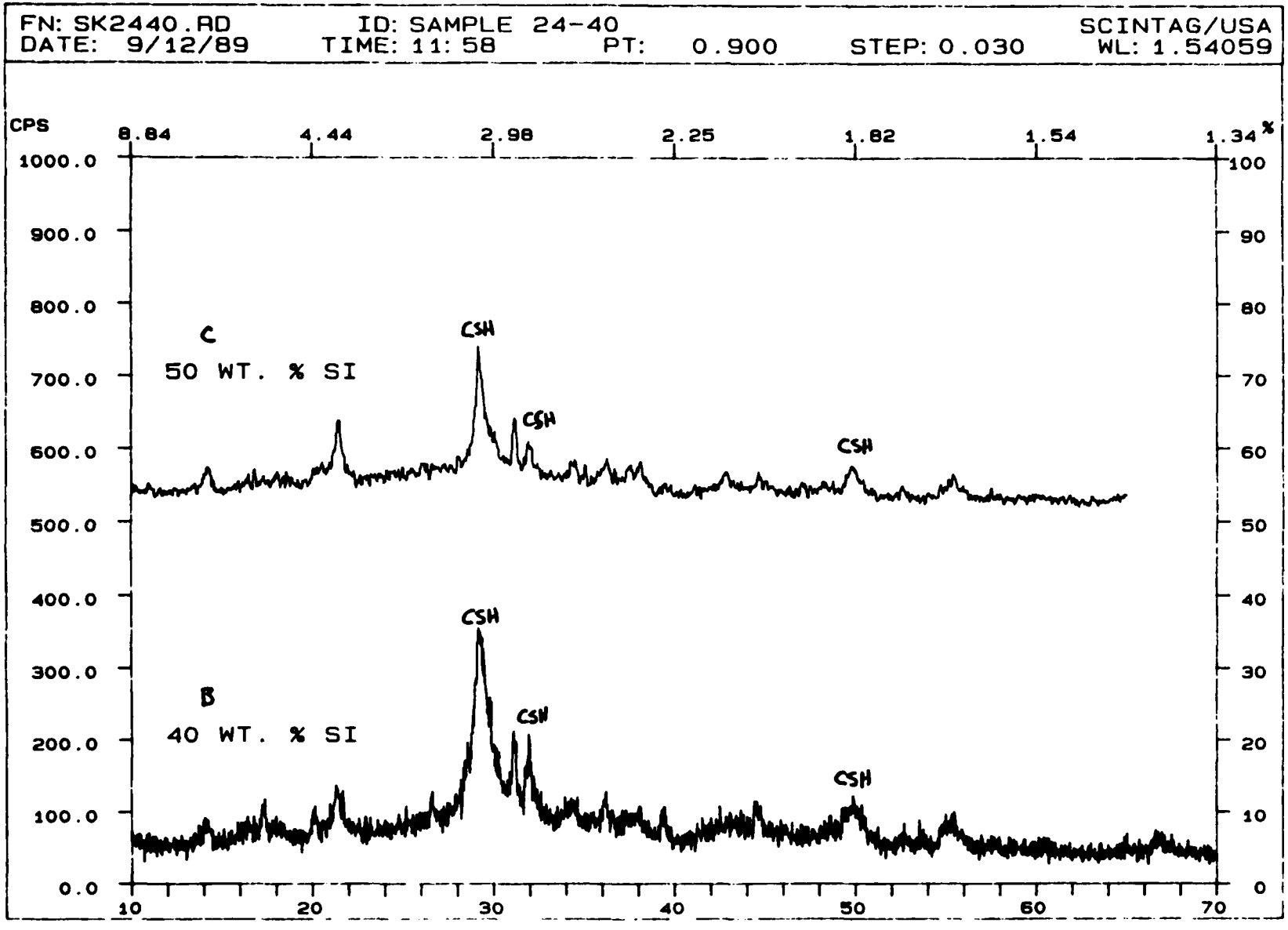

Figure 7. X-ray diffractograms of the two C-S-H phases along the 10 wt. % Al_2O_3 join.

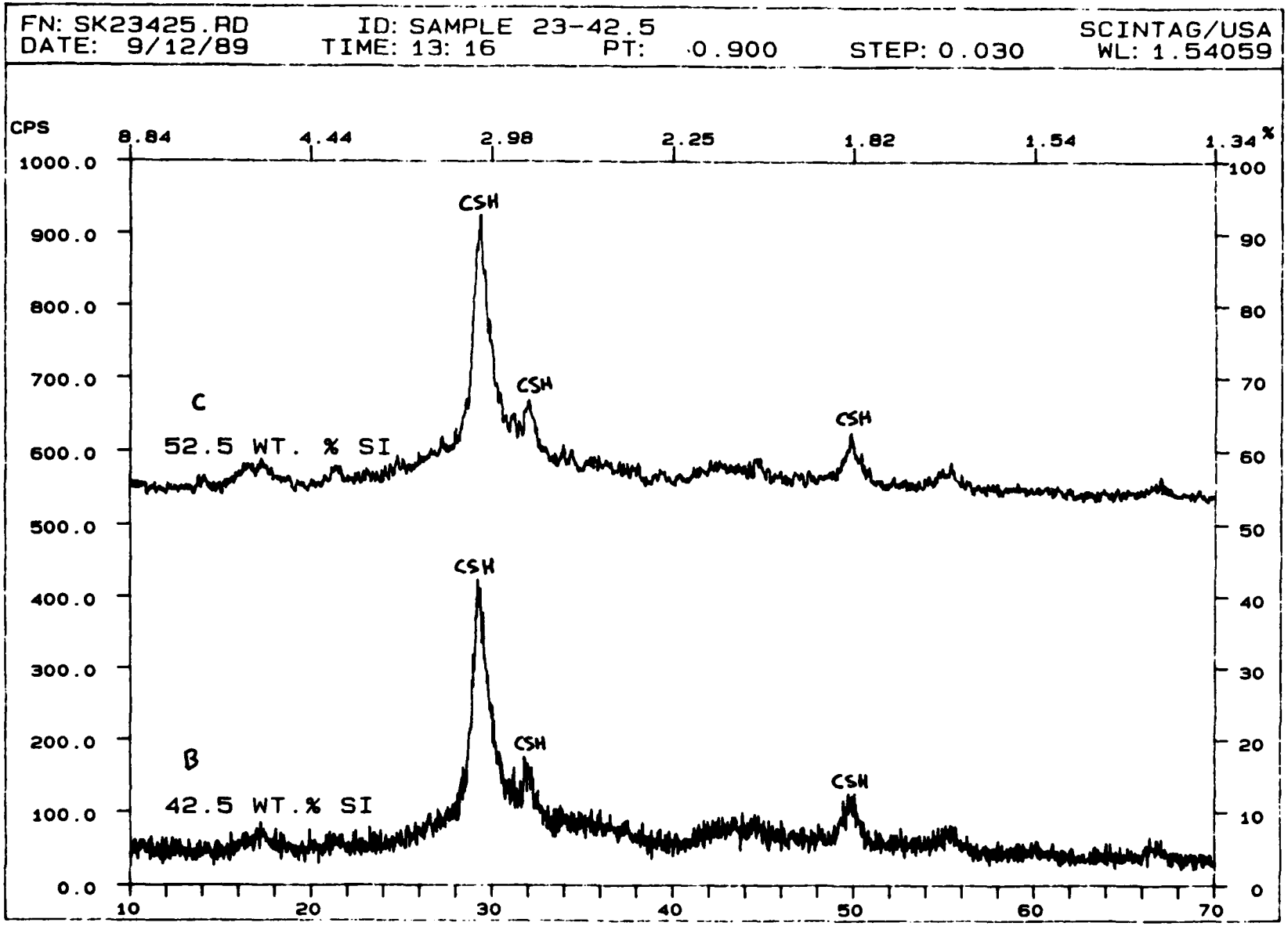

Figure 8. X-ray diffractograms of the two C-S-H phases along the 20 wt. % Al_2O_3 join.

Although, we would like to think that these C-S-H's are phase pure, both the 10 wt. % and 20 wt. % plots seem to contain traces of a second phase which increases as more Al_2O_3 is added to the system. Nevertheless, both the Ca-rich and Si-rich C-S-H still have identical patterns, patterns which also seem to be independent of alumina content.

X-ray diffraction data for samples containing 30 wt. % Al_2O_3 hydrated in deionized water and equilibrated at 60°C (A, B and C, Figure 6, top) also contained peaks and amorphous humps attributable to C-S-H, and silica gel. However, because of the relative richness of the mixtures in aluminosilicate content, strätlingite ($2CaO{\cdot}Al_2O_3{\cdot}SiO_2{\cdot}8H_2O$) rather than hydrogarnet was observed (see Figure 9). Coupled with studies mentioned earlier (x-ray and TEM), the production of complex aluminosilicate hydrates seems to strengthen the idea that the alumina is dissolving and taking part in the hydration reactions. As SiO_2 is added to the system (A→B→C), strätlingite and C-S-H peaks decrease while the silica gel amorphous hump increases.

The x-ray diffraction data for the 1.5M NaOH containing system (A, B, and C, Figure 6 bottom) is radically different. See Figure 10. The patterns show that the crystallinity of the samples are much higher than the ones hydrated in deionized water. As opposed to a decrease in crystallinity as the silica content increased (mixtures hydrated in DI water), the crystallinity of these samples increase as the silica content increase (A→B→C). As the composition of these mixtures are well within the traditional compositional range of zeolites, it is not unreasonable to assume that the peaks in the x-ray pattern are due to the presence of "zeolitic" materials, although at this time, their identity is still unknown.

MASNMR

The recent success of solid state magic angle spinning NMR, in particular ^{29}Si MASNMR, in the investigation of the structure of amorphous cementitious materials has been demonstrated in the literature. Whereas traditional diffraction methods are only sensitive to fairly long range structure, NMR is atom sensitive and structures can be studied by examining the shifting of peaks

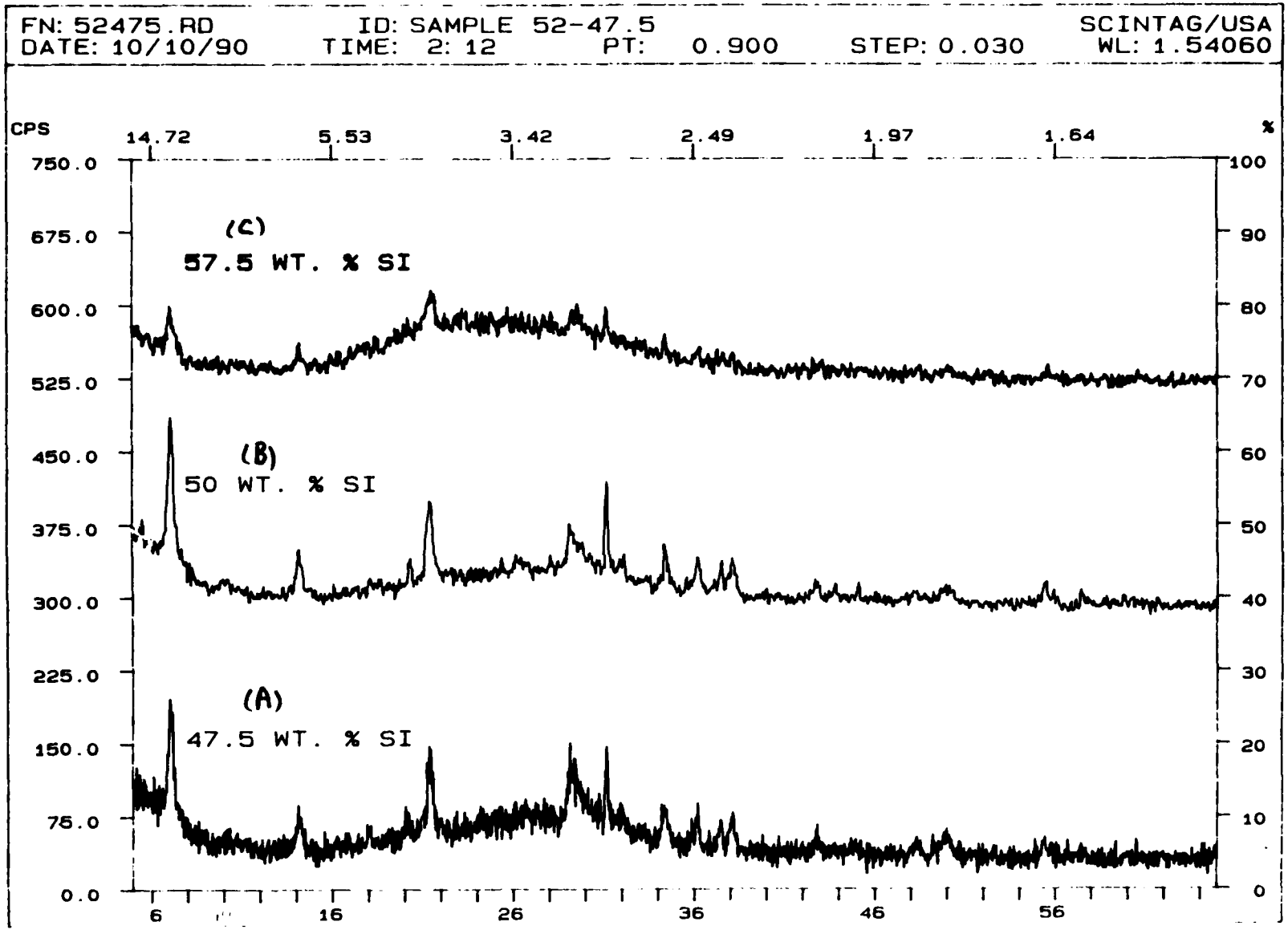

Figure 9. A comparison of x-ray diffraction patterns for mixtures along the 30 wt. % Al_2O_3 join. Mixtures A, B and C illustrate the effect of increasing SiO_2 content of the mixtures.

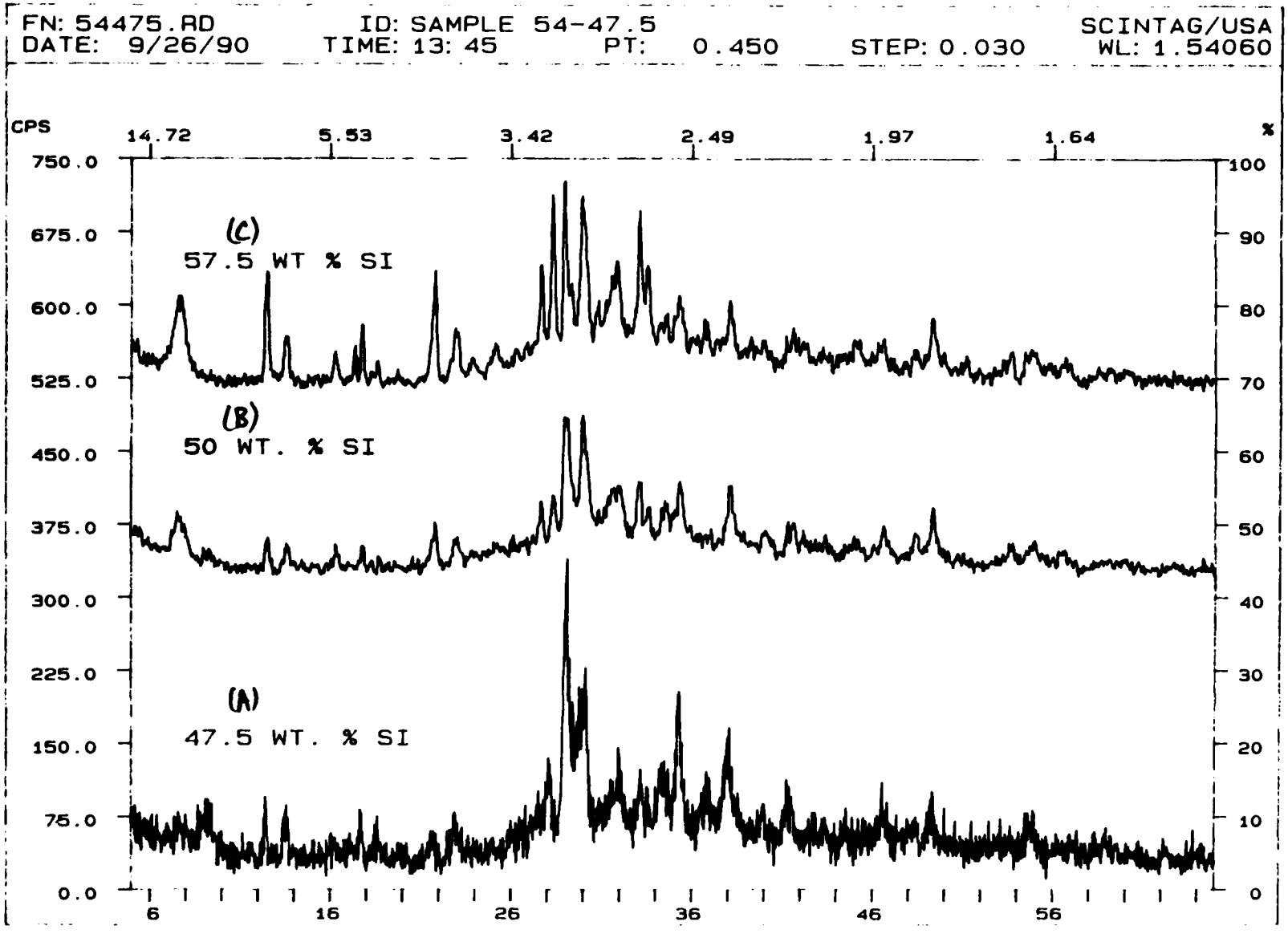

Figure 10. A comparison of x-ray diffraction patterns for NaOH-containing mixtures along the 30 wt. % Al_2O_3 join. Mixtures A, B and C illustrate the effect of increasing SiO_2 content of the mixtures.

due to nearest neighbor environments and longer range interactions. Therefore it can be used to study the structure of fine grained amorphous C-S-H gels.

Shown in Figures 11 and 12 are the ^{29}Si MASNMR spectra of the two proposed C-S-H phases (B and C in Figure 5) from the 10 and 20 wt. % Al_2O_3 sections, which were studied by x-ray diffraction. The spectra of the two samples from the 10 wt. % series (Figure 11) exhibited the expected change from a double peak gel containing Q_1+Q_2 [dimers (~-79 ppm) and chains (~-84 ppm] silica connectivity, to a single Q_2 (~-85 ppm) peak gel. This implies that, at about 50 wt. % silica, there is a change in the atomic level structure. However the samples from the 20 wt. % series had a different behavior. As can be seen from the NMR spectra in Figure 12, there is no compositional induced change in the structure of the C-S-H gel. This suggests that the stability field of the C-S-H gel consisting of dimers and chains does not extend past the 20 wt. % Al_2O_3 join and that the phase field of the silica rich C-S-H possibly "wraps" around the phase field of the lime rich C-S-H.

To further verify the existence of the two C-S-H stability fields and also study the effect of alumina on the structure, ^{27}Al MASNMR was used to study the same four samples. Figure 13 illustrates ^{27}Al spectra of the two 10 wt. % Al_2O_3 containing samples. There is a change of relative intensities of the peaks due to 6 (~10 ppm) and 4 (~60 ppm) coordinated Al atoms between the two samples. The Ca-rich C-S-H has a greater proportion of Al ions in 4-coordinated (silicate chain) sites. Likewise, ^{27}Al NMR spectra were also taken of the two samples containing 20 wt. % Al (Figure 14). Unlike the 10 wt. % samples, there is no change in the relative intensities between the two peaks representing 6 and 4 coordinated Al atoms; octahedral coordination is now more prevalent.

These data reinforce the idea that the stability field of the lime rich C-S-H does not extend past the 20 wt. % Al_2O_3 join, and that the silica-rich C-S-H is more stable at elevated alumina content.

Two samples were extracted from the series of mixtures containing 30 wt. % Al_2O_3 and hydrated in NaOH (A and C, Figure 6 bottom, Figure 10 x-ray pattern). ^{29}Si spectra were taken

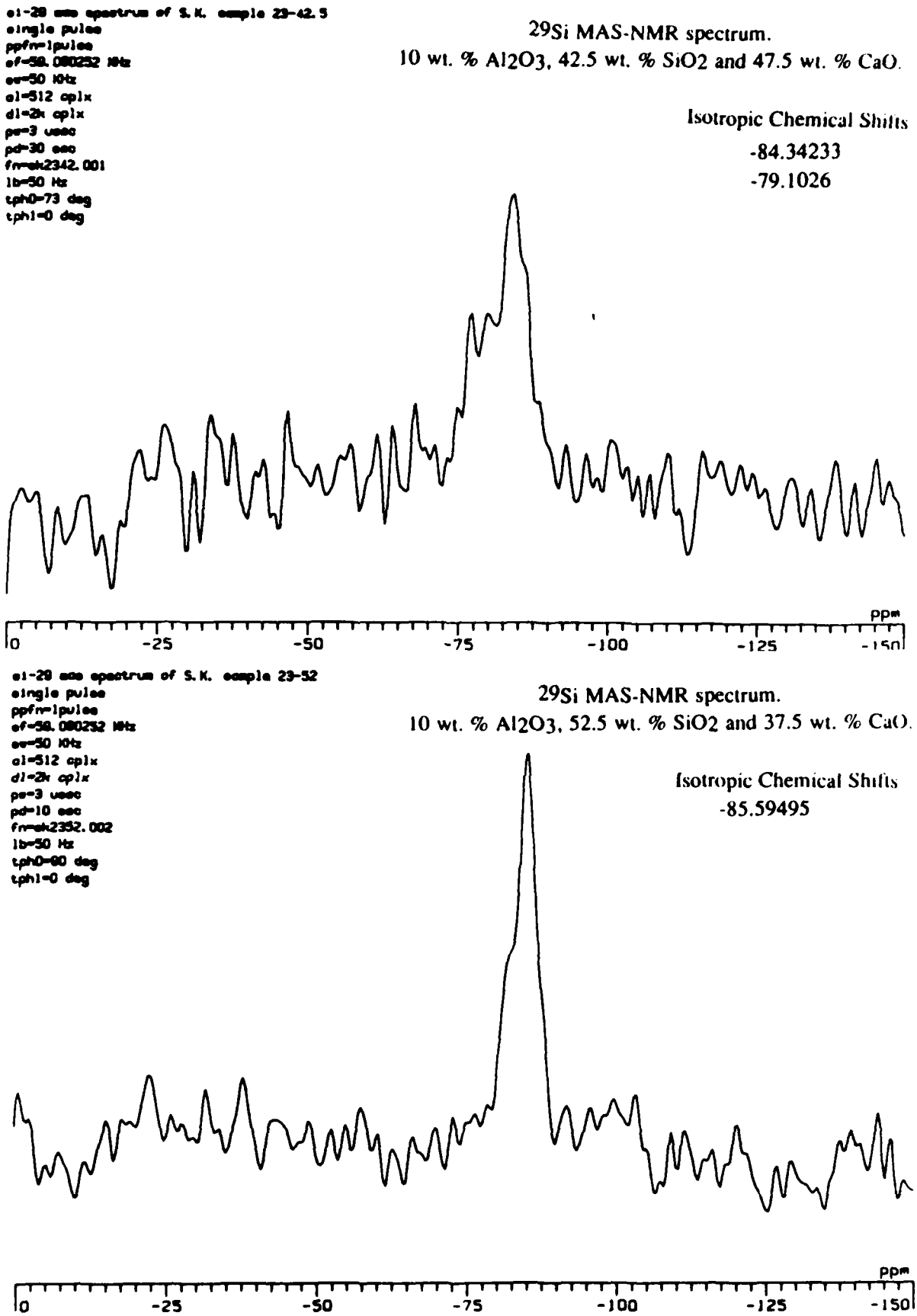

Figure 11. ^{29}Si MAS NMR spectra of the more Ca-rich C-S-H (upper) and the more Si-rich C-S-H (lower) present along the 10 wt. % Al_2O_3 join.

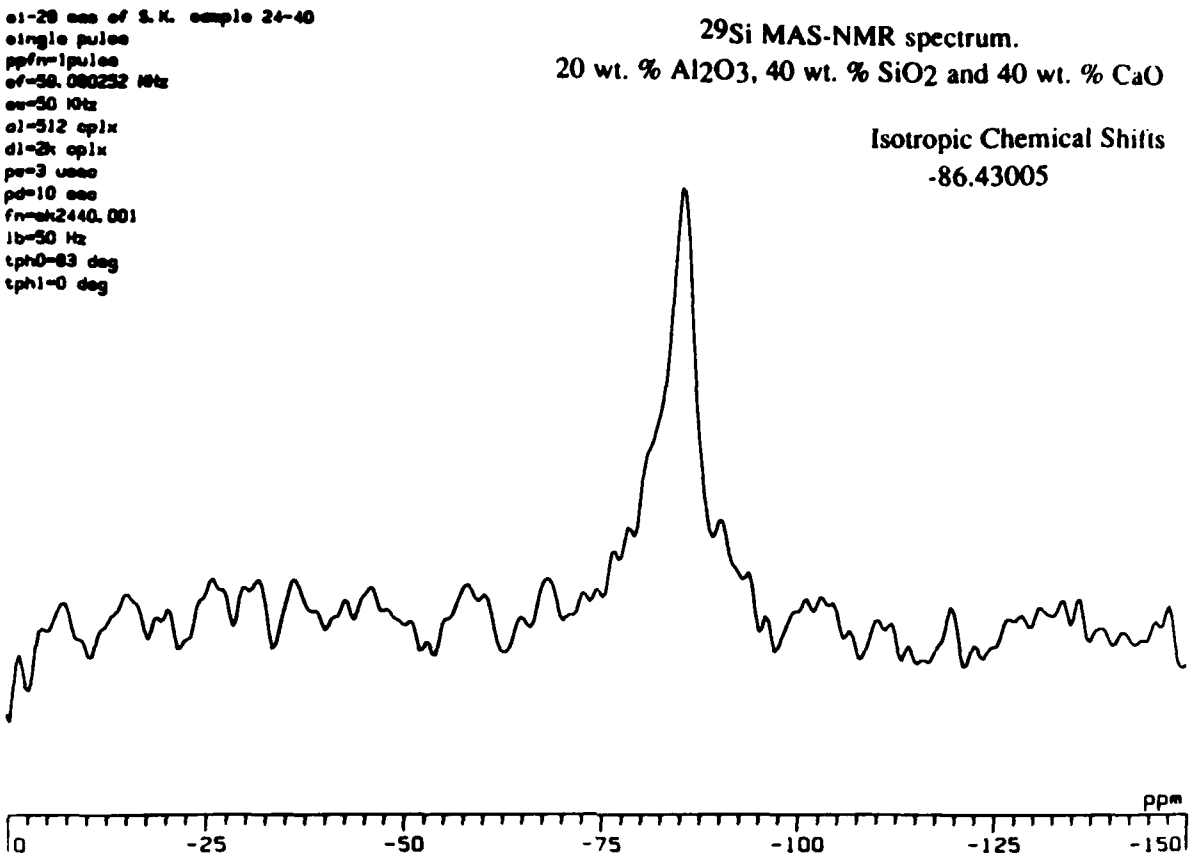

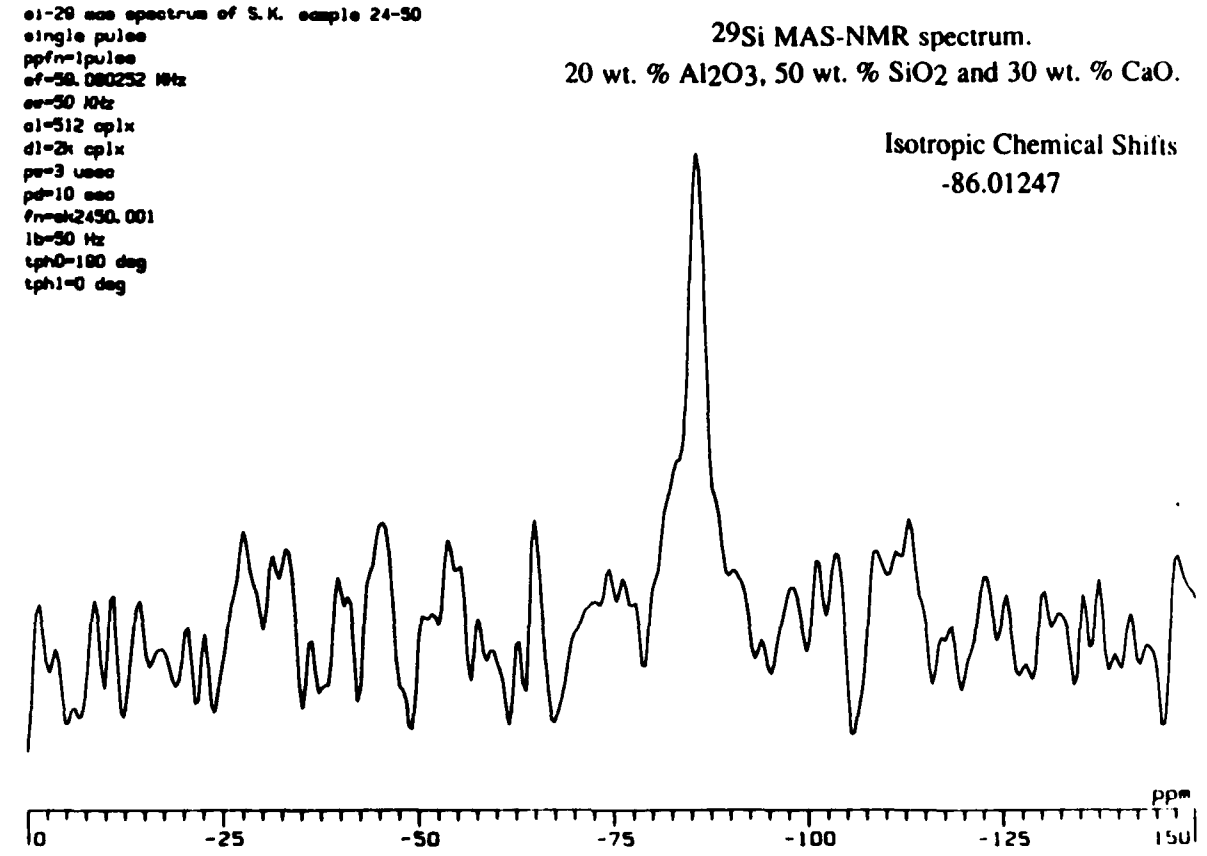

Figure 12. ^{29}Si MAS NMR spectra of the more Ca-rich C-S-H (upper) and the more Si-rich C-S-H (lower) present along the 20 wt. % Al_2O_3 join.

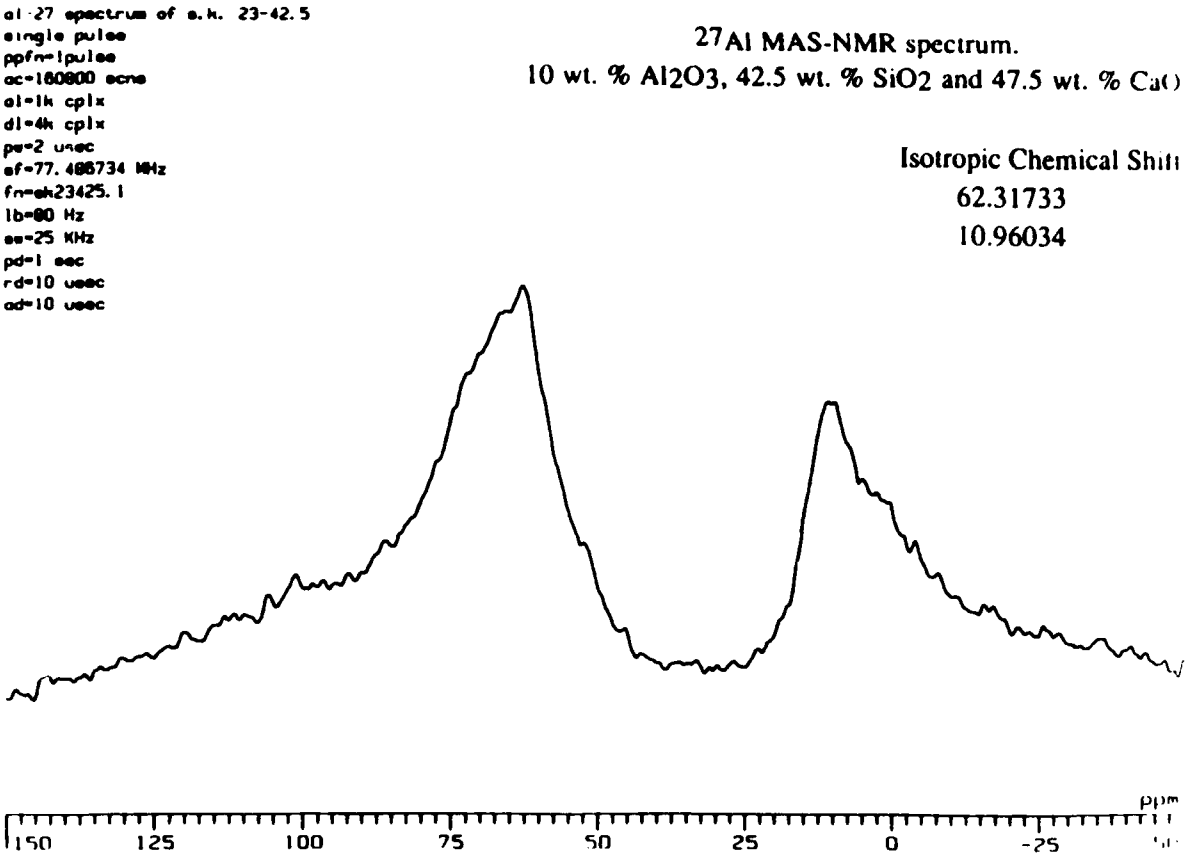

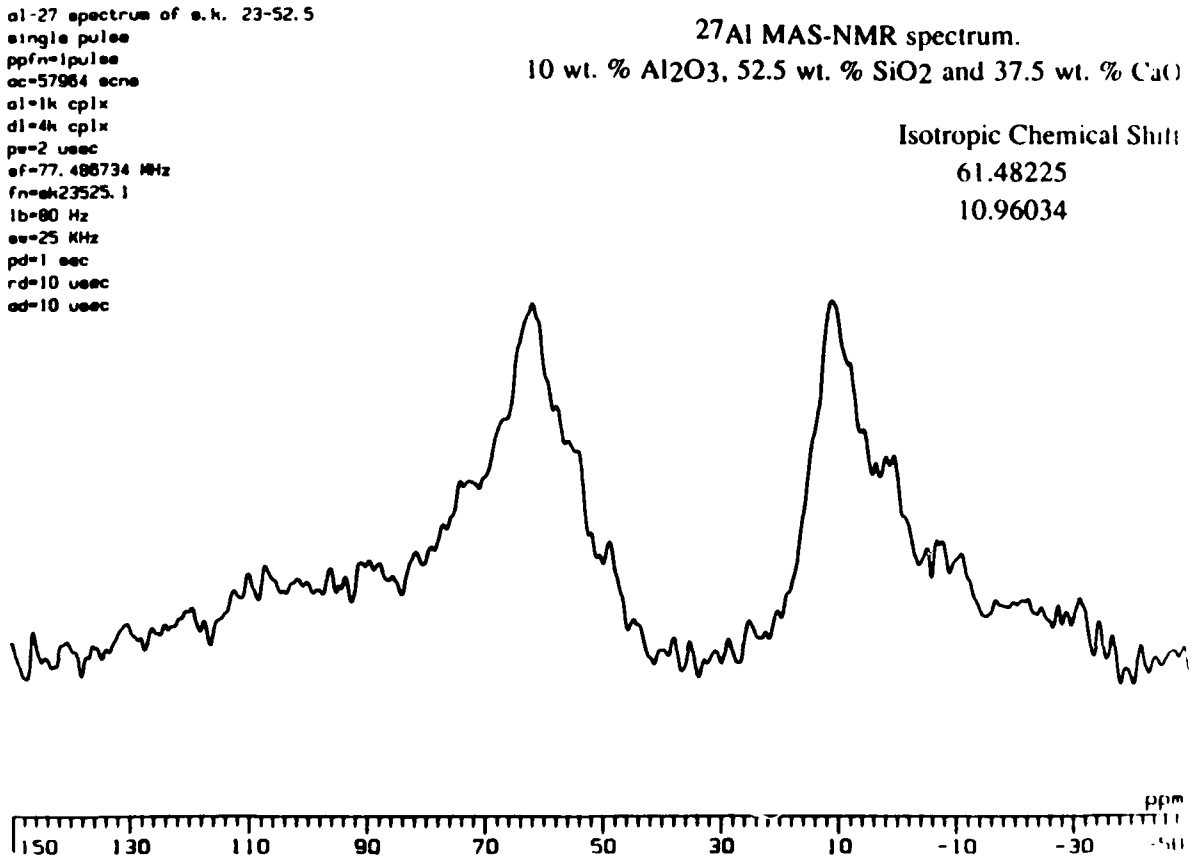

Figure 13. ^{27}Al MAS NMR spectra of the more Ca-rich C-S-H (upper) and the more Si-rich C-S-H (lower) present along the 10 wt. % Al_2O_3 join.

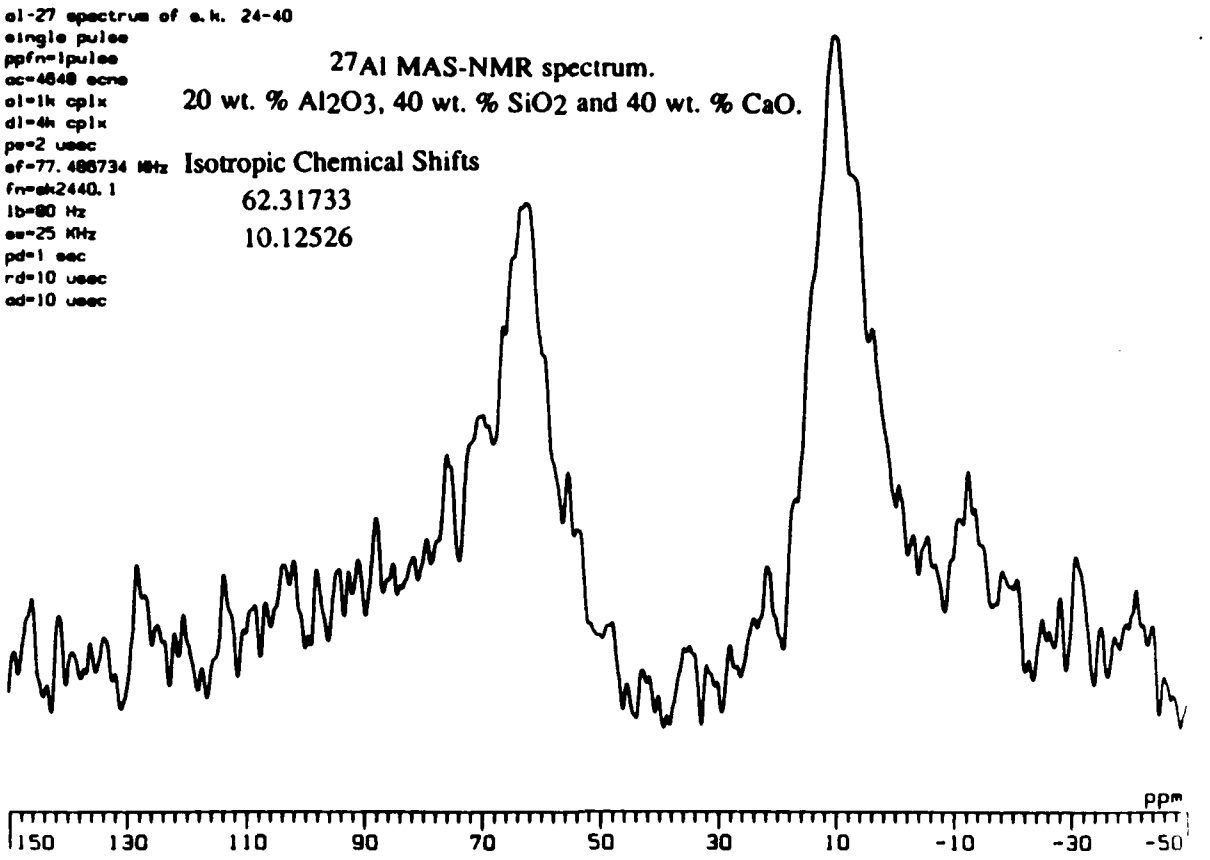

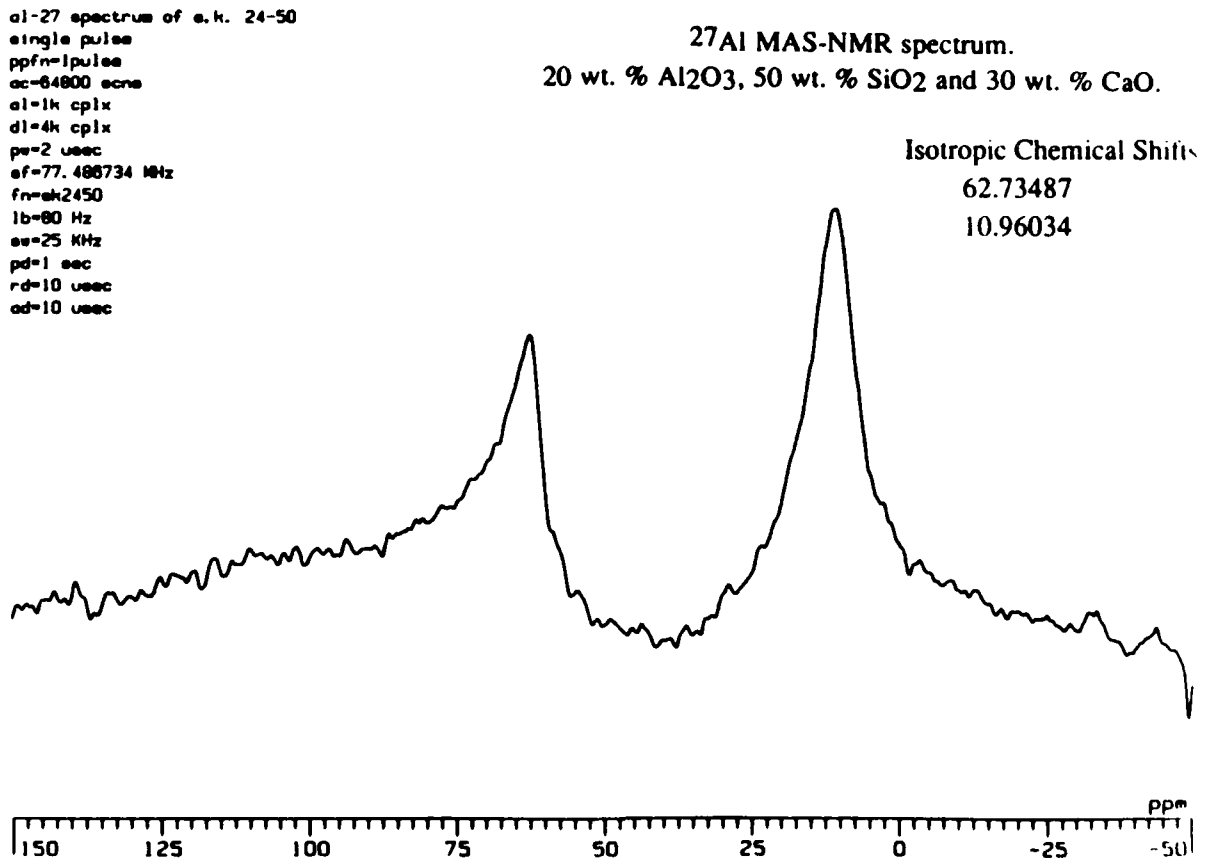

Figure 14. ^{27}Al MAS NMR spectra of the more Ca-rich C-S-H (upper) and the more Si-rich C-S-H (lower) present along the 20 wt. % Al_2O_3 join.

and the results are shown in Figure 15. These spectra contain Q_1+Q_2 peaks corresponding to dimers and long chains. These were different from the mixtures hydrated in deionized water (not shown here) in that the mixtures hydrated in water and having similar compositions consisted only of Q_2 peak material. This discrepancy arises from the sodium we have added to the system. It is known that a small amount of sodium can substitute into the structure of C-S-H gels and may modify its structure, but not to the degree indicated here. An alternate explanation may be that a new gel has been produced altogether. Although corresponding x-ray patterns (Figure 10) were filled with peaks of suspected "zeolites", the expected Q_3 and Q_4 (sheets and 3-D network respectively) ^{29}Si peaks are absent from these plots. The reason for this behavior is unknown.

Thermogravimetric Analysis

Thermogravimetric analysis (TGA) plots of the lime rich C-S-H and silica rich C-S-H without Al_2O_3 are shown in Figures 16 and 17, respectively. There are differences in their behavior during heating. The more lime-rich C-S-H exhibited weight loss in one large step followed by a smaller step. The more silica-rich C-S-H lost weight initially by a large step but then gradually afterward. The dehydration behavior of the two C-S-H gels containing 10 wt. % alumina again showed that there are distinctive differences between these two gels. The dehydration patterns of the two C-S-H gels are again very different. See Figure 18. The Q_1+Q_2 containing C-S-H lost 29.5 wt. % (H_2O) both gradually and in two steps, while the Q_1 containing C-S-H lost 25 % in one large step and gradually thereafter. The samples with 20 wt. % Al_2O_3 (Figure 19) reinforce earlier findings concerning the limited extent of the stability field of the Ca-rich C-S-H gel as there are no differences between the two samples. In addition, both C-S-H samples (B and C, Figure 5, bottom) lost ~ 25 wt. % H_2O.

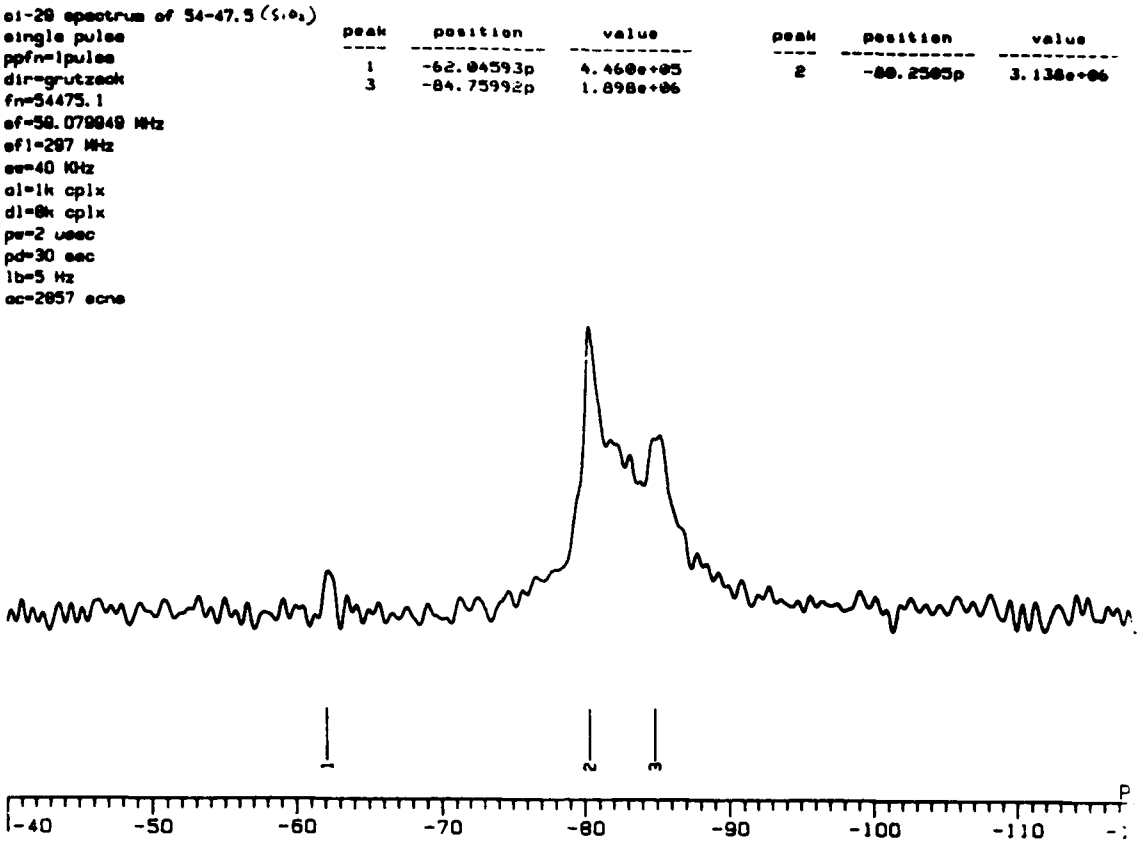

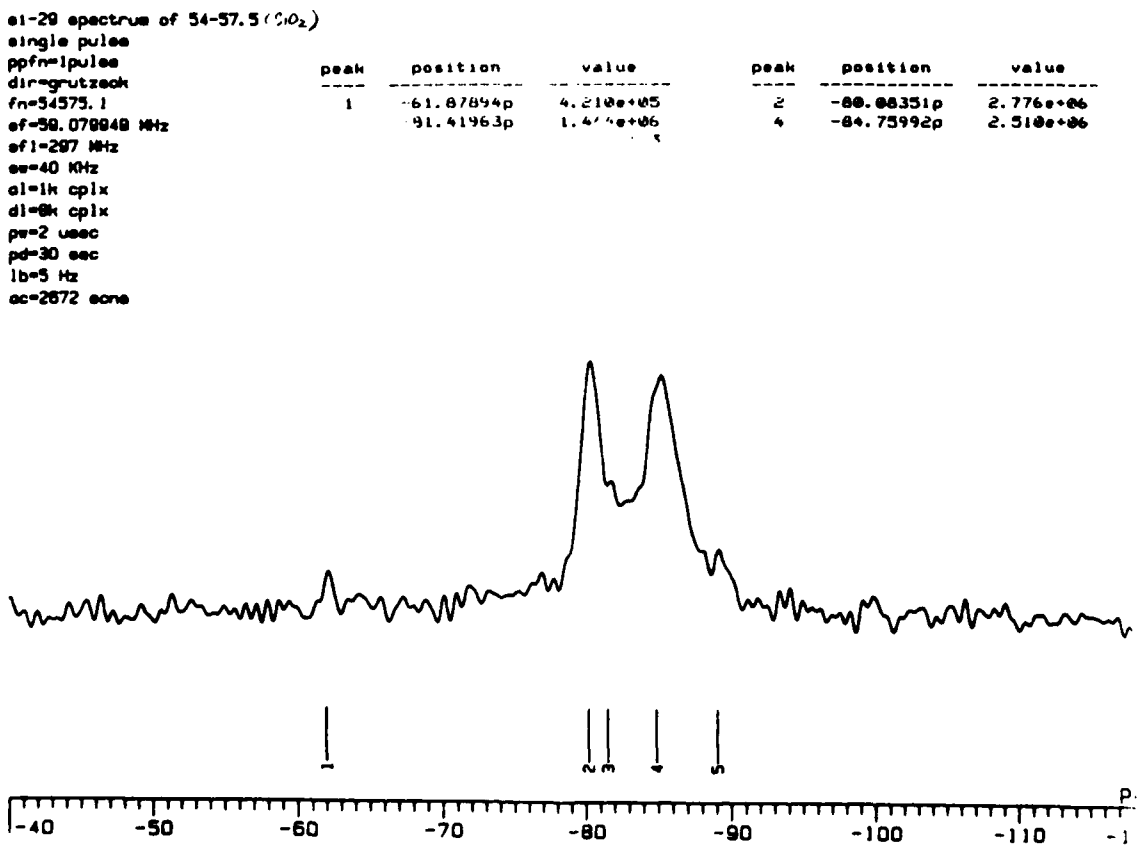

Figure 15. ^{29}Si MAS NMR spectra of NaOH-containing mixtures along the 30 wt. % Al_2O_3 join.

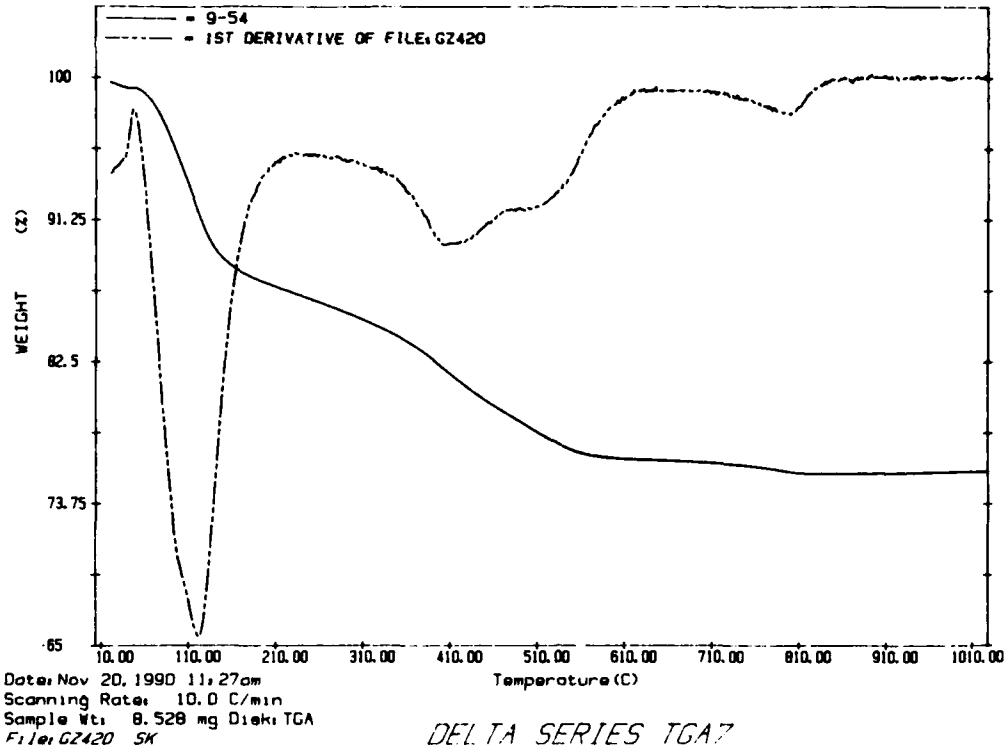

Figure 16. TGA and first derivative curve of Ca-rich C-S-H (alumina-free system).

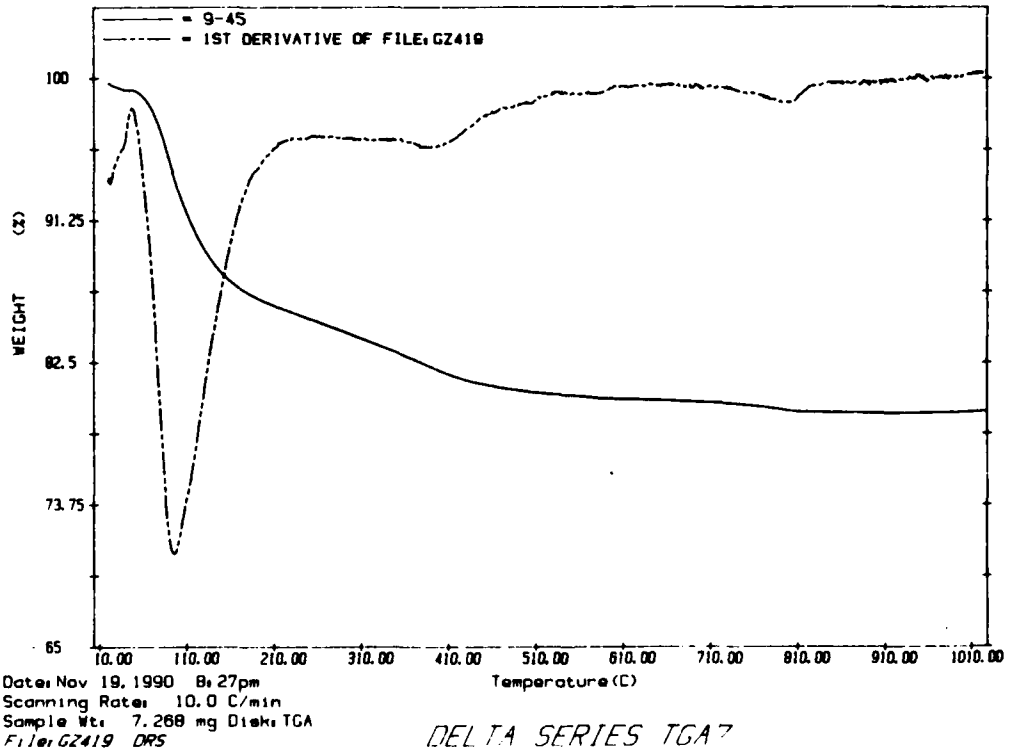

Figure 17. TGA and first derivative curve of Si-rich C-S-H (alumina-free system).

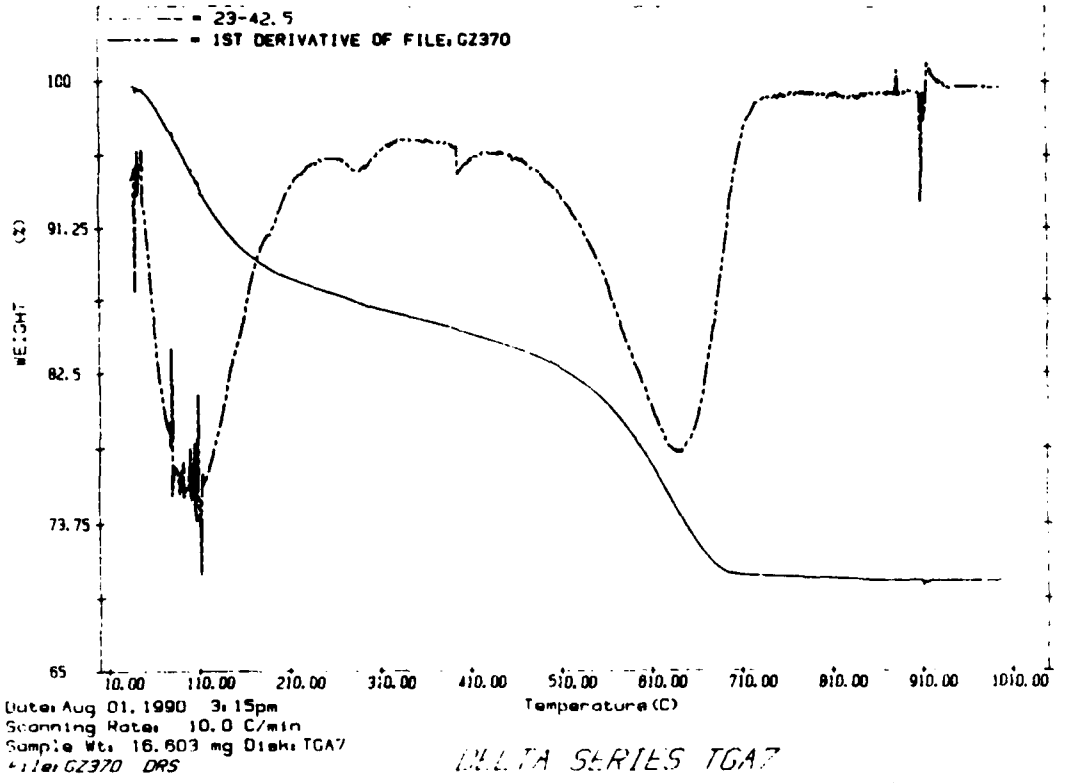

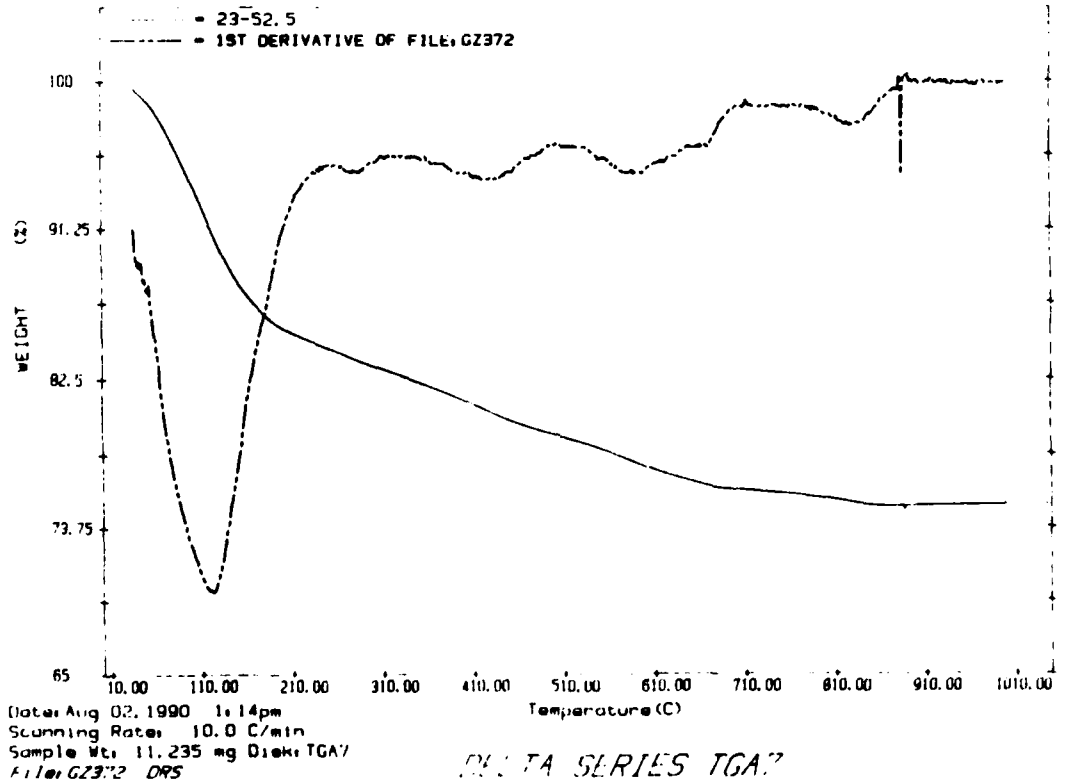

Figure 18. TGA and first derivative curves of Ca-rich C-S-H (upper) and Si-rich C-S-H (lower) occurring along the 10 wt. % isoalumina join.

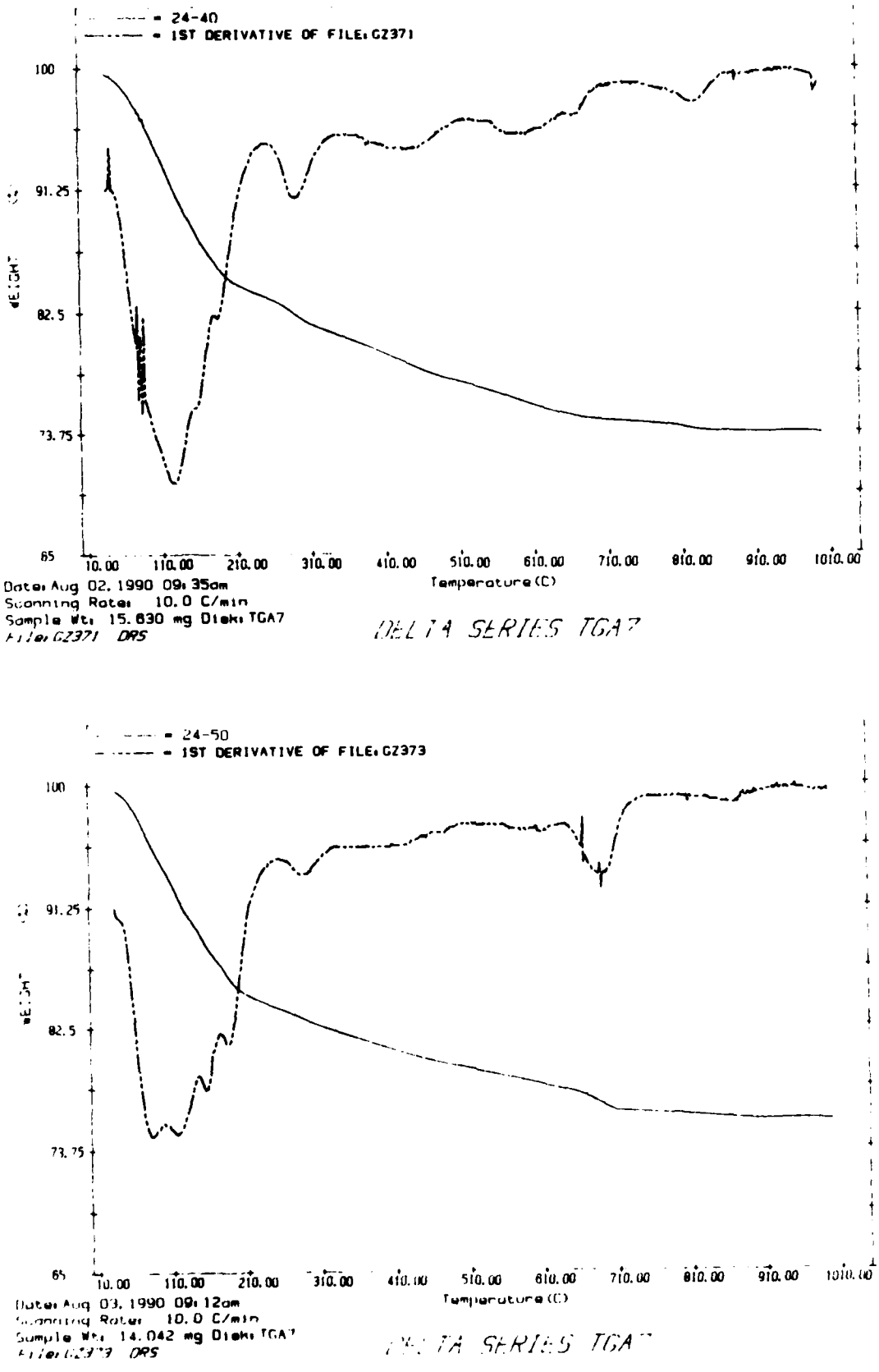

Figure 19. TGA and first derivative curves of Ca-rich C-S-H (upper) and Si-rich C-S-H (lower) occurring along the 20 wt. % isoalumina join.

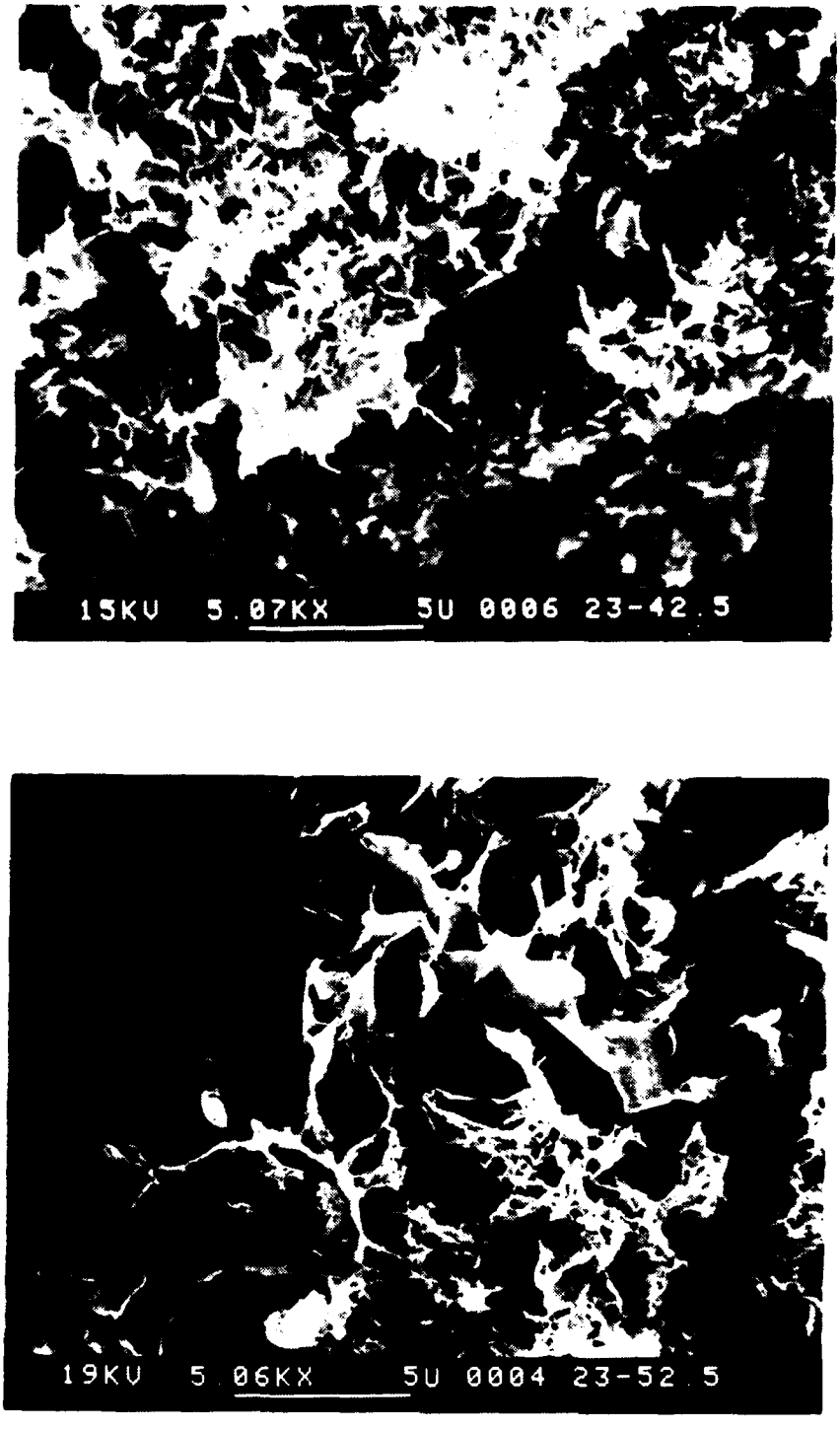

Figure 20. Typical SEM photomicrographs of Ca-rich C-S-H (upper) and Si-rich C-S-H (lower), with 10 wt. % Al_2O_3.

Electron Microscopy

The suggestion that two C-S-H gels exist can be confirmed by microstructural evidence given in Figure 20. Shown in this figure are typical SEM micrographs of the 10 wt. % Al_2O_3 samples studied above. The upper photo is typical of the more lime rich C-S-H. The lower photo represents the more silica rich C-S-H. As can be seen readily, the more silica rich C-S-H contains much larger foil like structure.

Shown in Figure 21 are SEM micrographs of the 20 wt. % Al_2O_3 samples. The upper photos represents the more lime rich C-S-H. There are crystals of hydrogarnet on the upper portion of the micrograph. In addition, large amount of plate like strätlingite can be seen growing out of a large grain of amorphous Al_2O_3. One can also see large areas of C-S-H gel surrounding the grain. Similarly, the micrograph of the more silica rich mixture contains large amount of strätlingite and reticulated gel-like C-S-H. In both cases the microstructure of the C-S-H appears similar, much more foil like, similar to the Figure 20 bottom silica rich C-S-H.

Figure 22 depicts the microstructure of the 30 wt. % Al_2O_3 containing mixtures. The upper photo is of an alkali free sample (C, Figure 6). In this instance large amounts of a hexagonal plate-like material is seen to coexist with reticulated C-S-H. This may be the strätlingite identified by x-ray diffraction (C, Figure 9). The sample made with NaOH (lower photo) has a radically different microstructure. The photo is dominated by prismatic crystals and gel-like masses. The prismatic crystals are probably the ones identified as being zeolitic in the accompanying x-ray patterns (C, Figure 10).

Discussion

Calcium silicate hydrate is the major cementing phase found in cementitious materials and thus the understanding of its structure is important if we are to utilize the properties of cement related products to their fullest. We have focused our efforts on investigating the structure of C-S-H gels using a variety of methods. However, C-S-H gels are x-ray amorphous, and thus common diffraction methods cannot be used to study their atomic structure. We have found that

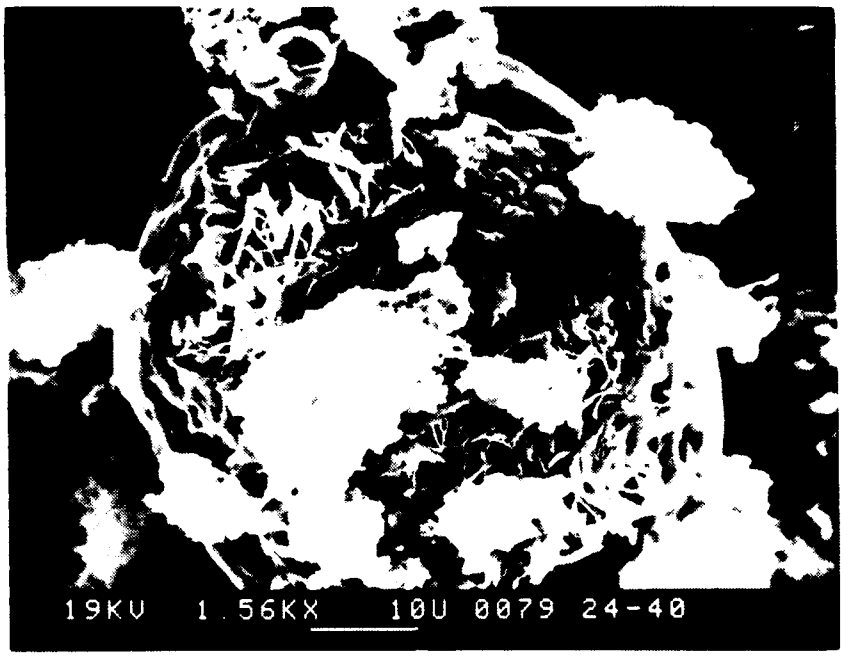

Figure 21. Typical SEM photomicrographs of Ca-rich C-S-H (upper) and Si-rich C-S-H (lower) with 20 wt. % Al_2O_3.

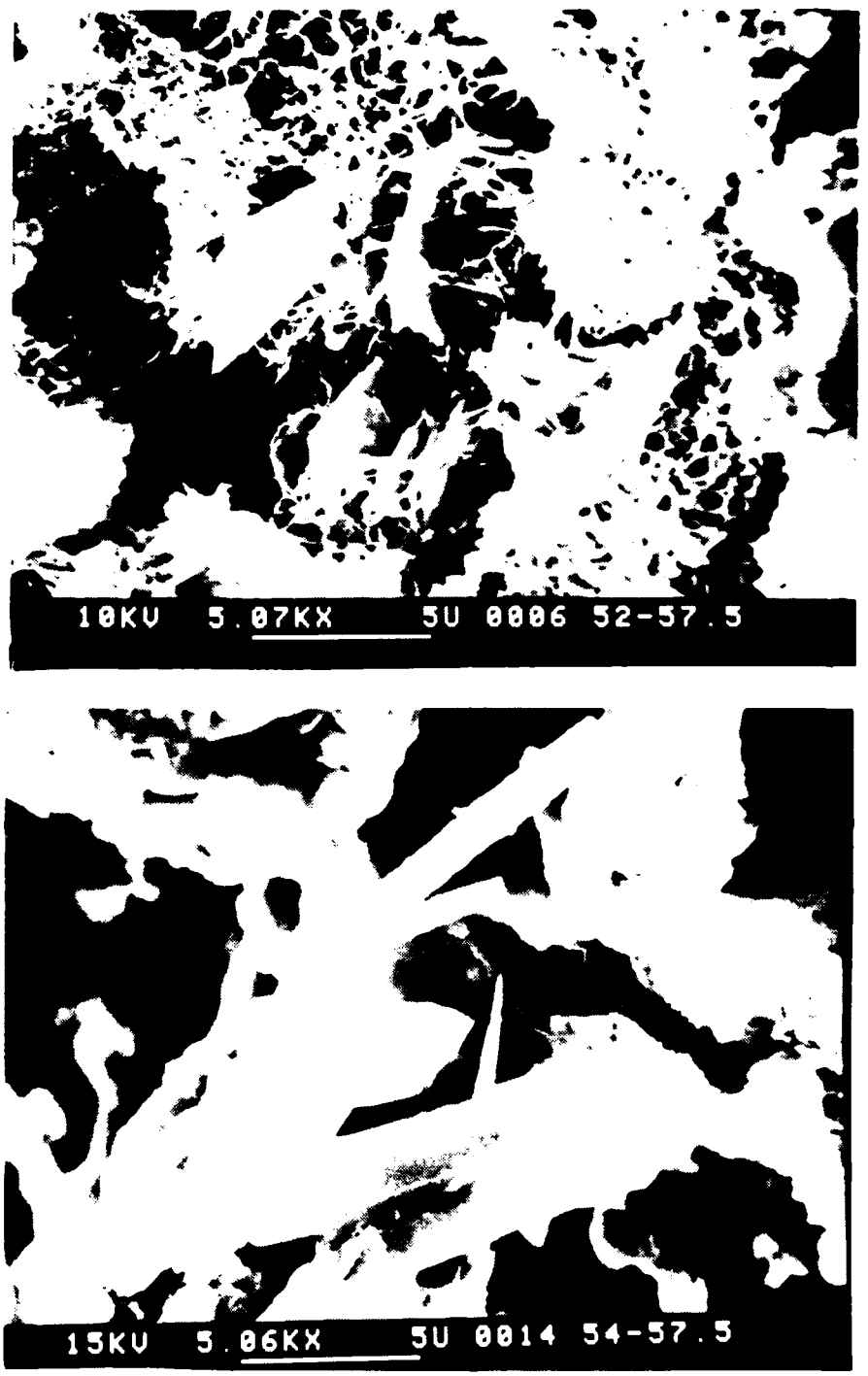

No Alkali

With Alkali

Figure 22. SEM photomicrographs of a silica-rich mixture (57.5/70) occurring along the 30 wt. % isoalumina join. Differences in microstructure reflect the effects of alkali content of the mixture.

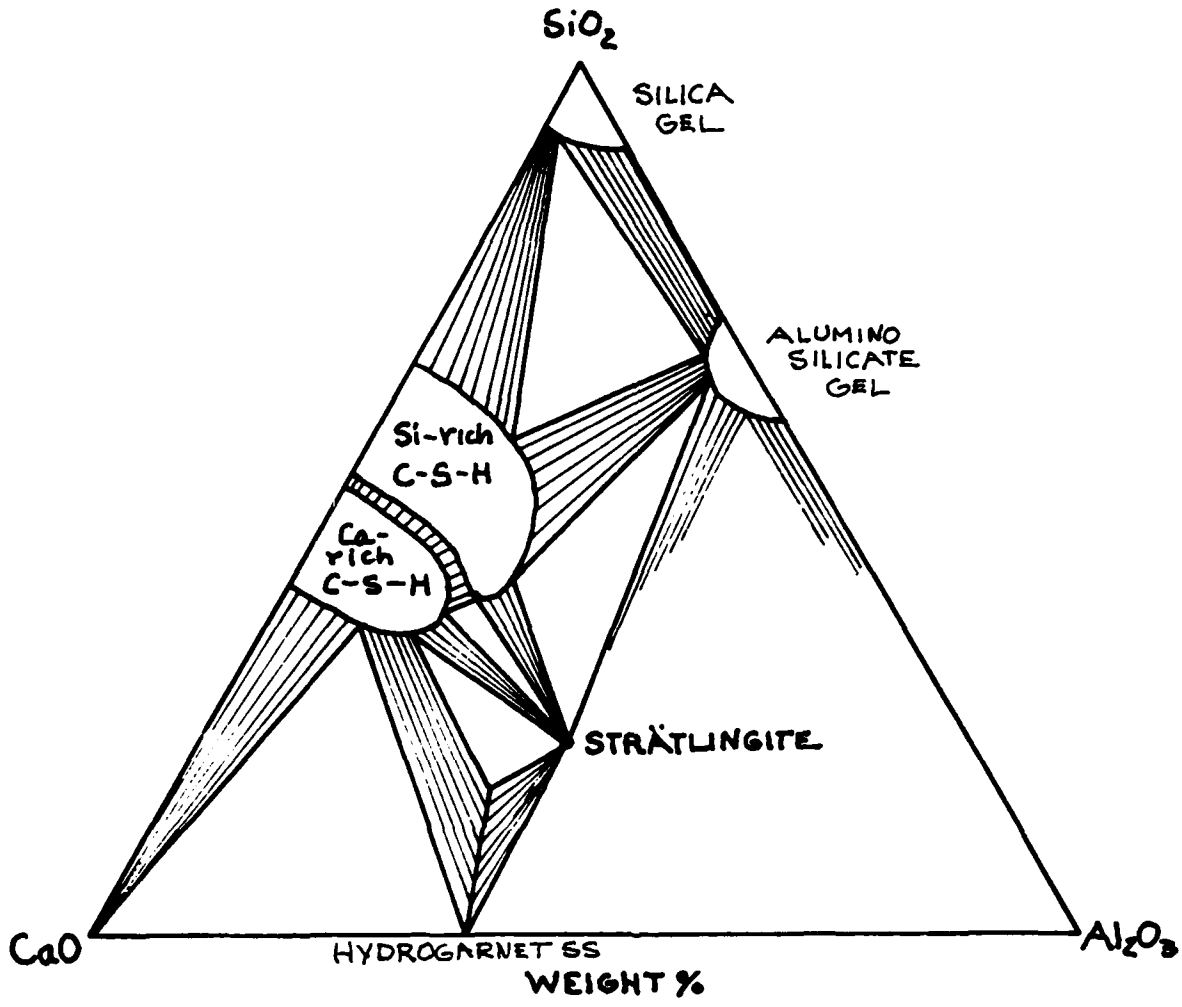

Figure 23. An internally consistent and somewhat schematic phase diagram constructed from the experimental data given earlier.

using phase equilibrium techniques as well as magic angle spinning NMR and associated supporting characterization methods, one can begin to map out the phase diagram of the system $CaO-Al_2O_3-SiO_2-H_2O$ (Figure 23) and thus gain an increased understanding of this system.

Part II. Kinetic Studies

Introduction

Work by Ramachandran (7) and Grutzeck and Ramachandran (8), which dealt with the evolution of microstructure and solution chemistry during the hydration of tricalcium silicate (Ca_3SiO_5-C_3S) at fixed pH, led them to conclude that two distinct C-S-H phases could exist, and that a potential phase change between the two could occur at pH 11.5. Although this suggestion was based upon an overwhelming amount of microstructural data and solution analyses, it was never actually demonstrated that the phases were distinctly different. The work reported in the following paragraphs is meant to addresses this shortcoming.

Experimental Procedures

A computer controlled pH stat, consisting of an IBM clone equipped with a data acquisition and controller board (MetraByte Corp.), Orion pH meter and Ross electrode, and a Sage syringe pump, was used to record pH of the solutions and also add HCL or NaOH in order to keep the pH at preselected levels. Temperature was kept at 25°C by a Haake circulating water both. The circulating water was used to drive a water driven magnetic stirrer immersed in the water bath. Hydration reactions were carried out in one liter wide mouth high density polyethylene bottles immersed in the water bath and placed on top of the stirrer. The lids of the bottles had three holes in them to accept the pH electrode, the syringe pump acid/base dispensing tube, and a stream of CO_2 free N_2 gas (to prevent carbonation by CO_2 in the air).

Ramachandran's original experiments (7) were repeated. However, in this instance three grams of C_3S were added to ~750 ml of freshly boiled deionized water and allowed to equilibrate at pH 11, 11.5, and 12. Because the introduction of C_3S to the solution causes the pH to rise

dramatically (~12), initial pH were adjusted manually for 3-8 minutes using a dropper filled with reagent grade HCL. Thereafter, dilute HCL was added automatically as the need arose. The IBM clone was used to measure a pH value every 5 seconds. Data were logged to a floppy disk every 60 seconds. The controller board was connected to a syringe pump filled with 0.25N HCl. The board controls the introduction of acid by comparing the pH value to a user defined value. The reaction was allowed to proceed for 3 days by which time the reaction of C_3S had more or less subsided. Figure 24 is a calorimetric plot of C_3S hydrated with deionized water. As can be seen from the plot, the rate of reaction reaches a maximum at about 8-10 hours and then slowly decreases. After 3 days of hydration, the pH meter was calibrated again to check for drift, which was minimal. Finally, the resultant mixture was removed from the wall and bottom of the bottle, filtered, and freeze dried to quench the reaction. These samples were analyzed as described in later sections. A pH 13 run was attempted using ~1.5N NaOH solution. However, what actually happened was that the basic character of the solution caused the pH electrode to drift downward, causing the pH stat to add more base than actually was needed. Although pH 13 was targeted, the actual pH may have been higher than 13.5. This experiment was discarded and repeated using a slightly different procedure. In this experiment, periodic measurements of the solution pH were made immediately after calibration of the electrode. Computer control was maintained, but between measurements (initially every few minutes, later every few hours), the electrode was removed from solution and the syringe pump was shut off. The pH of the solution was raised to $\geq$13 using 0.25N NaOH. Measurements showed that pH never dropped below 13. A final experiment, with no pH control was run as a comparison.

After freeze drying the hydrated C_3S powders, they were characterized using X-ray diffraction, ^{29}Si magic angle spinning nuclear magnetic resonance spectroscopy, thermogravimetric analysis and electron microscopy.

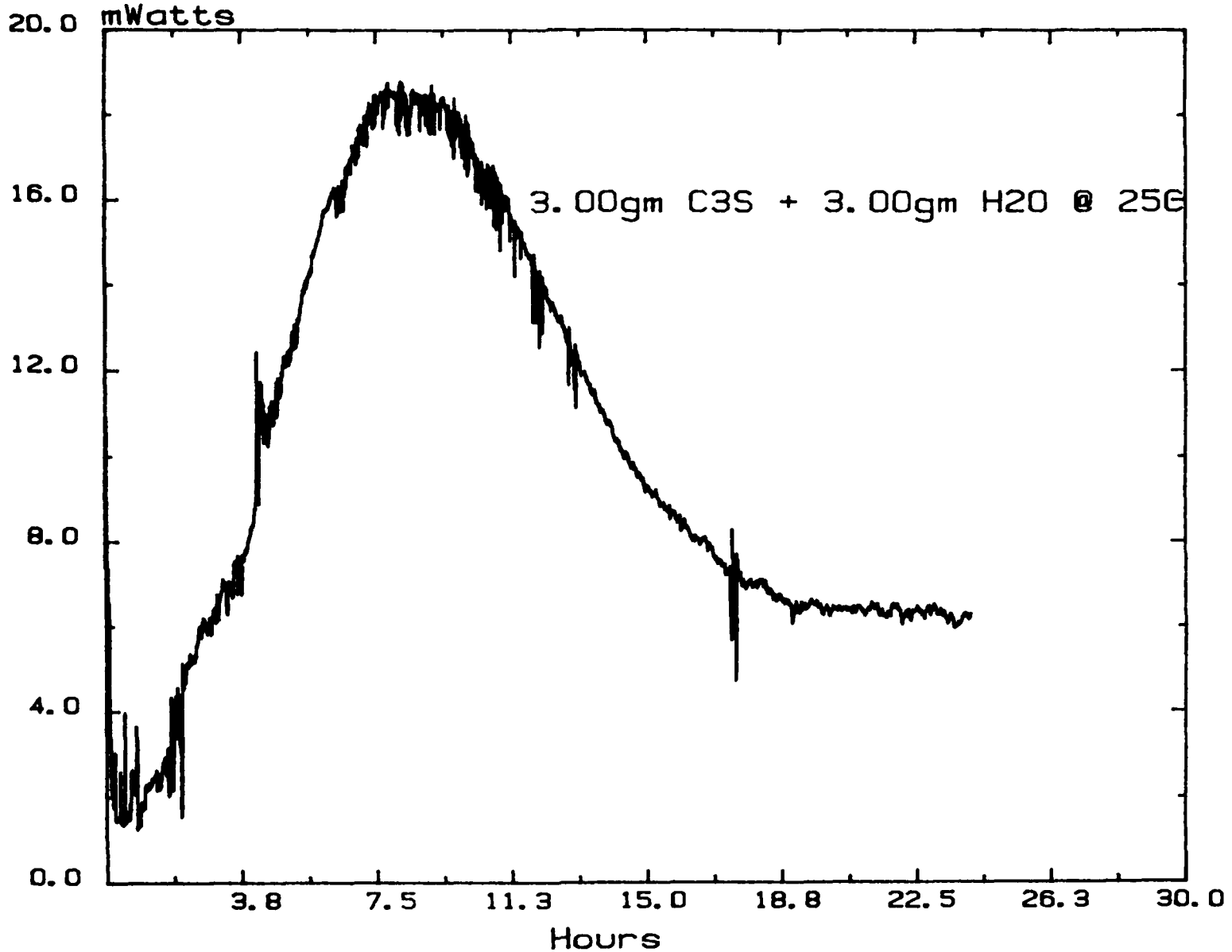

Figure 24. Isothermal calorimeter plot of C_3S hydrated in deionized water at 25°C. No pH control was attempted.

Results

X-ray diffraction. After 2-3 days the rate of acid/base additions tended to slow-all C_3S particles were found to be coated with thick rims of hydration products. Figure 25 is a x-ray pattern of the starting C_3S material. X-ray diffraction patterns of the C_3S hydrated for 3 days at pH 11, 11.5, 12, floating, and >13 at 25°C are given in Figure 26. Several distinctive features can be seen. As can be expected, the patterns of the pH float and pH 12 experiments are very nearly identical since the C_3S hydration with no pH control resulted in a final pH value very close to 12. The patterns for C_3S hydrated at pH 11, 12 and float are also very similar in that they all have peaks from the unreacted C_3S and very small peaks from $Ca(OH)_2$. During hydration of C_3S, the hydration process is controlled by diffusion. As C-S-H is formed on the outer surface of the C_3S grains, the thickening layers of hydrate hinder the hydration process. For some reason, the 11 and 11.5 runs exhibit a greater degree of hydration than the 12 or float samples.

However, the pattern from pH>13 is very much different from the others. The pH>13 samples exhibits large peaks from $Ca(OH)_2$, proportionally much smaller peaks from C_3S (even more reaction) and additional peaks from a yet unidentified phase(s) presumably resulting from the Na^+ ions added as NaOH.

^{29}Si magic angle spinning angle NMR spectroscopy. Given in Figure 27 is the ^{29}Si MASNMR spectrum of the pH 11 sample. There are two major peaks at ~-74 ppm and ~-85 ppm resulting from monomeric SiO_4 tetrahedra (Q_0) and silica chains (Q_2) respectively. These findings are similar to those obtained in previously described equilibrium solution/sol mixing experiments except for the presence of the Q_0 peak from the unreacted C_3S. This suggests that the silicate monomers present in C_3S combine with water to form long silicate chains when C_3S reacts with water at a pH of 11. Monomers were not observed in previous experiments because none were present in the starting materials (colloidal silica and lime).

On the other hand, the NMR spectrum of the pH 11.5 sample (Figure 28) shows peaks from Q_1 (dimers) at ~-80 ppm and chains (Q_2) at ~-86 ppm and no monomers (Q_0). This suggests that during hydration at pH 11.5 all of the C_3S has taken part in the hydration reaction

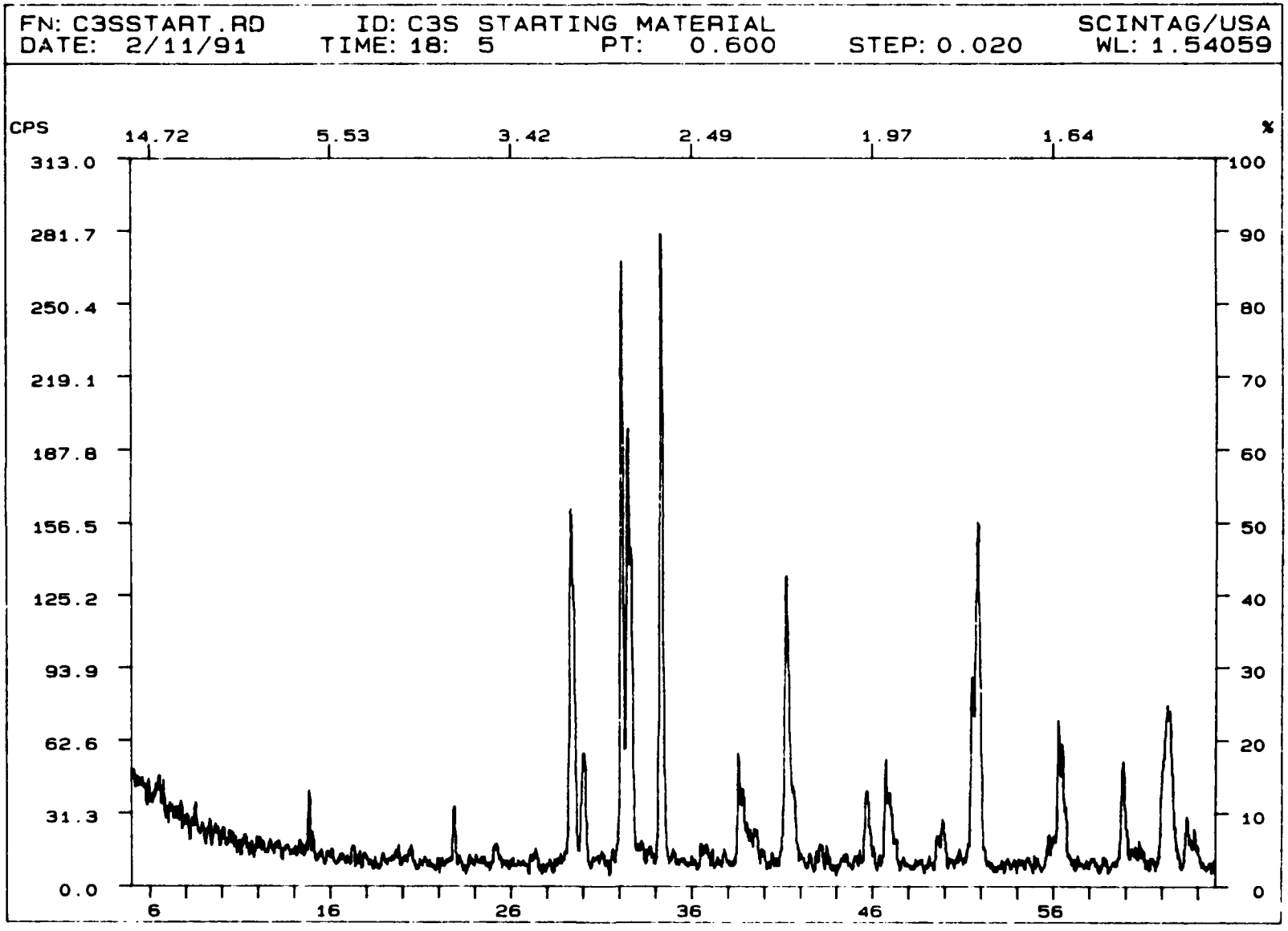

Figure 25. X-ray diffraction pattern of starting material C_3S.

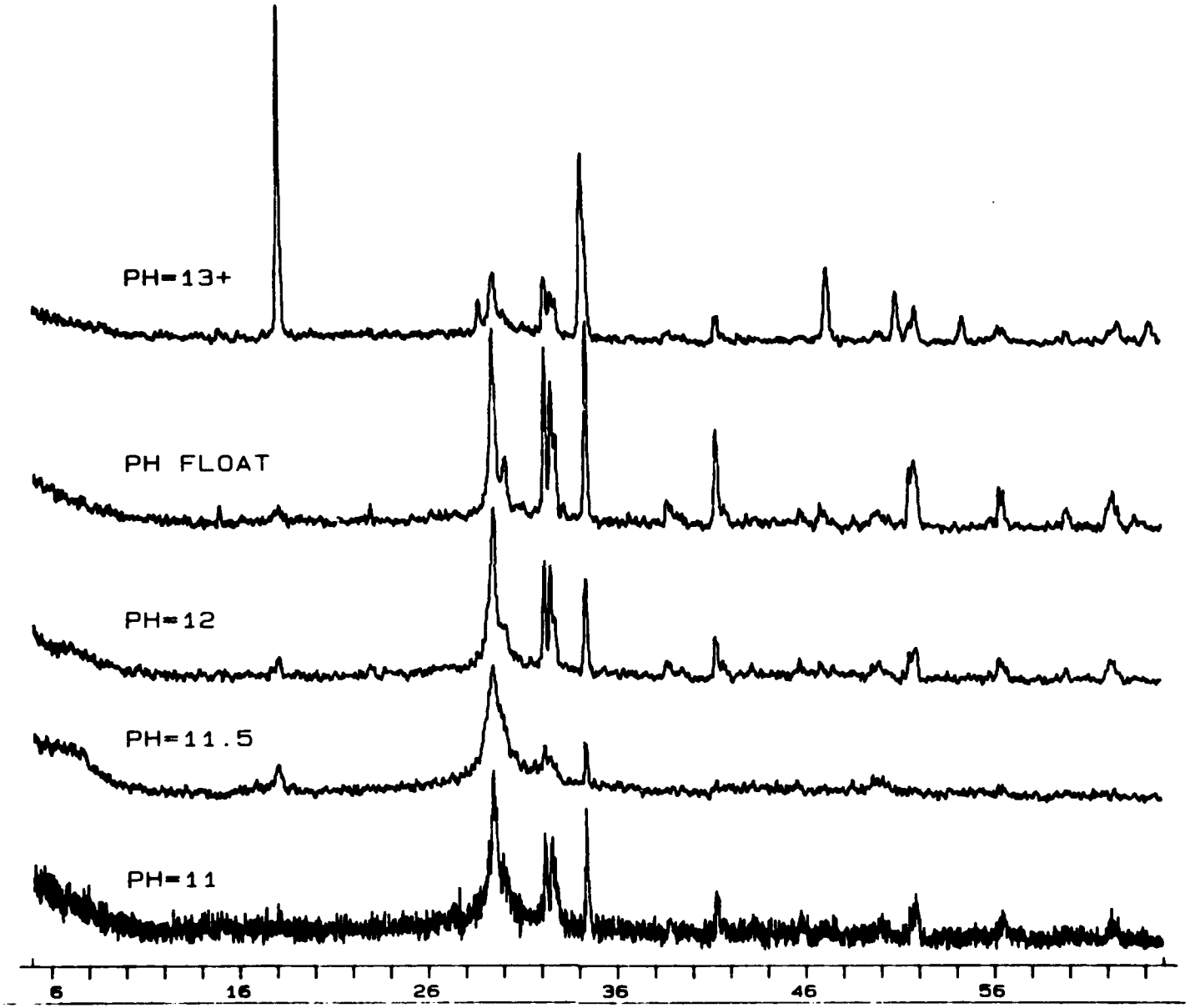

Figure 26. X-ray diffraction patterns of C_3S hydrated for 3 days at 25°C as a function of pH.

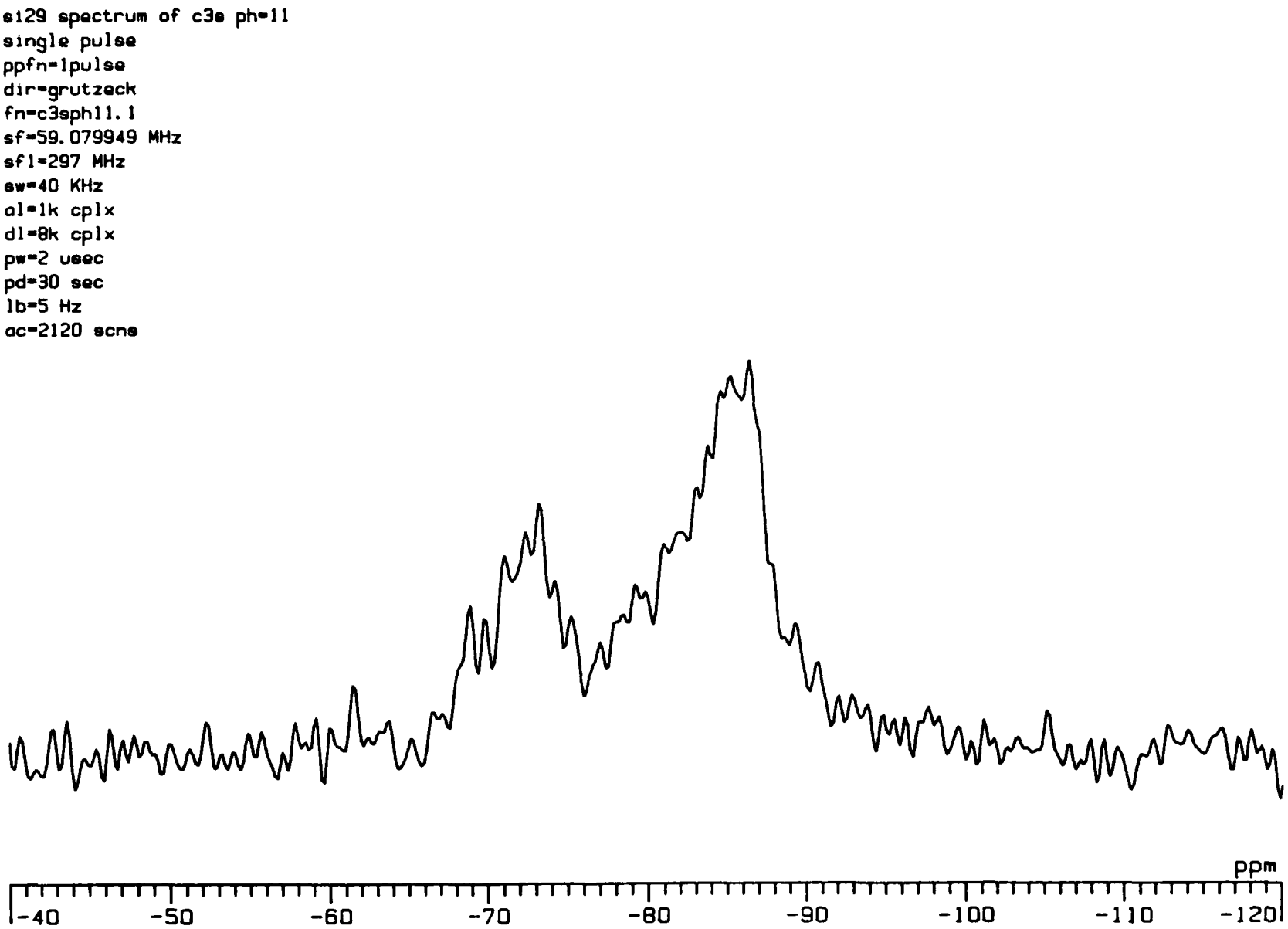

Figure 27. ^{29}Si MAS NMR spectrum of C_3S hydrated at pH 11.

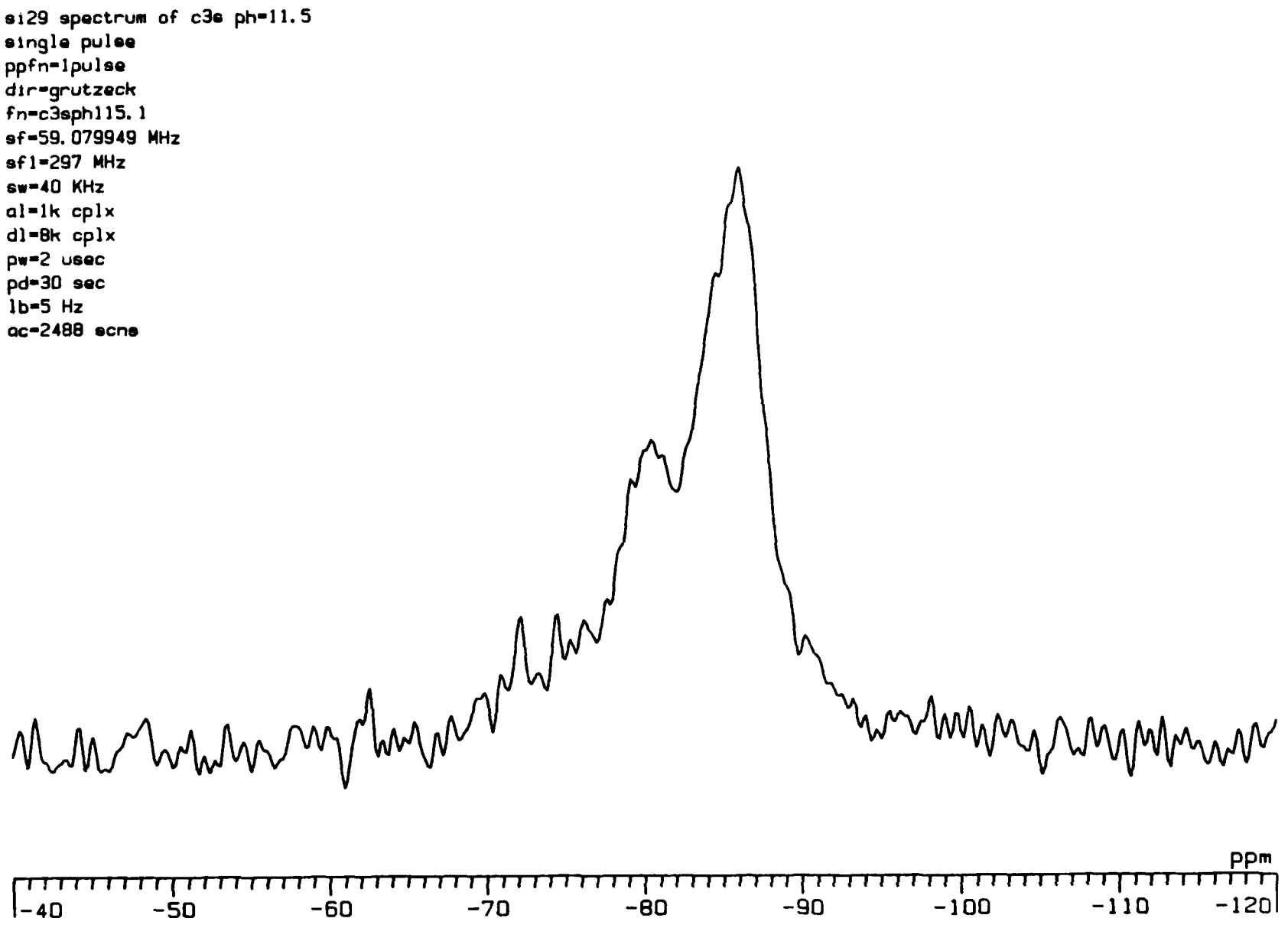

Figure 28. ^{29}Si MAS NMR spectrum of C_3S hydrated at pH 11.5.

(rates of hydration are faster-all monomers have been exhausted) and that dimers are formed in addition to chains.

Figure 29 shows the NMR spectrum of the samples that was hydrated at pH 12. Here we see that all three species, monomers (Q_0) from C_3S, dimers (Q_1) and chains (Q_2), are present. Comparing this data to the previous two spectra, one can see a trend developing which is similar to that observed in solution/sol mixing experiments using colloidal silica, lime and deionized water. As the pH of the hydration reaction is increased, the structure of the calcium silicate hydrate changes from predominantly chains (Q_2) to dimers and chains (Q_1+Q_2) with a transition region in the neighborhood of ~pH 11.5. From pH vs. composition plots (Part I of this report), it can be seen that pH 11.5 falls within an area of invariancy. This implies that at pH 11.5, the system might be in a transitional zone where two C-S-H gels could exist simultaneously with a solution phase.

Figure 20 is the NMR spectrum of C_3S hydrated in deionized water without any pH adjustment (pH float). The spectrum shows a major peak corresponding to monomers and also peaks from dimers (Q_1) and chains (Q_2). The relative intensities of the Q_1 and Q_2 peaks show that there are more dimers than chains. This is similar to spectra obtained from samples using colloidal silica, lime and water. However, the relative intensities of Q_1 vs. Q_2 in the pH 11.5 and pH 12 spectra are opposite that of pH float. This is probably due to the Cl^- added as hydrochloric acid. The Cl^-, in addition to accelerating the overall reaction, as shown by the greatly diminished Q_0 peak, somehow is promoting the polymerization of silica dimers into chains. Calcium chloride is often added to cements and concretes as an accelerator. The acceleration maybe be due to the more rapid polymerization of C-S-H gels.

Figure 31 shows the resultant NMR spectrum of the C_3S hydrated in 0.25N NaOH (pH>13). The spectrum contains peaks characteristic of monomers (Q_0) and dimers (Q_1) but no appreciable amount of chains (Q_2) were observed. Q_3 and Q_4 (silica sheets and networks respectively) species were also not observed. This behavior can be traced to the fact that Na^+ was introduce into the system and Na^+ ions are known to break up the structure of silica networks.

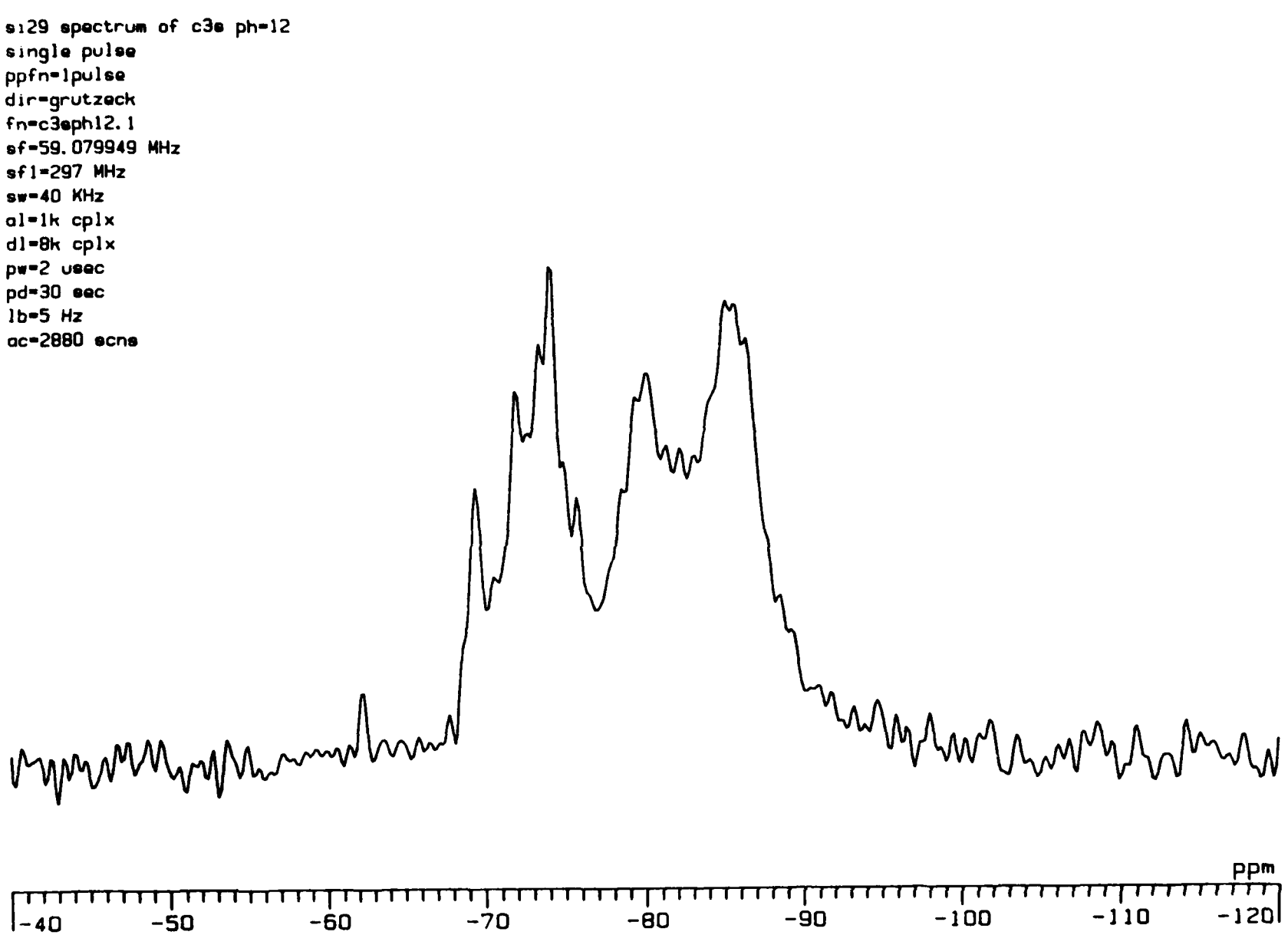

Figure 29. ^{29}Si MAS NMR spectrum of C_3S hydrated at pH 12.

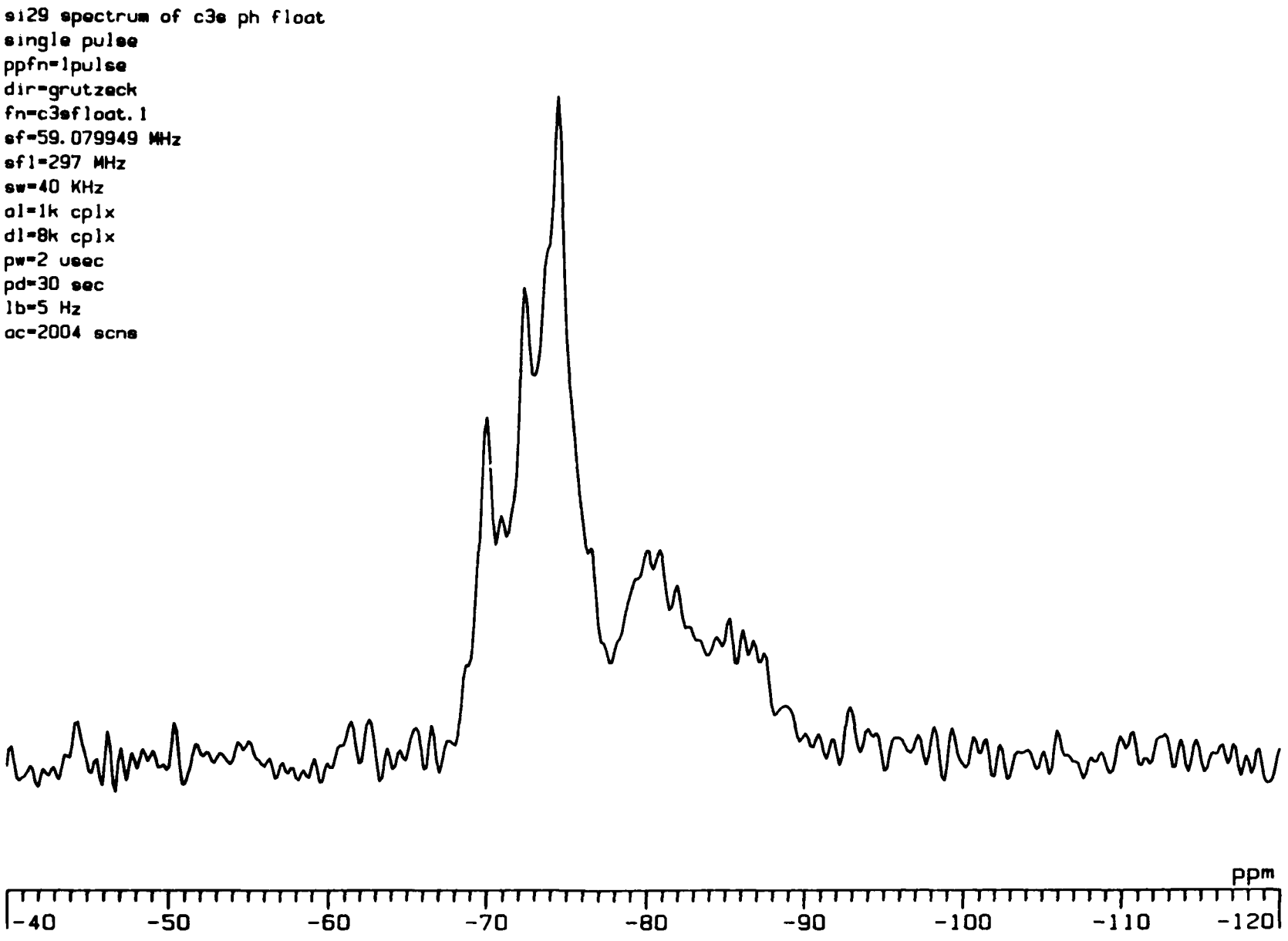

Figure 30. ^{29}Si MAS NMR spectrum of C_3S hydrated under floating pH conditions (no pH control).

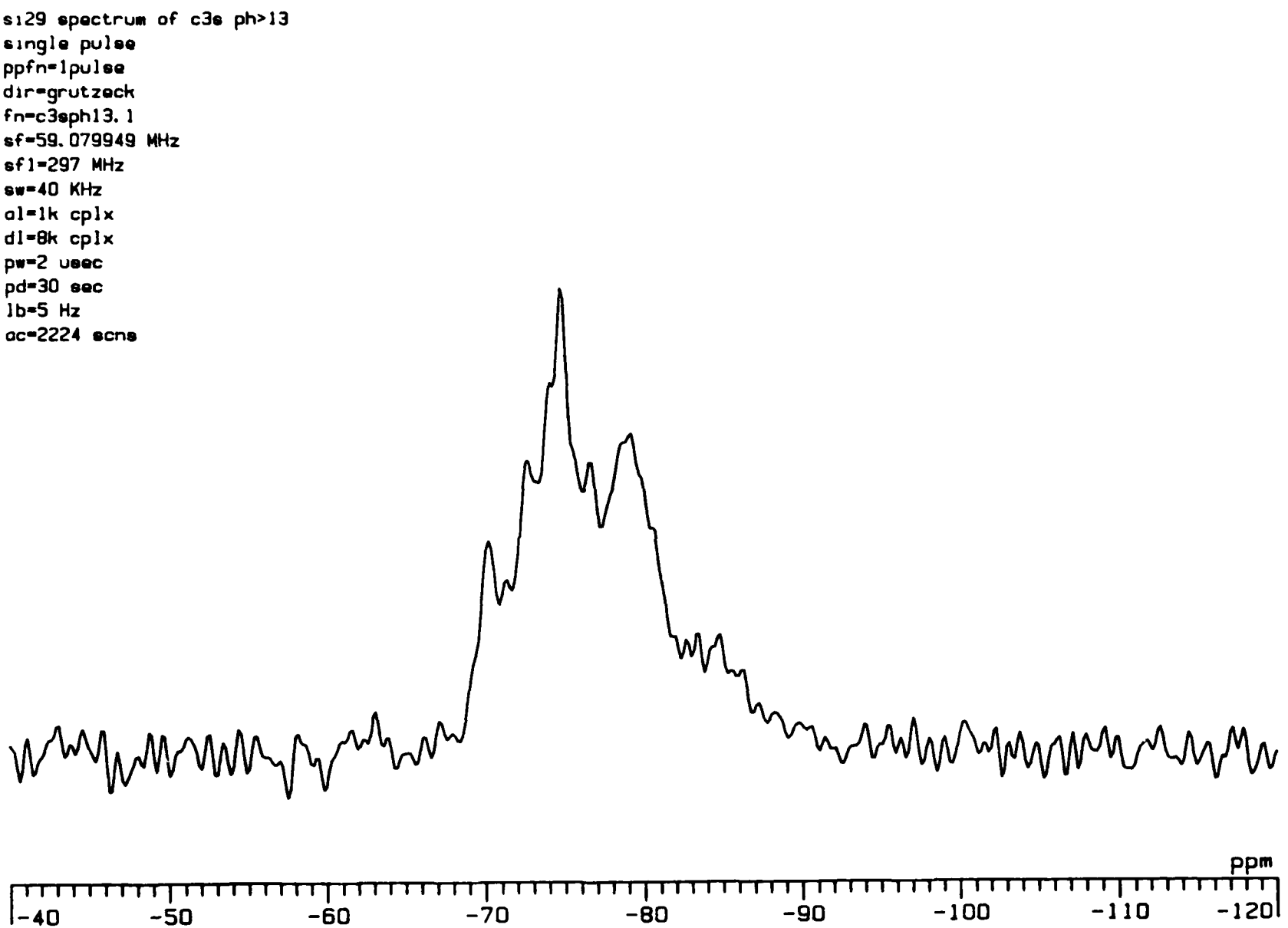

Figure 31. ^{29}Si MAS NMR spectrum of C_3S hydrated at pH ≥ 13.

Because of the high concentration of NaOH in the system, simple sodium silicate hydrates rather than calcium silicate hydrates may be forming.

Thermogravimetric Analysis. Thermogravimetric analysis was used to confirm the differences between the two C-S-H phases and the transition between them in terms of pH. In Figure 32, the TGA of the starting C_3S shows a slight weight loss due to adsorbed free water (a small loss at ~380°C and a slightly larger loss at ~650°C).

Figure 33 is a TGA plot of the sample hydrated at pH 11. Here it is seen that there is a fairly sizable weight loss due to free water (~100-150°C) and a larger weight loss at ~320°C. In addition, a very small weight loss was detected at ~600°C with the possible exception of the 600°C loss, none of these can be attributed to $Ca(OH)_2$.

In Figure 34 it is observed that the TGA plot of the pH 11.5 sample is significantly different from that of the pH 11 sample. Once again loosely bound water comes off at ~100-150°C. The large weight loss at 320°C is now practically non-existent. However, in its place there is a very sharp and significant weight loss at ~500°C. As will be shown later, this behavior was also observed in the TGA patterns of pH 12, float and 13. It is reasonable to assume that this is due to the decomposition of $Ca(OH)_2$ since it appears in the x-ray diffraction patterns (Figure 26) of these runs. A final difference is the disappearance of the weight loss at 600°C. An additional weight loss is now present at ~780°C.

The sample hydrated at pH 12 (Figure 35) exhibits two weight losses. They occur at ~120°C and at 500°C. The weight loss at 500°C is very sharp and at this pH it is probably due to $Ca(OH)_2$. XRD confirms the existence of $Ca(OH)_2$. This TGA is very similar to that of Ph float given in Figure 36. It too contains only weight losses due to loosely bound water and $Ca(OH)_2$. However, companion NMR data suggest that there are differences between the two hydrates in terms of the relative amounts of silicate chains (Q_2) and dimers (Q_1) present in the samples. The amount of weight loss by the pH 12 samples is smaller than that of the pH float. This was also shown in the NMR spectra by the intensities of the Q_0 peak. The sample with the smaller monomer peak (pH 12) had a larger weight loss. The pH 12 sample appeared to have been

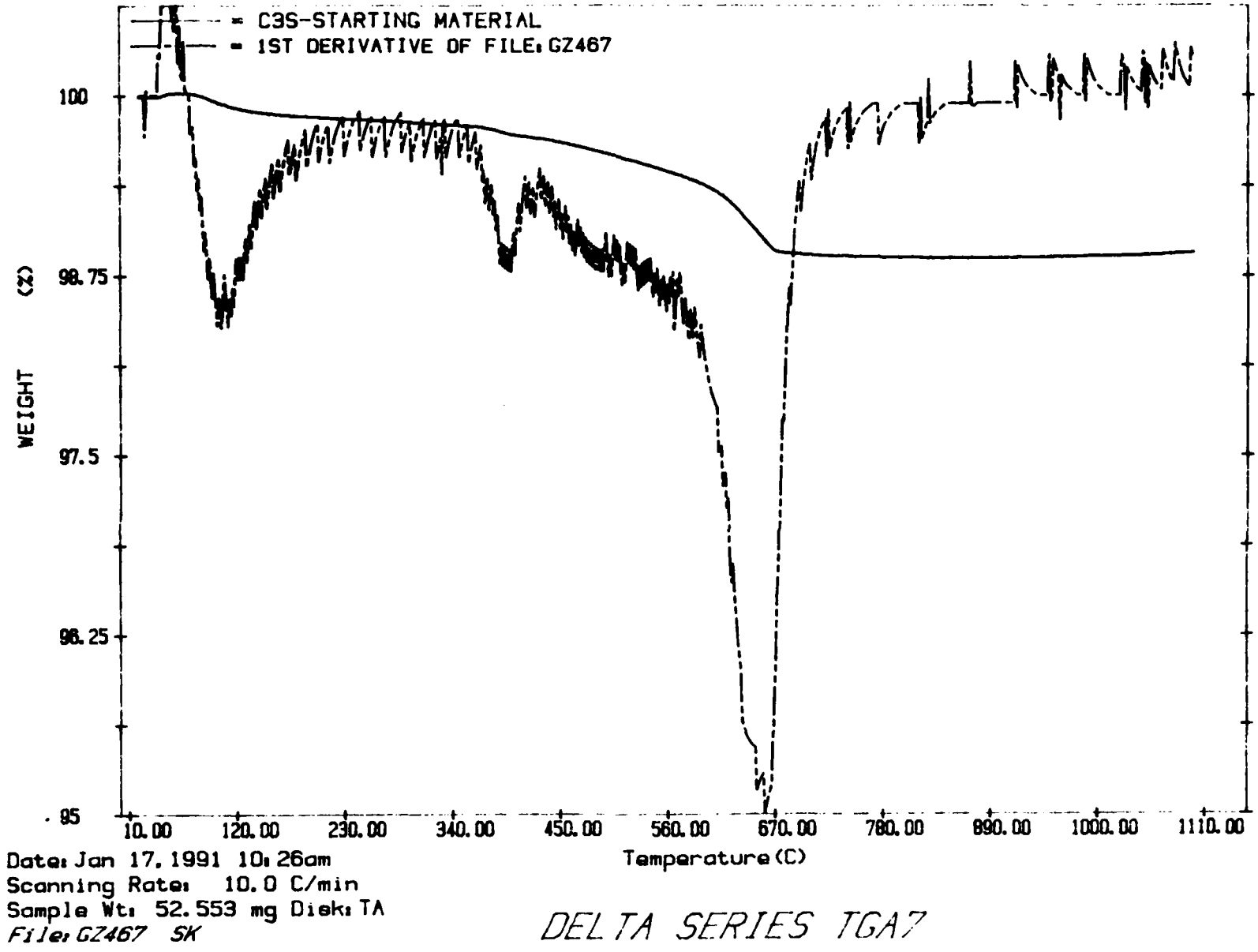

Figure 32. TGA plot of C_3S starting material.

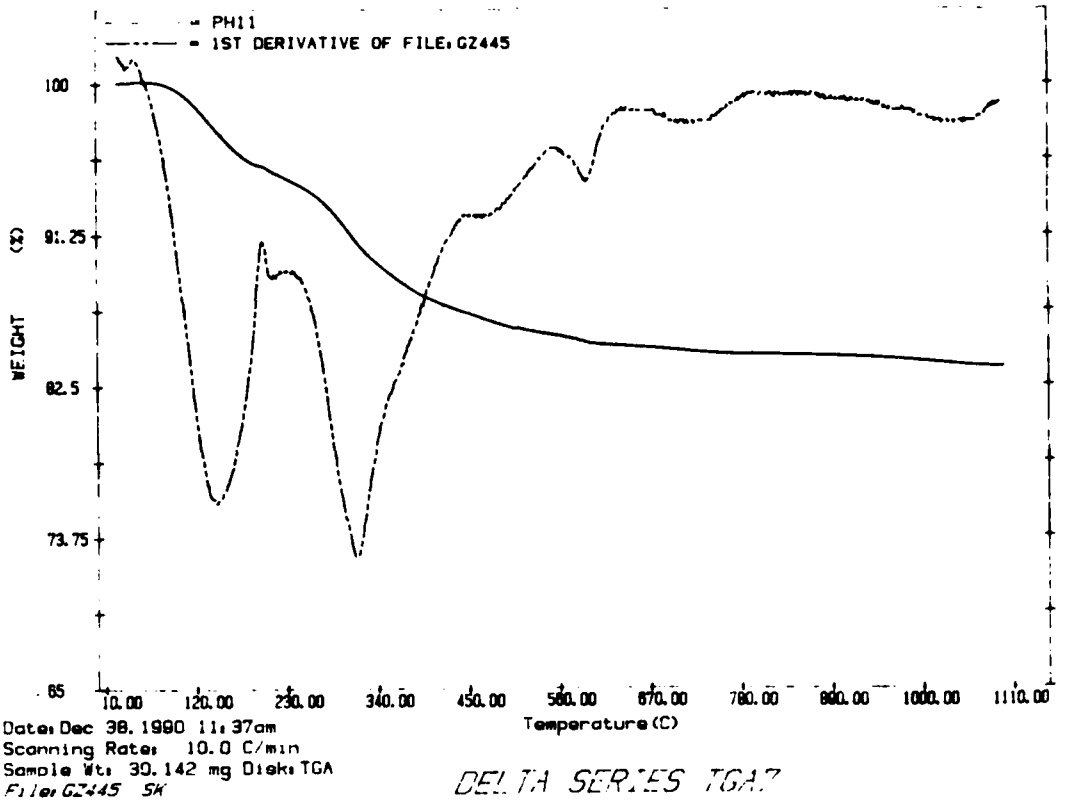

Figure 33. TGA and first derivative curves of C_3S hydrated at 25°C and pH 11 for 3 days.

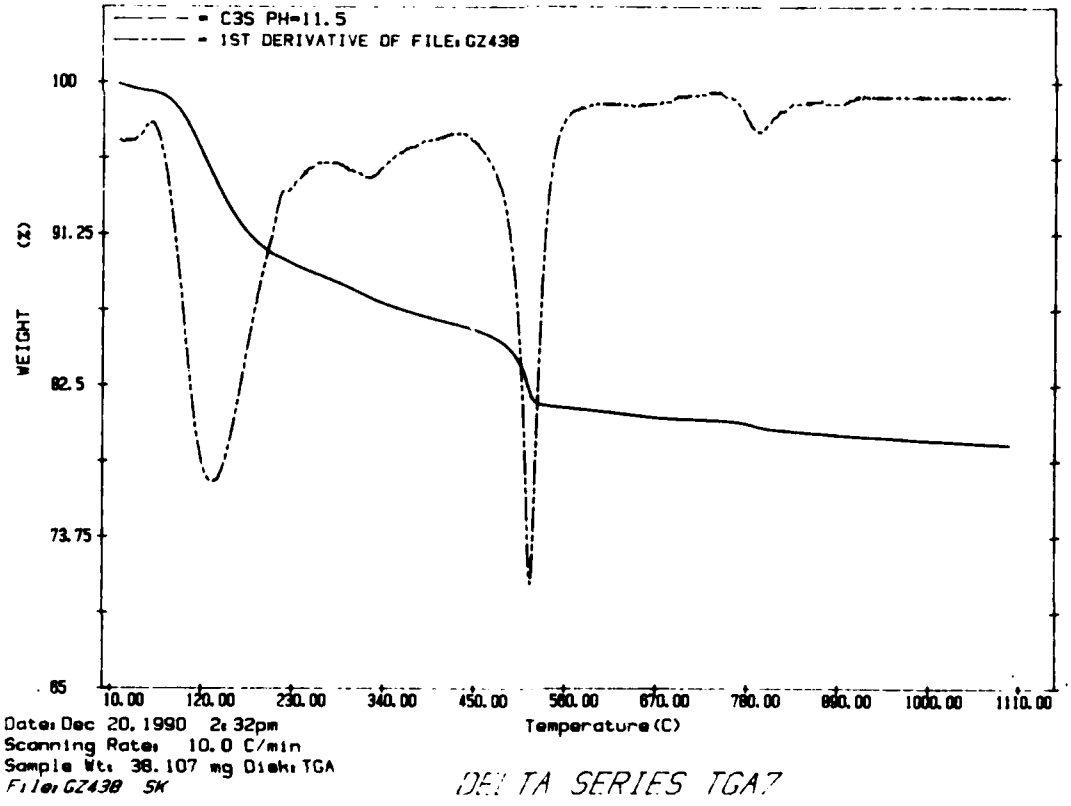

Figure 34. TGA and first derivative curves of C_3S hydrated at 25°C and pH 11.5 for 3 days.

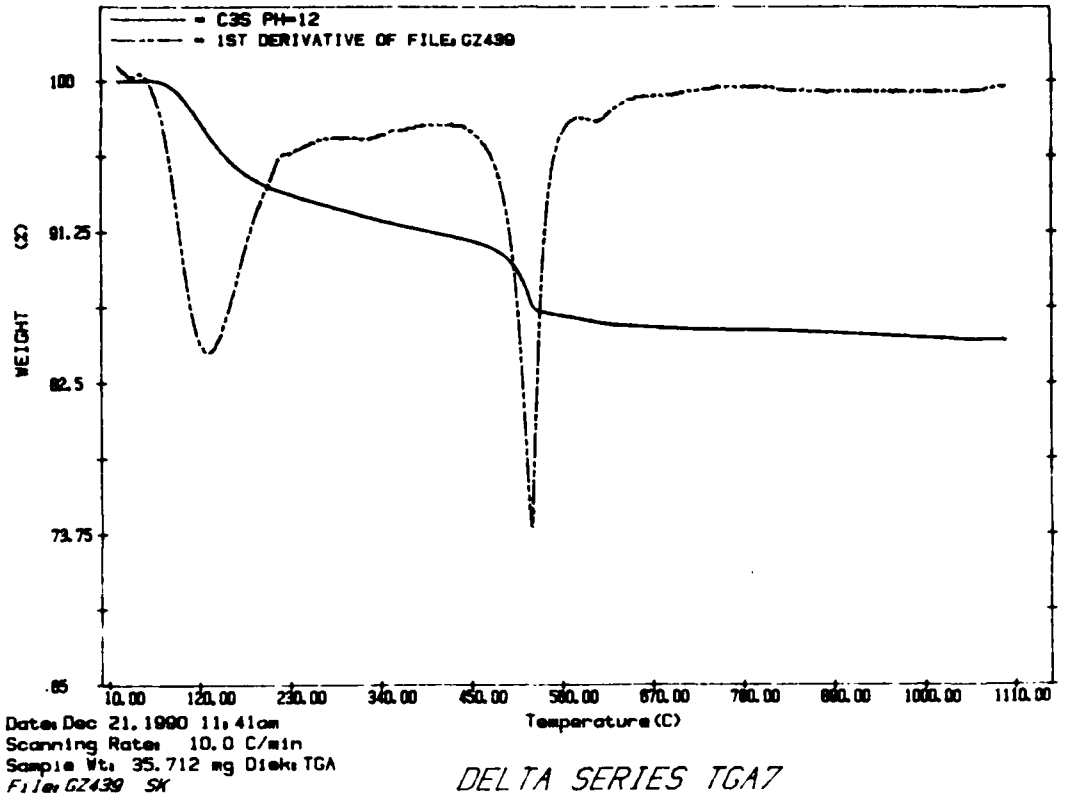

Figure 35. TGA and first derivative curves of C3S hydrated at 25°C and pH 12 for 3 days.

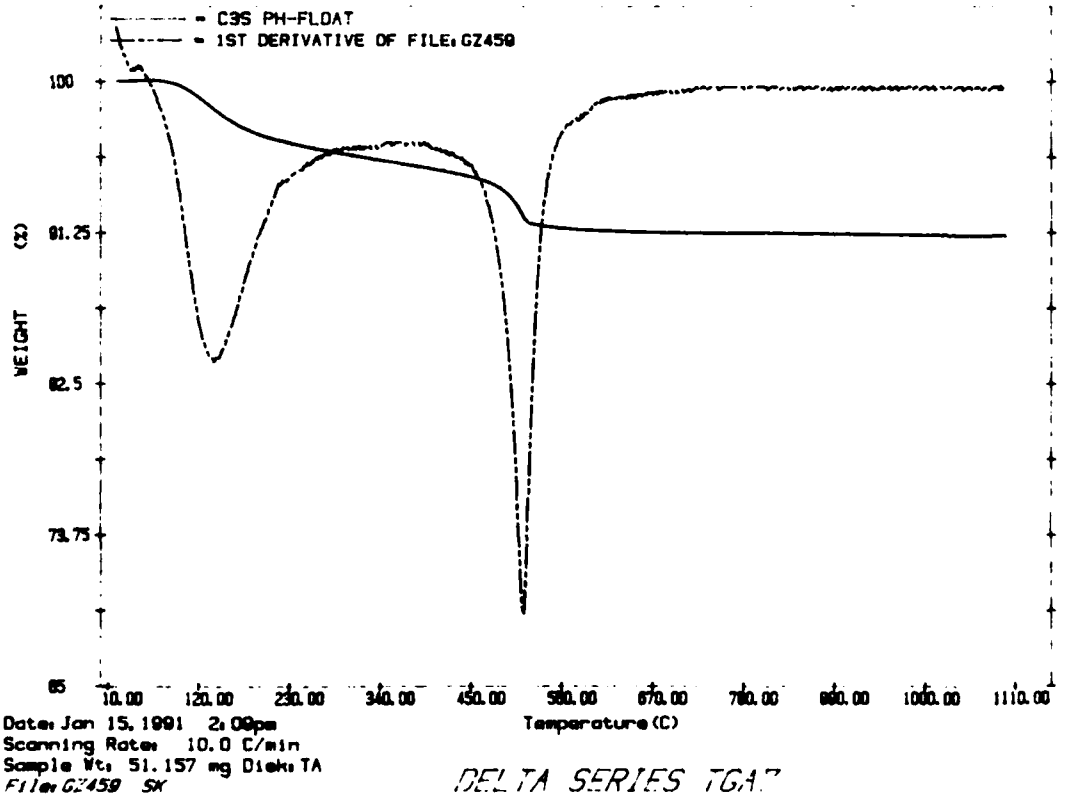

Figure 36. TGA and first derivative curves of C3S hydrated at 25°C under floating pH conditions (no pH control).

hydrated more extensively in the same time period compared to the pH float. As discussed previously, this may be due to the Cl^- added to the system.

The TGA plot of the pH>13 sample is given in Figure 37. The weight loss corresponding to the loss of water at 100°-150°C and decomposition of $Ca(OH)_2$ can be seen readily. However, there are three additional weight losses attributable to the addition of Na^+. This suggests that some of the Na^+ maybe incorporated into the structure of the lime-rich C-S-H gel or one maybe forming an entirely different gel. It is therefore safe to assume that the Na^+ incorporation may indeed be responsible for the apparent lack of silica chains, sheets and networks (Q_2, Q_3, Q_4), as shown by NMR, by breaking the bridging oxygens.

Discussion

The data apparently confirm Ramachandran and Grutzeck's suspected C-S-H phase change. Major differences are observed in the x-ray diffraction patterns, MASNMR spectra, and TGA dehydration curves of C_3S hydrated at pH 11 and 11.5. Earlier structural differences established in Section I of this report, tend to apply to the kinetic system as well. There is a distinct difference in the structure of the C-S-H formed at pH 11 (Q_2 only) versus that formed at pH 11.5 (Q_1, Q_2).

A second interesting observation concerns the apparent acceleration of the hydration of C_3S as progressively larger amounts of HCl were added tot eh solution. If one compares Figure 30 (floating pH ~12) with Figures 29 (pH 12) and 28 (pH 11.5), one is struck by the fact that monomer peaks (Q_0) due to the C_3S decreases while Q_1, Q_2 hydrate peaks increase. Unfortunately, the trend does not continue to the pH 11 samples, but then the Q_2 C-S-H has a different structure, perhaps not as susceptible to these effects.

At least for the (Q_1+Q_2 C-S-H, the data seem to suggest that the indirect formation of $CaCl_2$ in solution is in some way related to the observed acceleration. This finding leads us to speculate as to the cause of the $CaCl_2$ acceleratory effect observed in cement. By adding $CaCl_2$ to

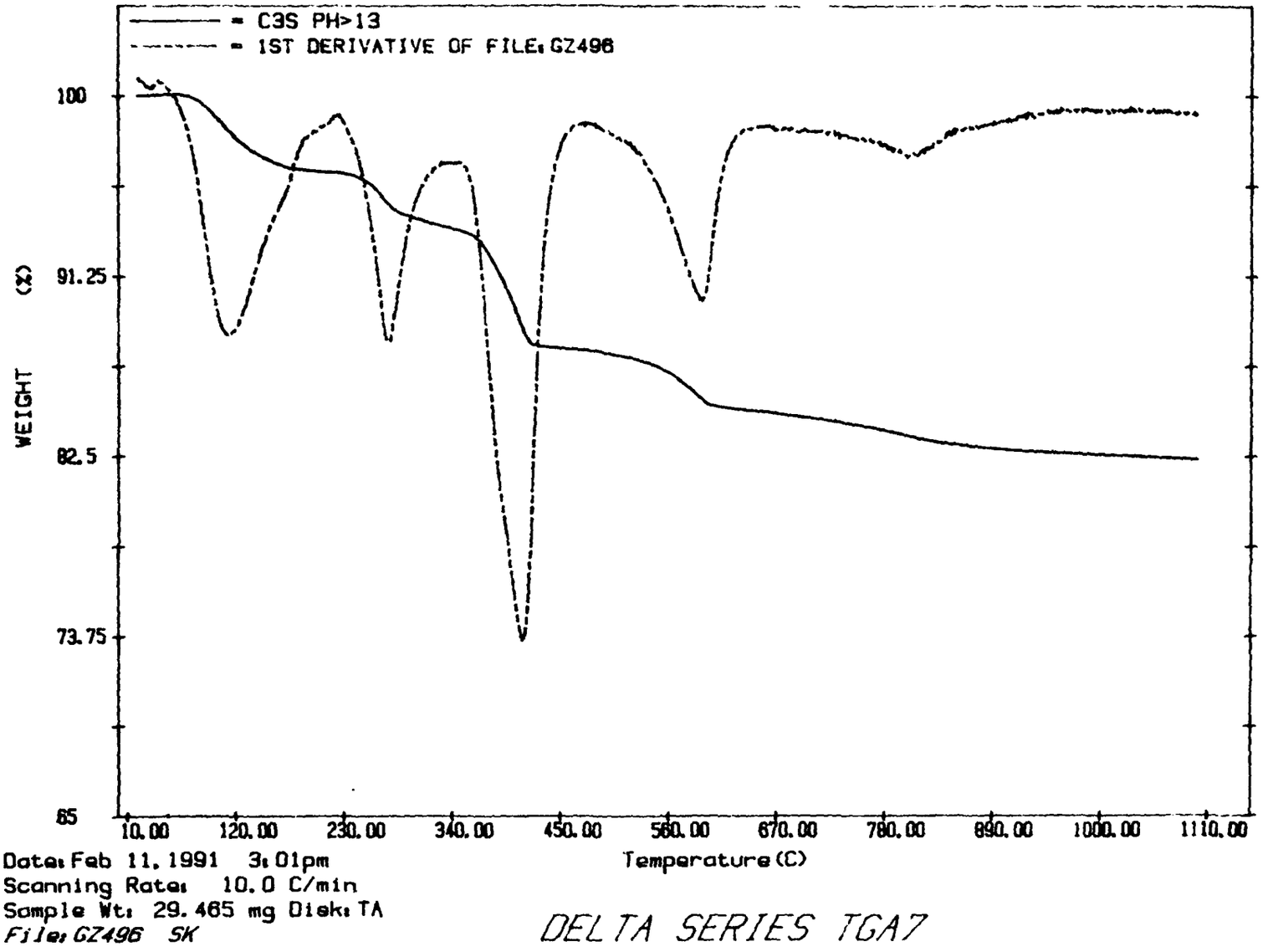

Figure 37. TGA and first derivative curves of C_3S hydrated at 25°C and pH ≥ 13.

cement, the OH^- concentrations may be suppressed enough so that rates of reaction are enhanced by the more acidic character of the solution.

Finally, the reaction of C_3S in pH>13 solution, which contains no chains (Q_2) but only dimers (Q_1) and monomer (Q_0 possibly due to residual C_3S but more likely due to newly formed alkali silicates) raises more questions than it answered. Clearly, major amounts of $Ca(OH)_2$ are formed and C_3S peaks are depressed (Figure 26) suggesting a high degree of reaction, but the presence of Q_0 peaks is puzzling. More work is needed to resolve some of these questions.

Part III. Zeolite Synthesis

Introduction

Equilibrium data presented earlier led us to speculate that, under certain hydration scenarios (composition, alkali content, temperature), C-S-H could coexist with a cogenerated zeolite-like material. However, in order for cogeneration to occur, the mixture in question has to be enriched both in alkali and aluminosilicate content. In an ordinary portland cement (OPC) system, alkalies are provided by the alkali sulfates present in the cement. Diamond (9) reports pore solution pHs of 13.1 and 13.8 for a w/c ratio 0.4 OPC paste at 4 hours and 4 days, respectively. These values are roughly equivalent to 0.13 and 0.63M alkali hydroxide solutions. Reactions of these solutions with alkali susceptible aggregate are thought to cause the well known alkali silica reaction. In a blended cement containing pozzolanic materials such as Class F fly ash, the aluminosilicate content of the system is elevated. It is possible that the alkalies and the aluminosilicates present in the mixture could combine to form zeolite-like materials (gels and/or crystalline). For example, Hoyle and Grutzeck (10) presented SEM photographs of cogenerated Cs-containing zeolites cemented with C-S-H. If this is true, one should be able to enhance/optimize the reaction and actually capitalize on the cogeneration of zeolites cemented by C-S-H. See Figure 38 for location of most promising formulations. By proper formulation one might be able to improve zeolite size and aspect ratio and thus toughen cement-based composite materials produced in this fashion. The work reported below is divided into three parts. It summarizes experiments in two areas:

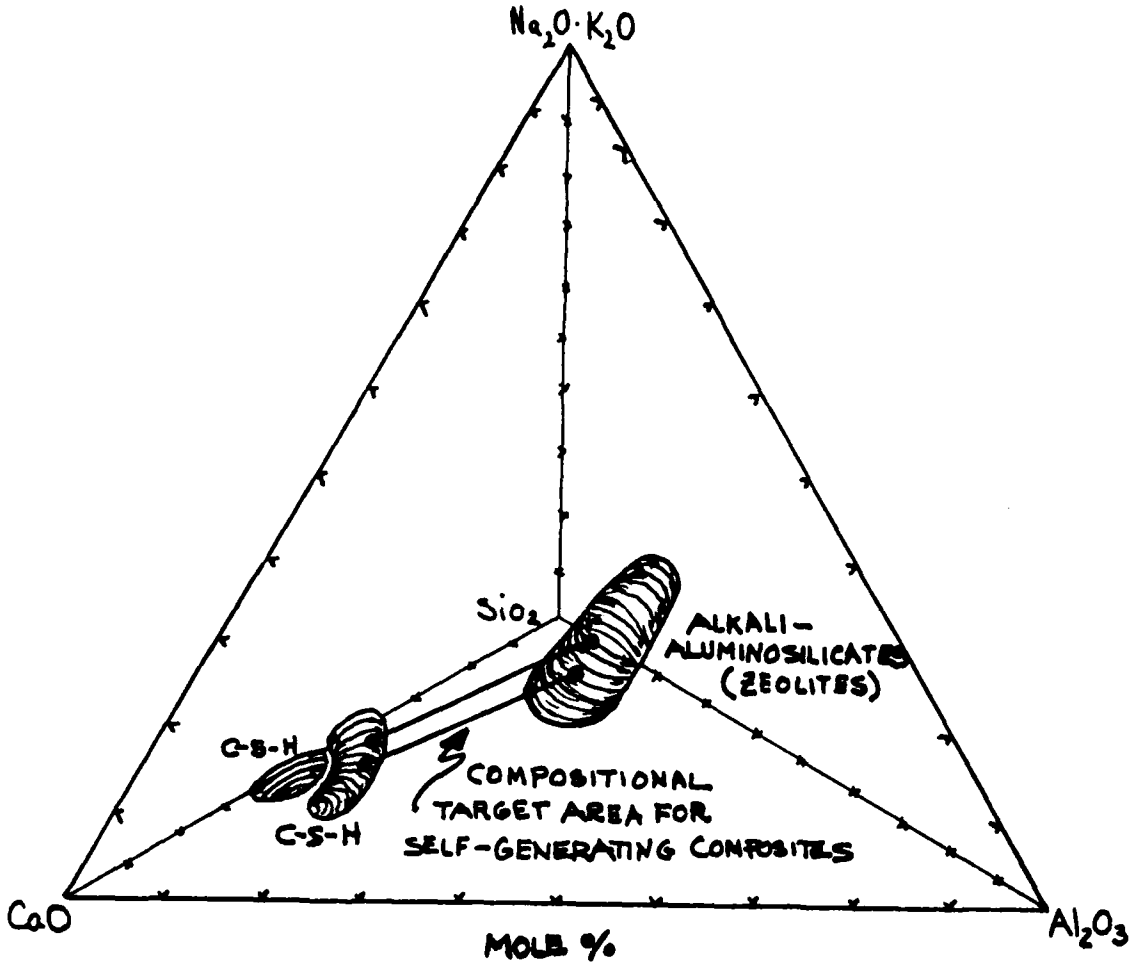

Figure 38. Schematic representation of possible phase relations in aluminosilicate enriched systems containing sufficient alkalies to simultaneously produce both zeolites and cementitious C-S-H.

synthesis of zeolites from synthetic and waste glasses (Sections 1 and 2) and preliminary attempts at producing actual zeolite-cement composite materials (Section 3).

Background

Naturally occurring zeolites and their synthetic counterparts are an extremely important class of materials. The majority of naturally occurring zeolites are alteration/hydration products of glassy volcanic ashes and rocks (11-13). As a geochemical process, the formation of zeolites takes a relatively long time. Diagenetic temperatures and pressures are relatively low and groundwater compositions fairly dilute. However, the use of hydrothermal vessels, more concentrated solutions and templating agents have shortened synthesis times to a few hours (14). For example, Ottana et al. (15) used Lipari pumice to synthesize zeolites in sodium hydroxide and sodium chloride solutions. The influence of NaCl on the degree of zeolitization as a function of NaOH concentration is discussed. Burriesci et al. (16) discussed the hydrothermal synthesis of zeolites from Sardinian perlite and Sicilian tuff in NaOH solution. They discuss the effect of the microstructure and chemical composition of the starting material, pH, NaOH concentration, reaction temperature and duration time on the zeolitization process. Faujasite-type zeolites can be synthesized from ground volcanic glass as discussed by Yoshida and Inoue (17). The yield of zeolites is affected by aging at ordinary temperatures, particle size of the glass powder, and the reaction time. After heating hydrothermally to 90°C for 24-72 hours, faujasite decreases and the species P zeolite, phillipsite and analcime are formed, respectively. Clinoptilolite was synthesized for the first time as a single phase from volcanic ash. It forms over a composition range of 2M K_2CO_3 to 2M Na_2CO_3 at 1 kbar pressure and a temperature of 145°C. A more potassium-rich solution produces phillipsite while mordenite, subordinate clinoptilolite and minor phillipsite are formed in a sodium-rich solution according to Hawkins et al. (18).

Zeolites can also be synthesized from other starting materials. Kuhl (19) used phosphates as complexing agents for a batch of metasilicate or waterglass from which phillipsite was synthesized. NaOH or KOH was added at a temperature of ~100°C. Barrier (20) obtained chabazite from Na_2O-Al_2O_3-nSiO_2 gels with the moles (n) of SiO_2 falling between 7 and 9 at

80°C and 200% excess NaOH. Fiedler et al. (21) investigated zeolite formation in the system Na_2O-Al_2O_3-SiO_2-H_2O. Zeolites were produced from highly reactive starting materials such as: aluminates, anhydrous silicic acid, fine-grained, glassy quartz wool, silica sol and added NaOH.

Although zeolite strengths are not very high, Davidovits (22) has claimed that zeolites and zeolite gels are an important ingredient in his "geopolymer" cements. Variations of his original formulation are being marketed by LoneStar Industries (Texas) under the name Pyrament. Additionally, Wu et al. (23) have shown that alkali activation of largely glassy blast-furnace slags could produce materials with compressive strengths up to 45 MPa, while Silsbee and Roy (24) have shown that alkali activation of fly ash pastes can produce bending strengths (MOR) in the 10 MPA range.

Previous Glass Hydration Work

In 1960, Locher (25) published a very interesting paper in which he discussed the various merits of different ways of activating glassy blast furnace slags. To do this he synthesized a number of glasses in the system CaO-Al_2O_3-SiO_2 and tested their reactivity as a function of time and activating agent. See Figure 39 for the location of his glass compositions. His conclusion was that certain compositional areas of the system CaO-Al_2O_3-SiO_2 produced materials with higher strength than others, but all of his glasses needed to be activated before hydration reactions could take place. This result was generally accepted by the scientific community until 1986 when MacDowell (26) of Corning Glass published his findings that calcium aluminosilicate glasses which fall in the approximate composition range 45-55% CaO, 12-26% SiO_2 and 22-40% Al_2O_3, formed hydraulic cements containing hydrogarnet and strätlingite. To some extent this compositional area overlapped Locher's (Figure 39), but by proper thermal treatment, rapid quenching and fine grinding, MacDowell was able to make his glasses react in a matter of hours without the addition of activators.

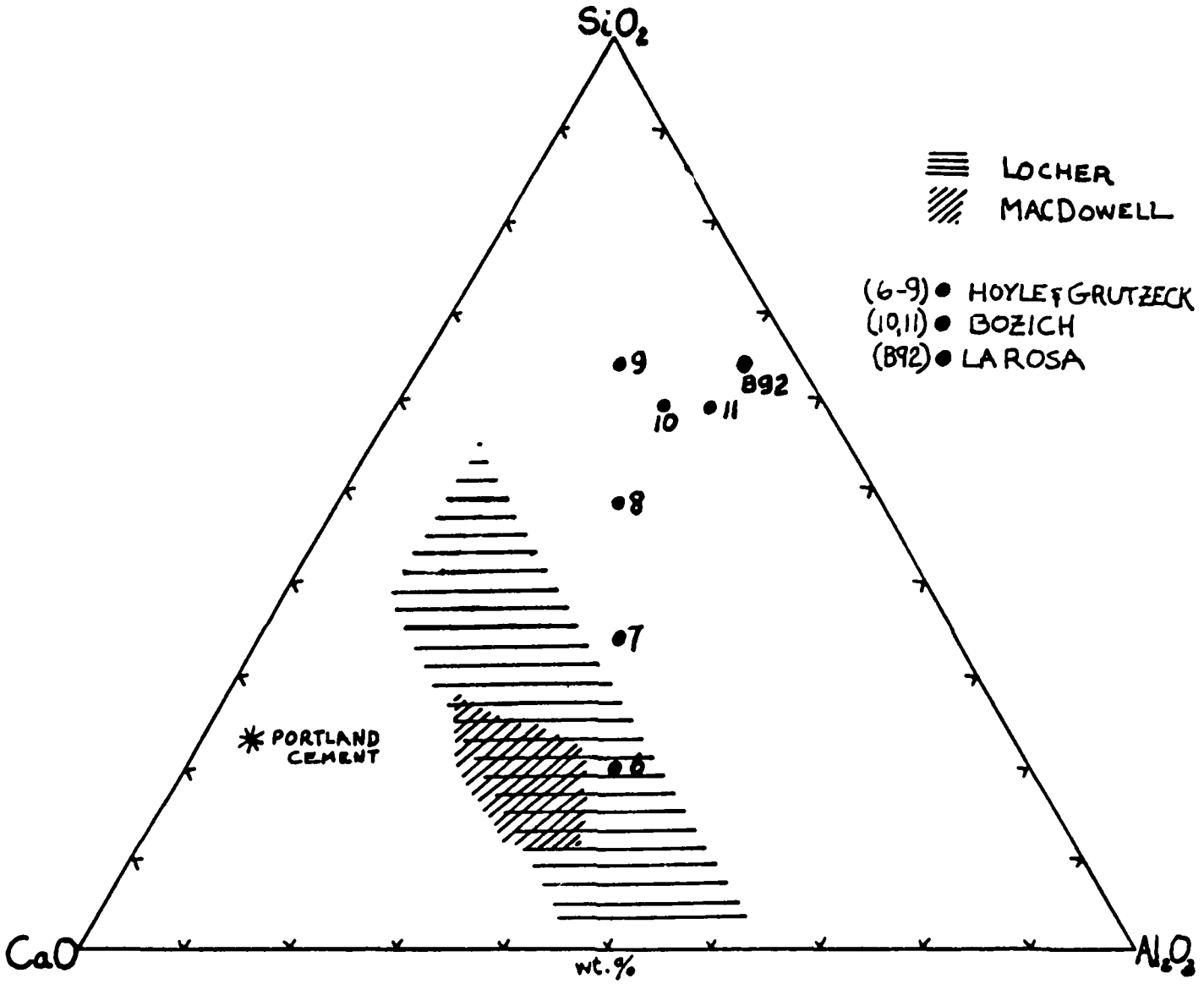

Figure 39. Composition diagram showing areas of previous and present glass hydration studies.

In related studies of zeolite formation in cement-based materials the author and his students were able to demonstrate that it was possible to grow zeolites in high aluminosilicate-enriched cement (10, 27, 28) as well as from calcium aluminosilicate glasses (10). By monitoring leach and pore solution compositions, Hoyle and Grutzeck (27,28) were able to demonstrate that aluminosilicate-enriched blends of cement and silica fume were much better waste forms for cesium than portland cement. They postulated that they were forming cesium-containing zeolites. Using this information they sketched a working phase diagram and synthesized a series of glasses numbered 6-9 in Figure 39. They mixed the glasses with CsOH solutions and monitored the progress of reaction with x-ray diffraction and the SEM. They found a correlation of zeolite formation with both composition and temperature. Glass 8 formed Cs-substituted herschelite ($Cs_4Al_4Si_8O_{24}.12H_2O$,) and Glass 9 formed pollucite [$Cs_2Al_2Si_4O_{12}.H_2O$ (10)]. In addition, the zeolites were observed to be cemented by a reticulated calcium silicate hydrate (C-S-H) which imparted strength to the material.

The work described below summarizes the results of similar hydration reactions using synthetic glasses 10 and 11, and fly ash (B92) as starting materials (see Figure 39 for their compositions). In each case the glasses were mixed with alkali solutions and cured at various temperatures as a function of time.

Zeolite Synthesis from Synthetic Glasses 10 and 11*

Experimental Procedures. Glasses 10 and 11 were made from reagent grade $CaCO_3$ and Al_2O_3, and 30 μm Min-U-Sil, a natural quartz. Stoichiometric mixtures were ball milled with ethyl alcohol and alumina media for ~24 hours. After drying and slowly heating to 1000°C to drive off the CO_2, the powders were fired in a MoS_2 furnace at ~1500°C in a Pt crucible. After 2-3 hours the glasses were quenched by immersing the entire crucible in chilled deionized water.

* The work described in this section is part of a B.S. Thesis in Ceramic Science and Engineering (Bozich, 1990).

The glasses were analyzed (Table 1) and ground to -850 μm mesh. After grinding, 10 grams of each glass were mixed with 25mL of 0.8M NaOH solution and placed in a 125 cc HDPE bottle. These samples were cured at room temperature. Companion samples cured at 70° and 90°C were placed in Teflon bottles. Weights were monitored to see if the containers were leaking; they were not. Samples were shaken occasionally rather than continuously, and pHs were measured to track reaction progress. The room temperature runs showed little or no reactivities and therefore were abandoned early in the program. Data for the 70° and 90°C experiments are presented below.

Results

pH versus time plots are given in Figure 40. The pH of the 90°C samples exhibit a more rapid rate of change than do the companion 70°C samples. Interestingly, not very much happens for the first 3 days of reaction. Apparently this "soaking" period is necessary to build up the activation energy necessary to initiate nucleation and growth of zeolites. After 90 days of hydration, glass 11 had consumed all of the available water, and only a white powder remained in the bottle.

Typical x-ray diffraction patterns of the hydration products after 80 days of hydration at 70° and 90°C are given in Figures 41 and 42 (glass 10 and 11, respectively). In both cases, gobbinsite ($Na_5Al_4Si_{11}O_{32}\cdot 11H_2O$) was forming. It was also observed that gobbinsite formed from an intermediate zeolite earlier in the hydration reaction. The identity of the intermediate is still unknown, but because it had a larger d-spacing; it is assumed to be a more water-rich version of gobbinsite.

Figure 43 gives an example of the microstructure of the gobbinsite which forms. The crystals are massive and highly striated. Evidence of glass shards were hard to find. Judging from the Figure 40 pH plots, reactions were nearly complete by this time.

Table 1. Glass analyses.

Oxide	Glass 10	Glass 11
CaO	14	11
Al_2O_3	26	31
SiO_2	61	61
Total	101	103

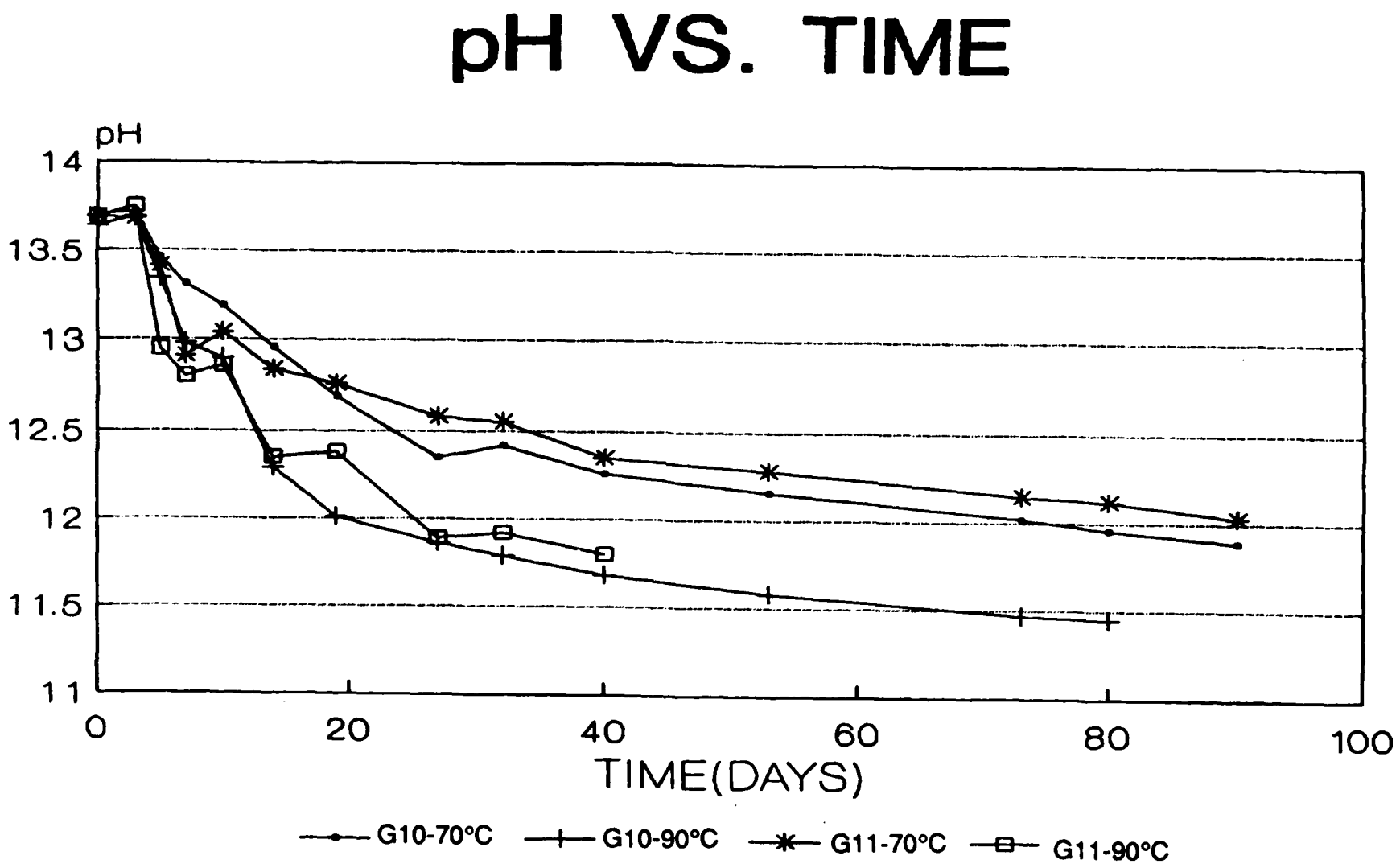

Figure 40. pH versus time plots for glasses 10 and 11 hydrated in 0.8M NaOH solution at 70° and 90°C.

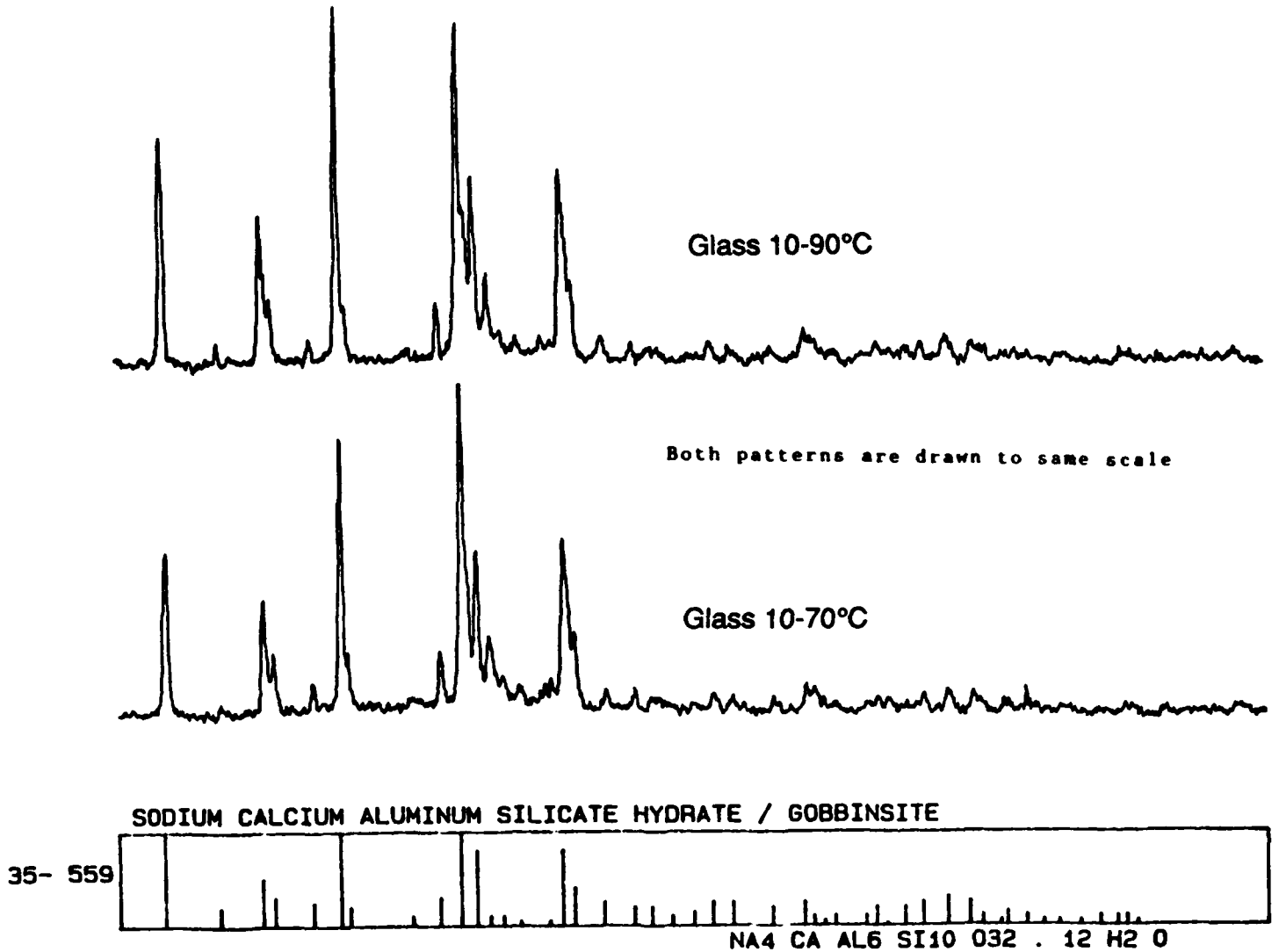

Figure 41. Glass 10 hydrated at 70° and 90°C for 80 days. Hydration products match JCPDS No. 35-559 for gobbinsite.

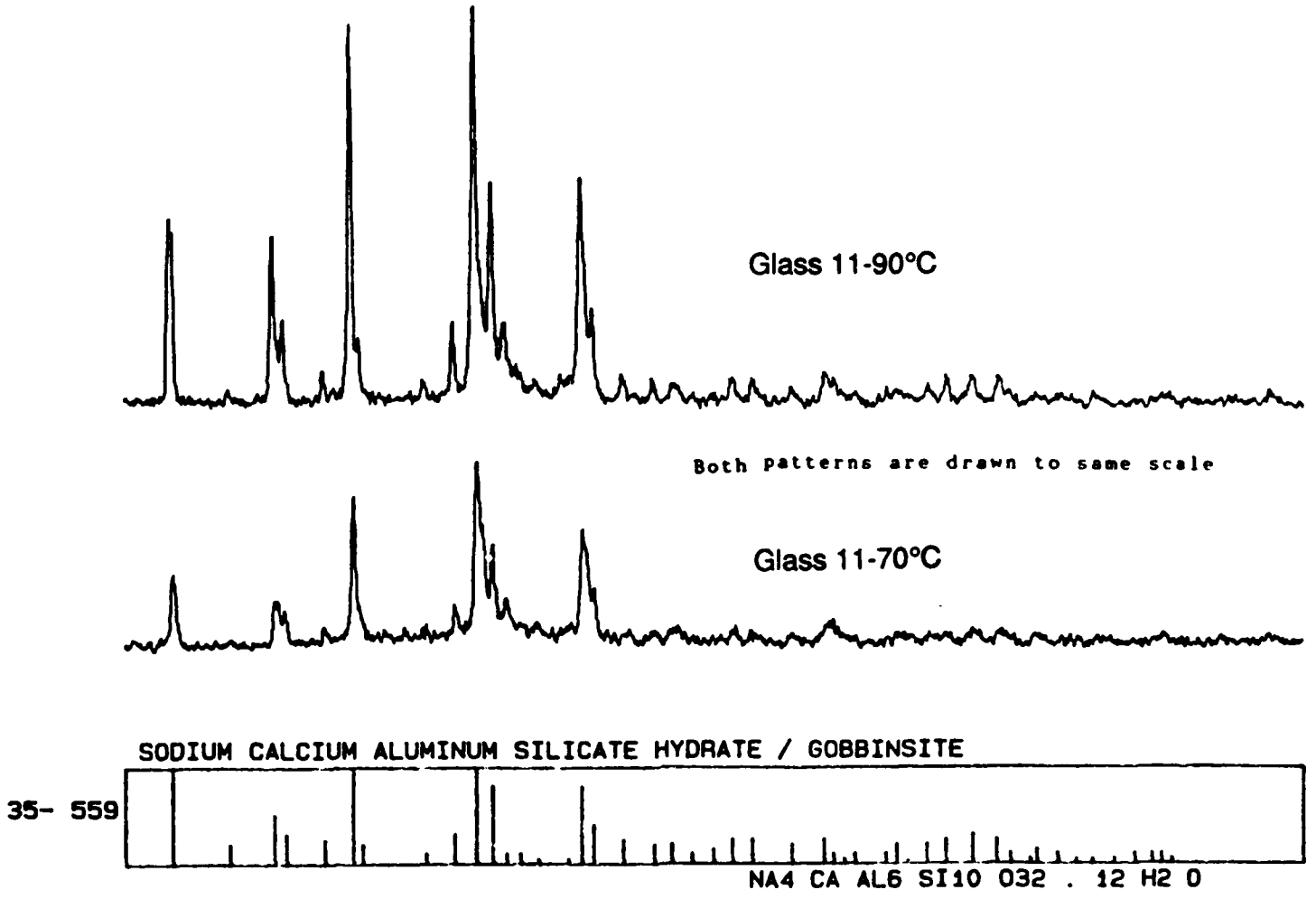

Figure 42. Glass 11 hydrated at 70° and 90°C for 80 days. Hydration products match JCPDS No. 35-550 for gobbinsite.

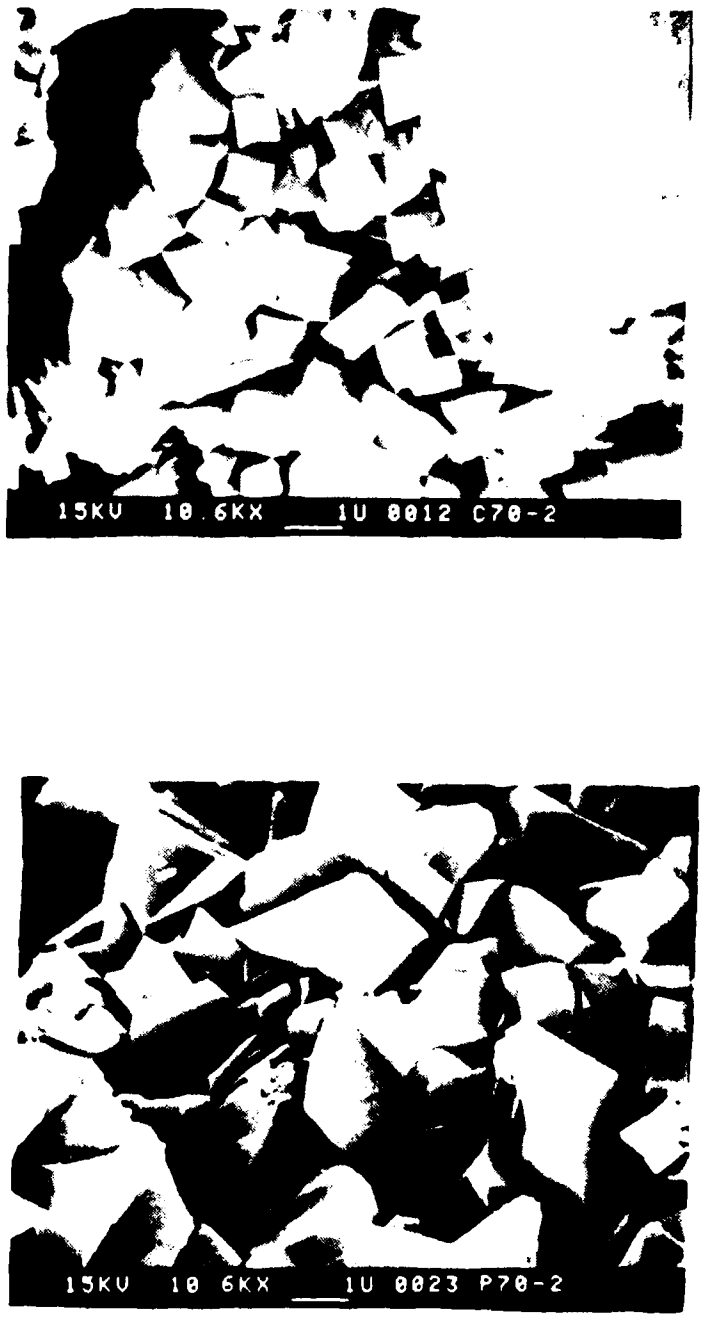

Figure 43. SEM photomicrographs of gobbinsite microstructure. Glass 10 top, Glass 11 bottom after 80 days at 70°C.

Zeolite Synthesis from Fly Ash

Introduction. In a parallel study, Class F fly ash (B92) was hydrated in the presence of different concentrations of NaOH and KOH solutions and cured at various temperatures. Occasionally a high-lime Class C fly ash (G07) or a blast furnace slag (G24) were substituted for the B92. In some instances, additional alumina or silica were added to the fly ash in order to explore the effect of such additions on the nature and microstructure of the zeolites which formed during the hydration reaction. Successful synthesis of zeolites in these experiments led to attempts at synthesizing zeolites in blended-cement pastes. Again, Class F B92 fly ash was a constituent along with ordinary portland cement (OPC) and substitutions/additions of Class C G07 fly ash, blast furnace slag G24, hydrated aluminum hydroxide, and silica fume. Several factors were varied, and their effect on phase development and microstructure were studied. These factors included: percentage and type of starting materials, concentration and type of alkali hydroxide solution, water to solids (w/s) ratio, and curing temperature. Finally, a set of pastes were made from fly ash, cement, and natural zeolites in an attempt to seed the materials in order to promote the growth of zeolites.

Procedure and Results. Experimental procedures were similar to those described in the previous section. Any differences are detailed within the text. In a set of preliminary experiments, zeolites were successfully synthesized from fly ash and alkali-hydroxide solutions. Most of these samples were made with a Class F fly ash (B92). Its composition is given in Table 2. X-ray diffraction and TEM confirmed the presence of small amounts of quartz, mullite, and graphite in the predominantly glassy fly ash. The diffraction pattern given in Figure 44 shows the presence of a glassy phase as evidenced by the amorphous hump centered around 24° 2θ. The accompanying SEM micrograph of the fly ash indicates that the sizes of the fly ash spheres range from ~1 to 20μm. In addition to the Class F fly ash, a few samples were made with either a Class C high-lime fly ash (G07) or a blast furnace slag (G24), both of which have a higher CaO content than the Class F material. Compositions of the Class C fly ash and the slag are also given in Table 2.

Table 2. Chemical analyses of the fly ashes, slag and portland cement (weight %).

Oxide	Class F fly ash B92	Class C fly ash G07	Slag G24	Portland cement I23
SiO_2	53.2	39.5	34.3	19.4
Al_2O_3	26.0	16.9	10.2	6.18
TiO_2	1.38	--	0.48	0.33
Fe_2O_3	7.95	6.4	0.67	2.50
MgO	0.97	6.3	11.4	3.13
CaO	3.57	24.8	40.61	61.85
MnO	0.041	--	0.510	0.155
Na_2O	0.29	1.44	0.19	0.41
K_2O	2.59	0.53	0.45	0.75
C	1.65	--	--	--
P_2O_5	--	--	0.02	0.34
SO_3	0.59	1.99	--	2.9
SrO	--	--	0.05	--
BaO	--	--	0.05	--
S	--	--	1.31	--
Loss of Ignition (750°C)	2.22	0.22	--	2.7
Totals	100.45	98.08	100.24	100.64

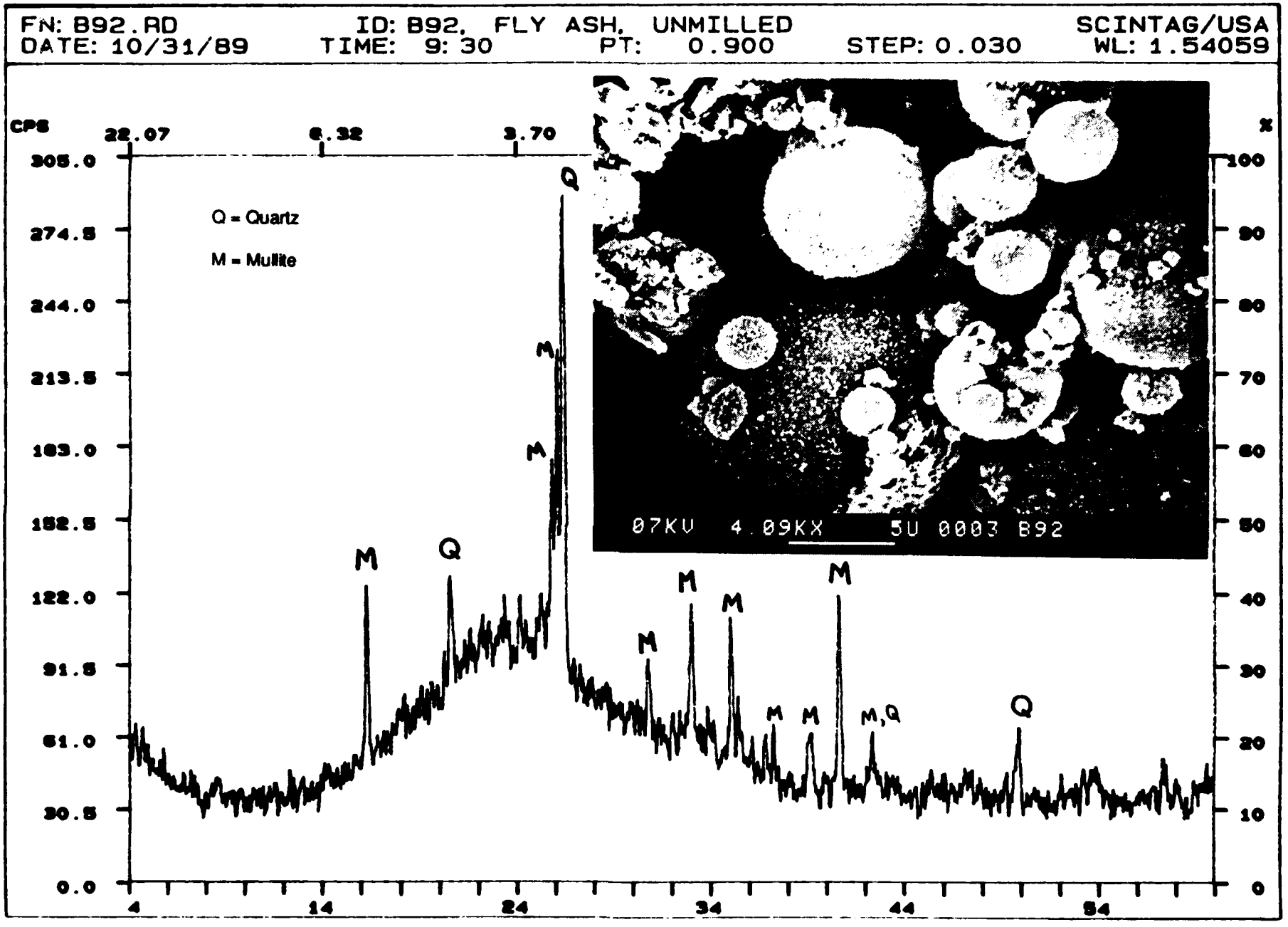

Figure 44. X-ray diffraction pattern and SEM photomicrograph of starting material B92 fly ash. M = mullite, Q = quartz.

2.8M KOH or NaOH solutions were added to fly ash alone or to mixtures of the fly ash and either $Al(OH)_3 \cdot xH_2O$ or condensed silica fume. Table 3 lists the amounts and kinds of materials used in each sample. The samples were cured using a procedure suggested by Yoshida and Inoue (17); samples were kept at room temperature for two days (presumably a "soaking" period) followed by six days of curing at ~80°C. The water to solids (w/s) ratio, by weight, was kept constant at 2.5. Table 3 also lists the phases identified using x-ray diffraction analysis. The zeolite Linde B1 ($0.95\ Na_2O\text{-}Al_2O_3\text{-}3.35SiO_2$) was found to be the crystalline phase present in sample B92N (Figure 45). Zeolites were found in other samples as well although actually determining the number and identity of the zeolitic phases has been very difficult and is still in progress.

Selected diffraction patterns and micrographs of other fly ash samples are presented in Figures 46-48. A variety of phases and microstructures are found in these materials. For example, B92N in Figure 45 contains both crystalline phases and a reticulated phase. B92NAL given in Figure 46, which is identical to B92N except that it contains 57.5% hydrated aluminum hydroxide, contains a needle-like phase along with some unusual looking particles consisting of intersecting disks. The accompanying x-ray diffraction pattern is very crystalline, but the identity of this zeolite is unknown. The B92K sample shown in Figure 47, which is similar to B92N except that it was mixed with KOH, illustrates the affect of KOH solution versus NaOH solution. In this case, the fly ash has clearly reacted; however, there is little crystallinity present. The x-ray diffraction pattern given in Figure 47 confirms this observation. Figure 48 represents phase development in B92KAL. When compared to Figure 46 (B92NAL), one can see that the KOH sample contains similar phases but is slightly less crystalline.

After the success of these preliminary experiments, the next step was to reproduce the results in cement pastes. A typical chemical composition of the Type I ordinary Portland cement (I23) used in these pastes is given in Table 2.

The pastes consisted of various combinations of fly ash, cement, and other additions as specified in Table 4. As before, either NaOH or KOH solutions were added to the powders. In

Table 3. Formulation of flash ash-alkali solution mixtures.

Sample	wt.% solids	w/s[a]	solution	Curing temp. (°C)	Phases present
B92N	100 B92	2.5	2.8M NaOH	80	Zeolite Linde B1, B92[b]
B92K	100 B92	2.5	2.8M KOH	80	B92, undetermined zeolite
B92NAL	42.5 B92 57.5 $Al(OH)_3 \cdot xH_2O$	2.5	2.8M NaOH	80	B92, undetermined zeolite
B92KAL	42.5 B92 57.5 $Al(OH)_3 \cdot xH_2O$	2.5	2.8M KOH	80	B92, undetermined zeolite
B92NS	42.5 B92 57.5 silica fume	2.5	2.8M NaOH	80	B92
B92KS	42.5 B92 57.5 silica fume	2.5	2.8M KOH	80	amorphous
G07N	100 G07	2.5	2.8M NaOH	78	quartz, undetermined
G24N	100 G24	2.5	2.8M NaOH	78	undetermined

[a]w/s = (wt. of solution)/(wt. of solids).
[b]Implies presence of quartz and mullite.
Sample code: B92 = Class F fly ash; G07 = Class C fly ash, G24 = blast furnace slag; N = NaOH solution containing; K = KOH solution containing; AL = alumina containing; S = silica containing.

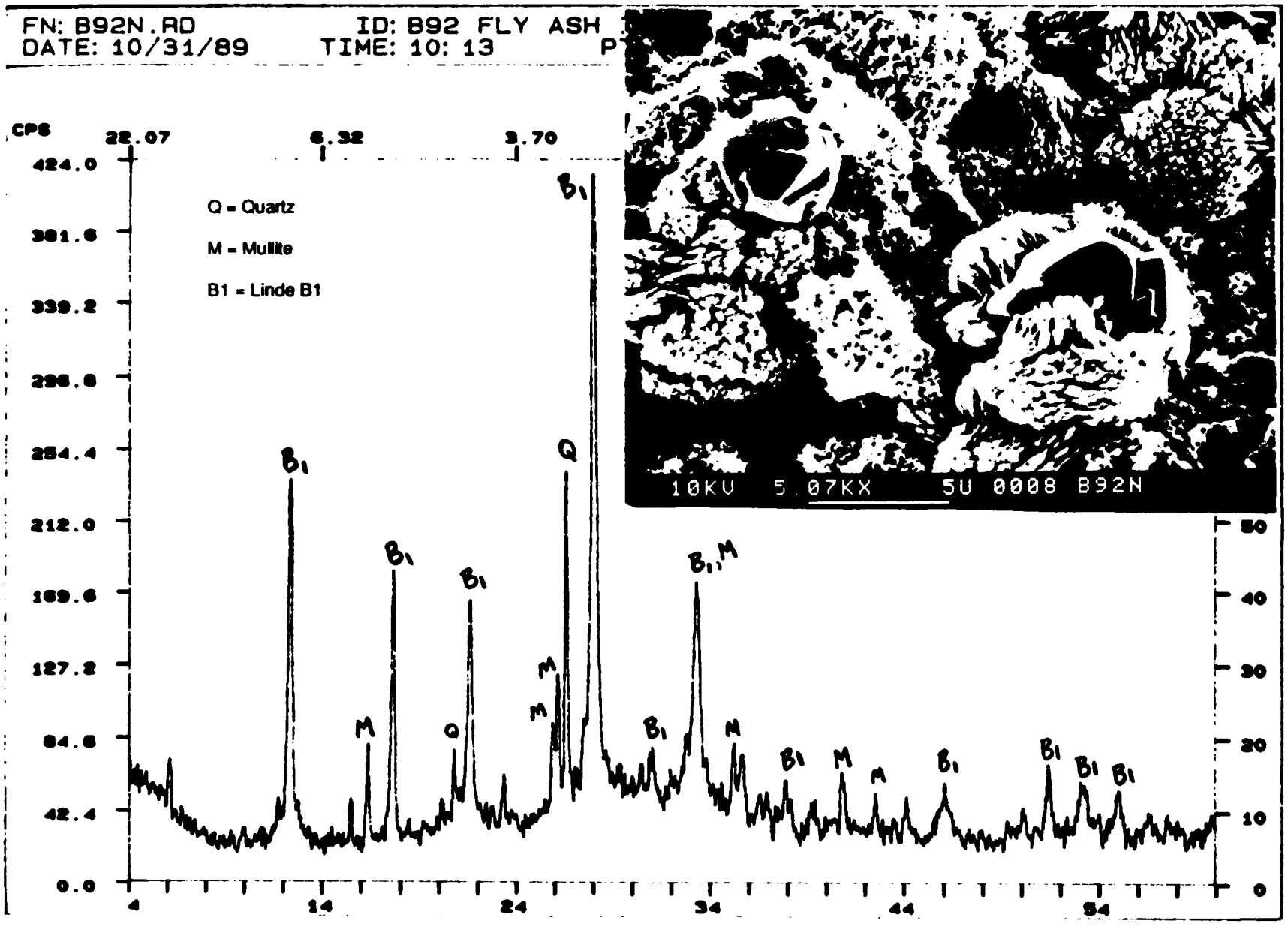

Figure 45. X-ray diffraction pattern and SEM photomicrograph of B92N (Class F fly ash + NaOH). B_1 = Linde B, M = mullite, Q = quartz.

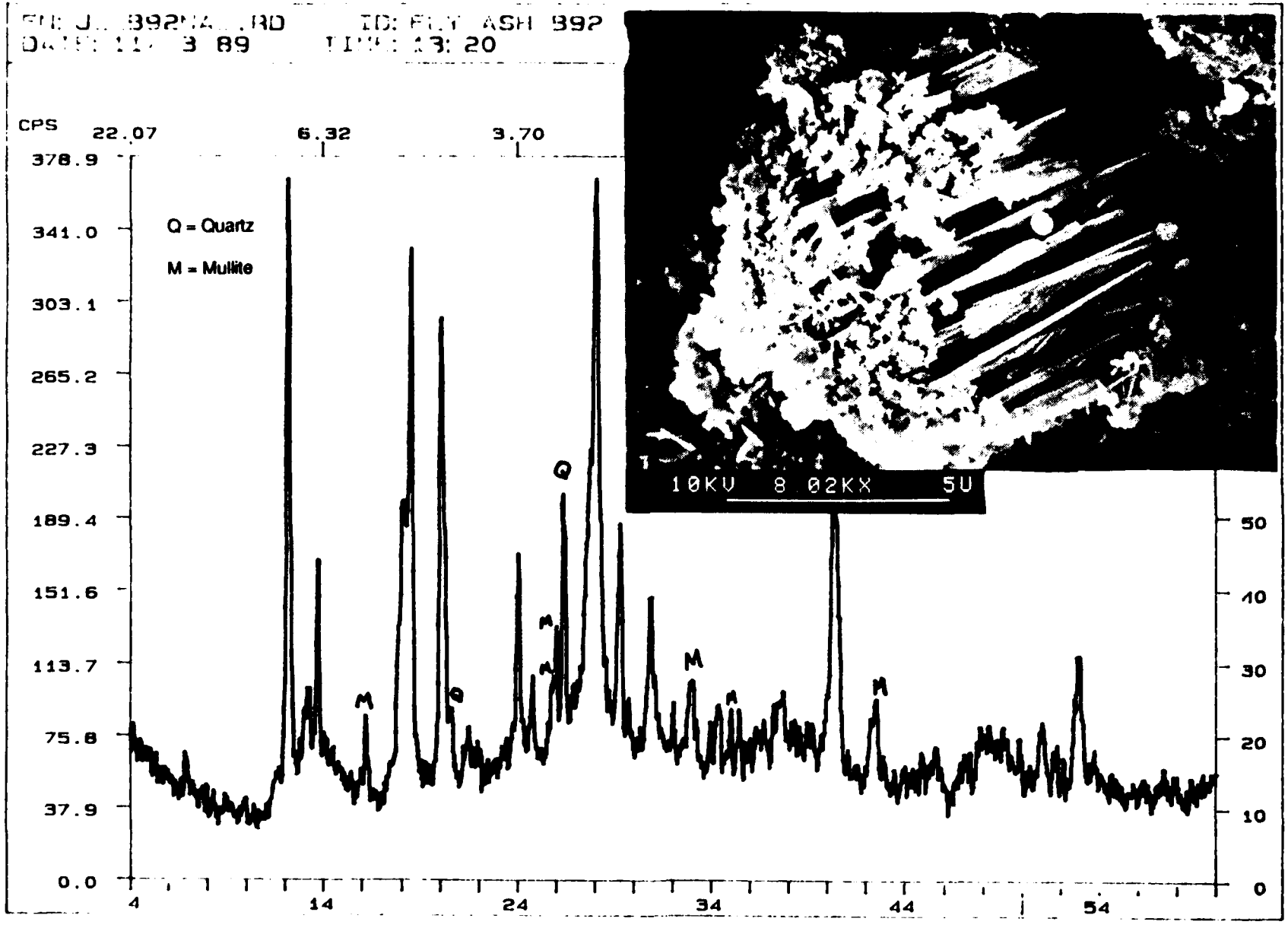

Figure 46. X-ray diffraction pattern and SEM photomicrograph of B92NAL (Class F fly ash + NaOH + $Al(OH)_3 \cdot xH_2O$). Unknown phases are more common than the mullite and quartz peaks from the B92 fly ash.

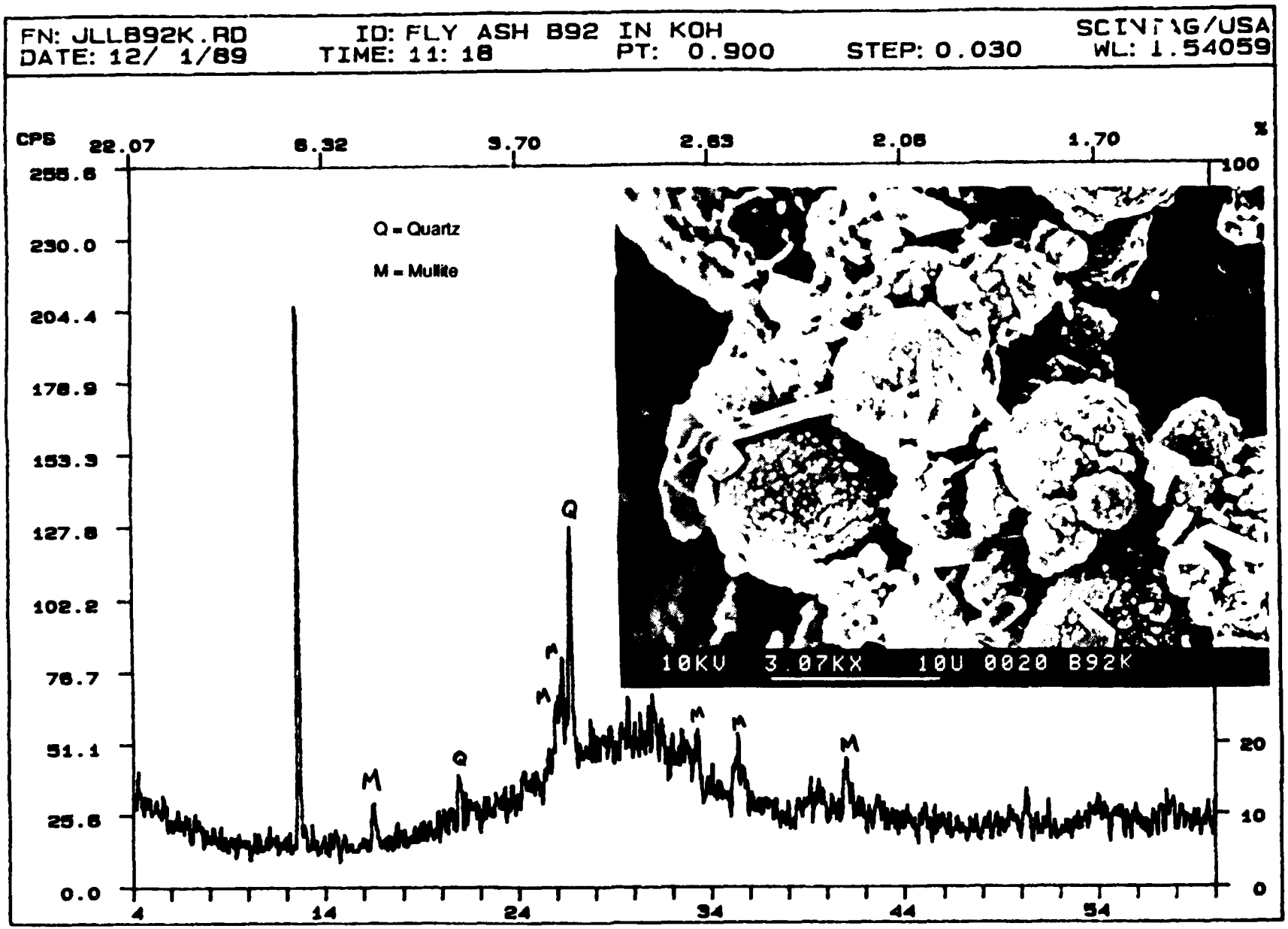

Figure 47. X-ray diffraction patterns and SEM photomicrograph of B92K (Class F fly ash + KOH). Hydration products are amorphous in nature. Only mullite and quartz from the B92 fly ash are present. The identify of the large peak at 13° 2θ is unknown.

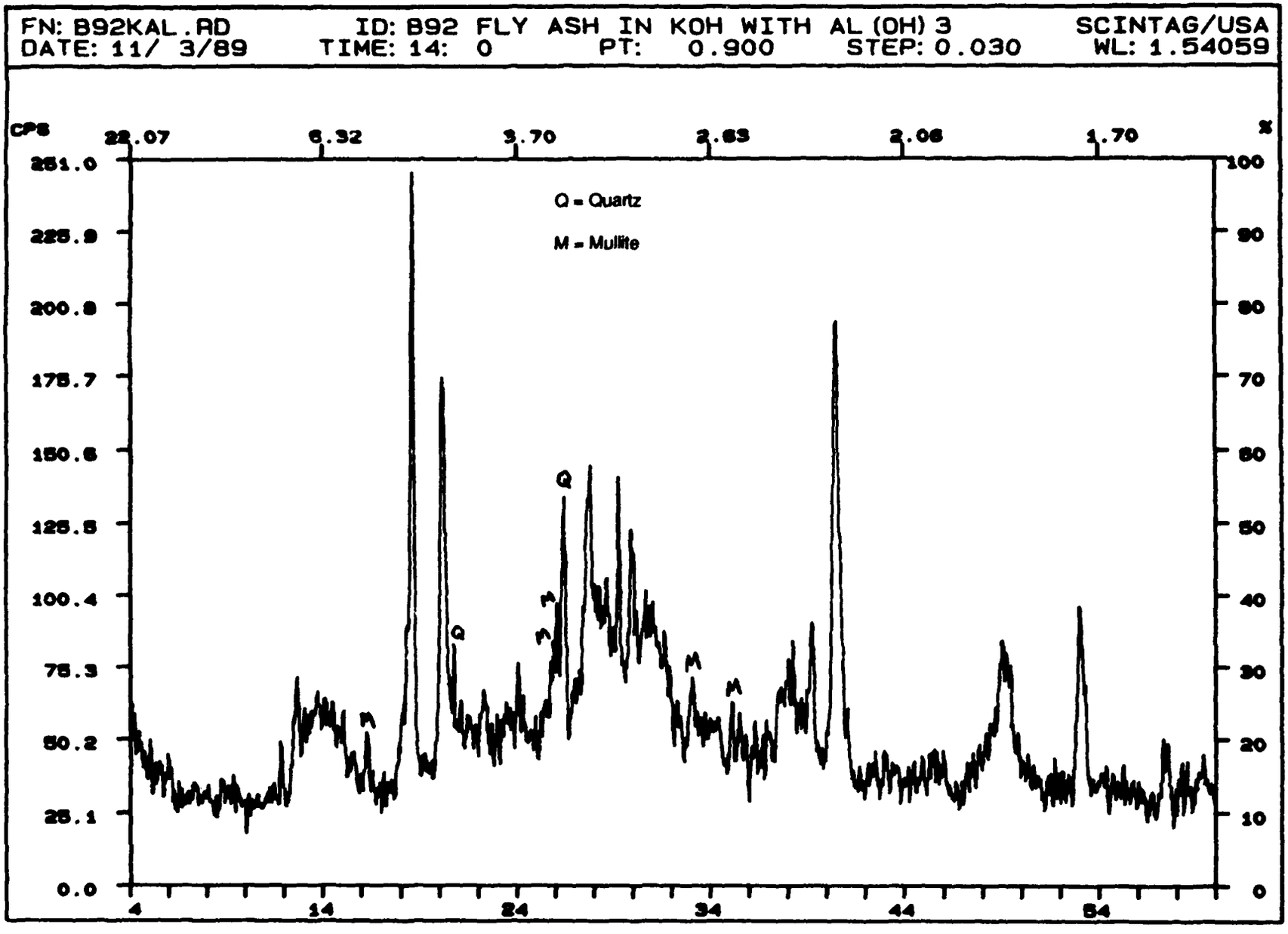

Figure 48. X-ray diffraction pattern of B92KAL (Class F fly ash + KOH + $Al(OH)_3 \cdot xH_2O$). The identity of the large peaks are unknown. Mullite and quartz are present in the B92 fly ash.

some cases (Pastes 8,9, and 12-18), the mixture was divided in two, and approximately 1 weight % sucrose, a commonly used cement retarder, was added to one of the samples. In Table 4 and throughout the text, samples containing sucrose have been labelled with a "B" while samples without sucrose are either specified with an "A" or contain no letter at all in the sample's name.

After two days at room temperature, all pastes made without sucrose (i.e, Pastes 1-7, 8A, 9A, 10, 11, and 12A-18A) had hardened and were broken into three pieces so that each piece could be cured at a different temperature for six days. In the case of pastes 1-12, the pieces to be cured at the higher temperatures of 78° and 90°C were placed in screw-top plastic bottles. A small piece of wet paper towel was put into each of these bottles to provide a high relative humidity. The bottles were then tightened and further sealed with a strip of electrical tape. Since 8B and 9B had not yet hardened, they were essentially poured into the bottles and sealed in the same manner. In the case of pastes 13-18, all samples (A and B)were kept in plastic petri dishes (which contained a moist piece of paper towel) and were sealed in zip-lock bags. In addition, bars of pastes 12A and 12B were cast and placed in a plastic container with water for two days. For the six day curing at 78°C, these bars were demolded and placed in a heat-resistant, plastic cooking bag.

Samples have been labelled according to the paste from which they were made, whether or not they contain sucrose, and the curing temperature. For example, P0178 is Paste 1, without sucrose, cured for six days at 78°C. P8ART is Paste 8, without sucrose, cured at room temperature (RT); and P9B90 is Paste 9, with sucrose, cured for six days at 90°C.

Of the 79 samples reported in Table 4, twenty-two have been examined with the SEM, and x-ray diffraction patterns for all but fifteen (14B-18B) have been collected.

Selected micrographs illustrating typical microstructure are presented in Figures 49-55. Again, the resulting phases are quite diverse. In some cases, there is little or no crystallinity while in others, zeolites did form. In P0278 which contains 80% B92 fly ash and 20% cement (Figure 49), the fly ash has reacted with the NaOH solution, and the cement has hydrated to form calcium silicate hydrate (C-S-H). P0778 in Figure 50, which is similar to P0278 but contains 46%

Table 4. Formulation of cement pastes.

Sample	wt.% solids	w/s	solution	Curing temps. (°C)[b]	Phases present
P01	80 B92, 20 PC[a]	0.40	2.8M KOH	RT	B92, CSH
				78	B92, CSH, unkonwn
				90	B92, CSH
P02	80 B92, 20 PC	0.40	2.8M NaOH	RT	B92, CSH
				78	B92, CSH, unknown
				90	B92, CSH, unknown
P03	80 G07, 20 PC	0.40	2.8M NaOH	RT	amorphous
				78	unknown, CSH
				90	unknown, CSH
P04	80 G24, 20 PC	0.40	2.8M NaOH	RT	CSH
				78	CSH, unknown
				90	CSH, unknown
P05	34 B92, 20 PC, 46 SiO_2 fume	0.61	2.8M NaOH	RT	amorphous, some B92, CSH
				78	B92, CSH
				90	B92, CSH
P06	34 B92, 20 PC, 46 $Al(OH)_3 \cdot xH_2O$	0.61	2.8M KOH	RT	amorphous, Q, CSH, unknown
				78	B92, CSH, unknown
				90	amorphous, some B92
P07	34 B92, 20 PC, 46 $Al(OH)_3 \cdot xH_2O$	0.85	2.8M NaOH	RT	CSH, Q, unknown
				78	CSH, Q, unknown
				90	CSH, Q, unknown
P8A	80 B92, 20 PC	0.80	5M NaOH	RT	B92, CSH, unknown
				78	B1, Chab., B92, CSH, unknown
				90	B1, Chab., B92, CSH, unknown
P8B	same as P8A plus ~1 wt. % sucrose			RT	B92, CSH, unknown
				78	Chab., B92, CSH, unknown
				90	Chab., B92, CSH, unknown
P9A	80 G07, 20 PC	0.80	5M NaOH	RT	Q, CSH, unknown
				78	Q, CSH, unknown
				90	Q, CSH, unknown
P9B	same as P9A plus ~1 wt. % sucrose			RT	Q, CSH, unknown
				78	Q, CSH, unknown
				90	Q, CSH, unknown
P10	50 B92, 50 PC	0.80	5M NaOH	RT	B92, CSH, unknown
				79	CSH, M, unknown
				90	B1, CSH, B92, unknown

Table 4. Continued.

Sample	wt.% solids	w/s	solution	Curing temps. (°C)[b]	Phases present
P11	20 B92, 80 PC	0.80	5M NaOH	RT	CSH, B92, unknown
				79	CSH, unknown
				90	CSH, unknown
P12A	80 B92, 20 PC	0.40	5M NaOH	78 (bar)	B92, Chab., CSH, unknown
				80	B92, Chab., CSH, unknown
P12B	Same as P12A plus ~1 wt. % sucrose			78 (bar)	B92, CSH, unknown
				80	B92, CSH, unknown
P13A	80 B92, 20 PC	0.40	5M NaOH	RT	B92, CSH
				38[c]	B92, CSH, unknown
				60	B92, Chab., CSH, unknown
P13B	Same as P13A plus ~1 wt. % sucrose			RT	B92, amorphous
				38[c]	B92, CSH, amorphous
				60	B92, CSH, unknown
P14A	80 B92, 20 PC	0.40	2.8M NaOH	RT	B92, CSH, unknown
				38[c]	B92, CSH, unknown
				60	B92, CSH, unknown
P14B	Same as P14A plus ~1 wt. % sucrose			RT	Samples have
				38[c]	not been
				60	analyzed.
P15A	80 B92, 20 PC	0.40	DI water	RT	B92, amorphous
				38[c]	B92, CSH, unknown
				60	B92, CSH, unknown
P15B	Same as P15A plus ~1 wt. % sucrose			RT	Samples have
				38[c]	not been
				60	analyzed.
P16A	65 B92, 35 PC	0.40	5M NaOH	RT	amorphous, B92, CSH
				38[c]	CSH, B92, unknown
				60	B92, CSH, Chab., unknown
P16B	Same as P16A plus ~1 wt. % Sucrose			RT	Samples have
				38[c]	not been
				60	analyzed.
P17A	65 B92, 35 PC	0.40	2.8M NaOH	RT	B92, CSH, unknown
				38[c]	B92, CSH, unknown
				60	B92, CSH, unknown

Table 4. Continued.

Sample	wt.% solids	w/s	solution	Curing temps. (°C)[b]	Phases present
P17B	Same as P17A plus ~1 wt. % sucrose			RT 38[c] 60	Samples have not been analyzed.
P18A	65 B92, 35 PC	0.40	DI water	RT 38[c] 60	B92, CSH, unknown B92, CSH, unknown B92, CSH, unknown
P18B	Same as P18A plus ~1 wt. % sucrose			RT 38[c] 60	Samples have not been analyzed.

[a]Sample code: B92 = Class F fly ash; G07 = Class C fly ash, G24 = blast furnace slag; N = NaOH solution containing; K = KOH solution containing; AL = alumina containing; S = silica containing; PC = Type I portland cement (I23); DI = deionized; CSH = calciumsilicate hydrate; B1 = Linde B1; Chab. = chabazite.
[b]Pieces of each sample were cured at each of the temperatures shown.
[c]Cured in a humidity chamber.

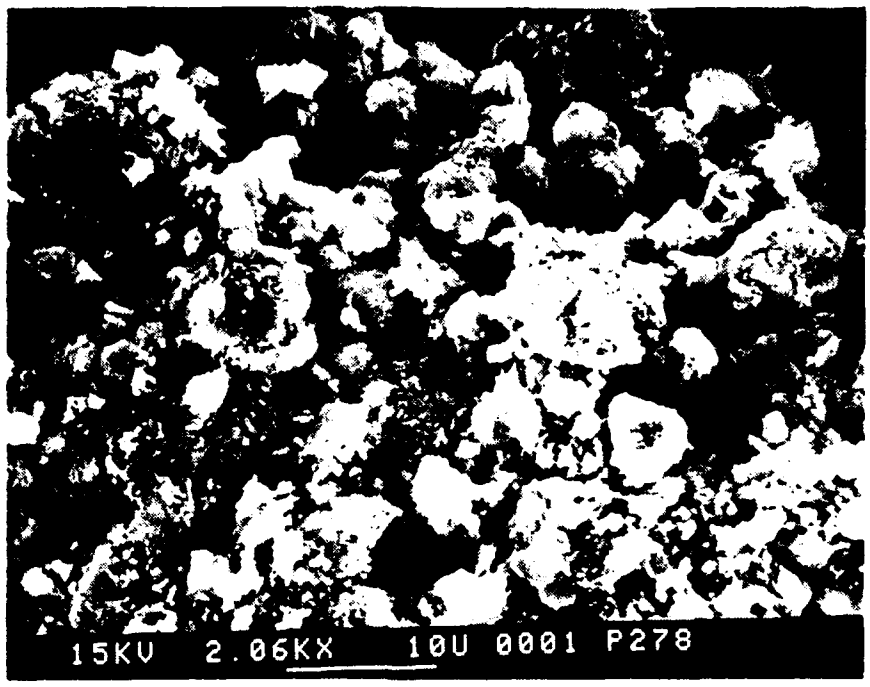

Figure 49. SEM photomicrograph of P0278 (80 % B92, 20% cement, w/s = 0.4, 2.8M NaOH) cured at 78°C for six days. Phases: B92, C-S-H, plus an unidentified phase.

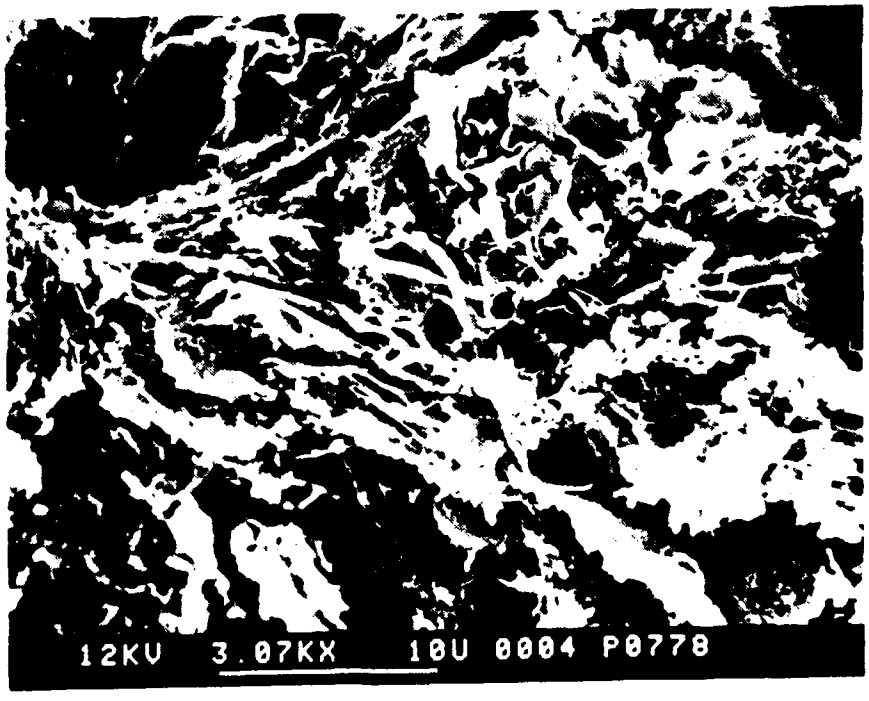

Figure 50. SEM photomicrograph of P0778 (34% B92, 20% cement, 46% $Al(OH)_3 \cdot xH_2O$, w/s = 0.85, 2.8M NaOH) cured at 78°C for six days. Phases: C-S-H plus an unidentified phase.

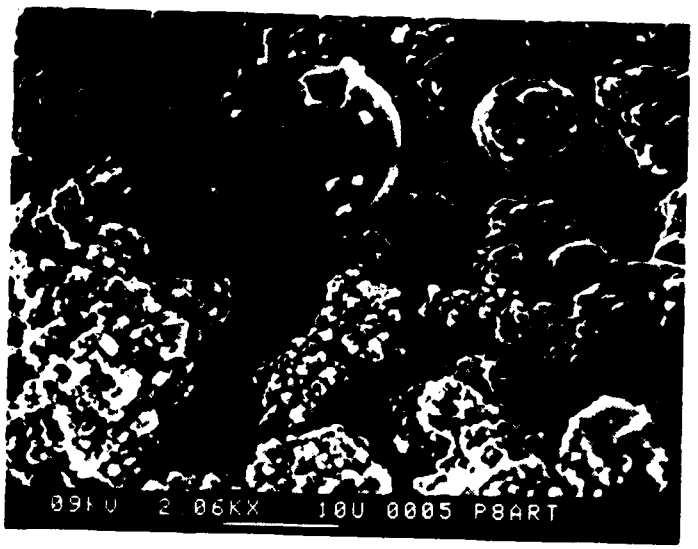

a)

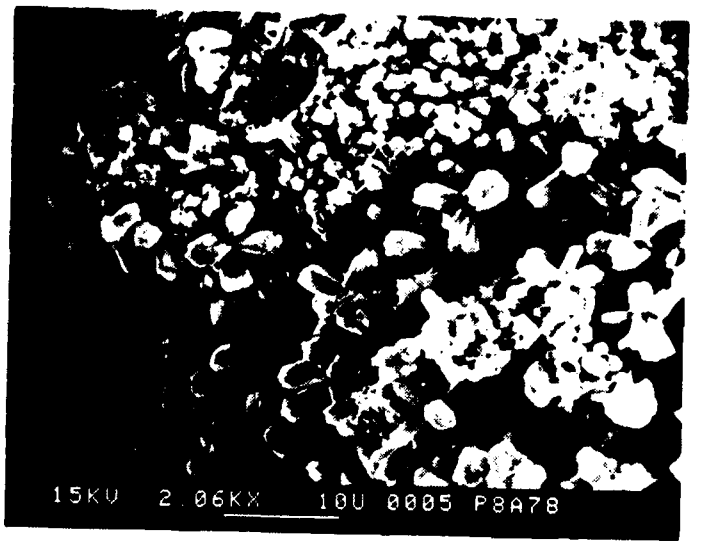

b)

c)

Figure 51. (a) SEM photomicrograph of Paste 8 (80% B92 and 20% cement, w/s = 0.8, 5M NaOH) P8ART cured at room temperature contains B92, C-S-H and an unidentified phase; (b) P8A78 cured at 78°C and (c) P8A90 cured at 90°C both contain Linde B1, chabazite, B92, C-S-H and an unidentified phase.

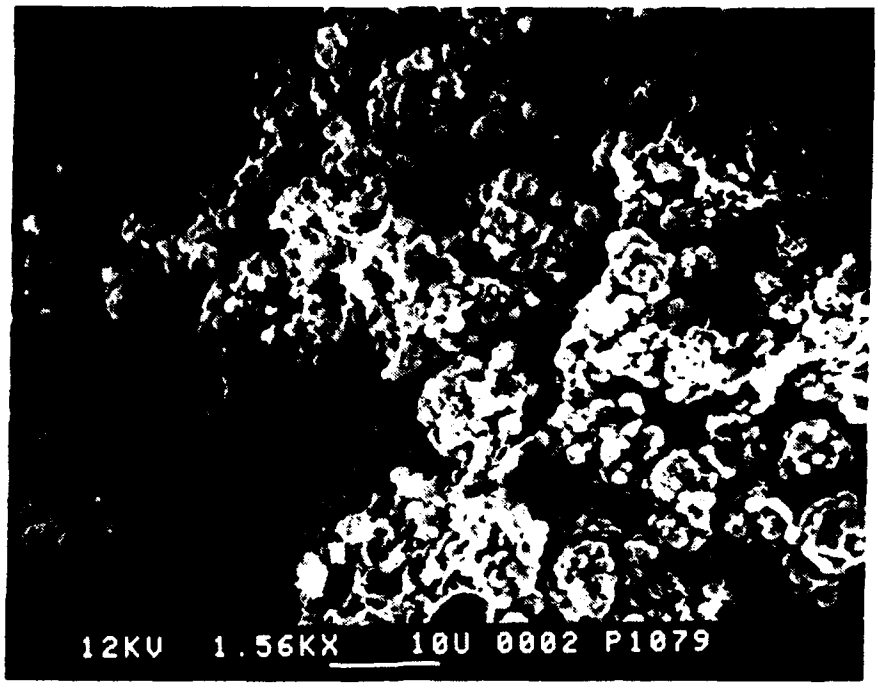

Figure 52. SEM photomicrograph of P1079 (50% B92, 50% cement, w/s = 0.80, 5M NaOH) cured at 79°C for six days. Phases: C-S-H, mullite and an unidentified phase.

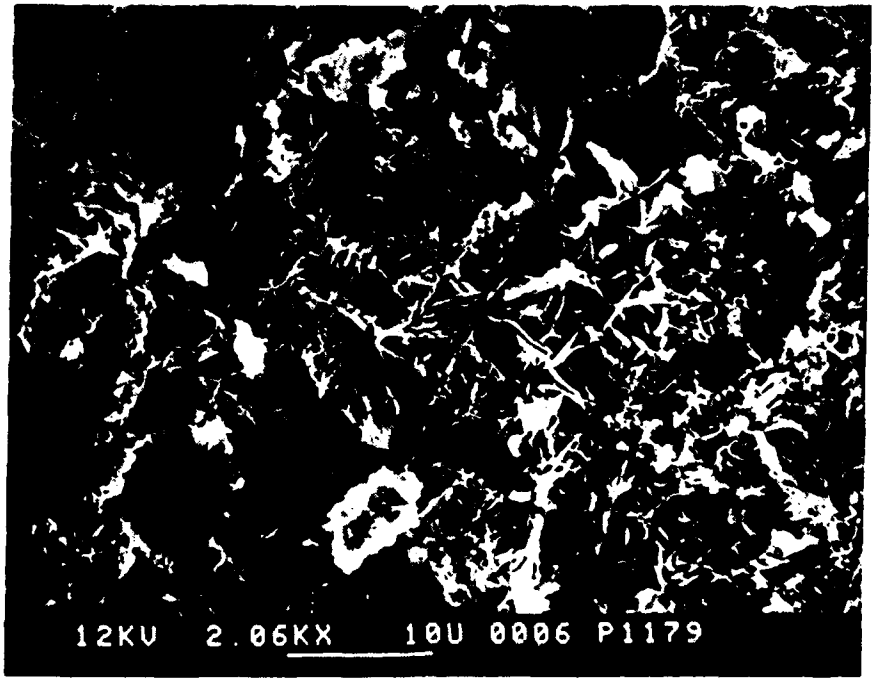

Figure 53. SEM photomicrograph of P1179 (20% B92, 80% cement, w/s = 0.80, 5M NaOH) cured at 79°C for six days. Phases: C-S-H and an unidentified phase.

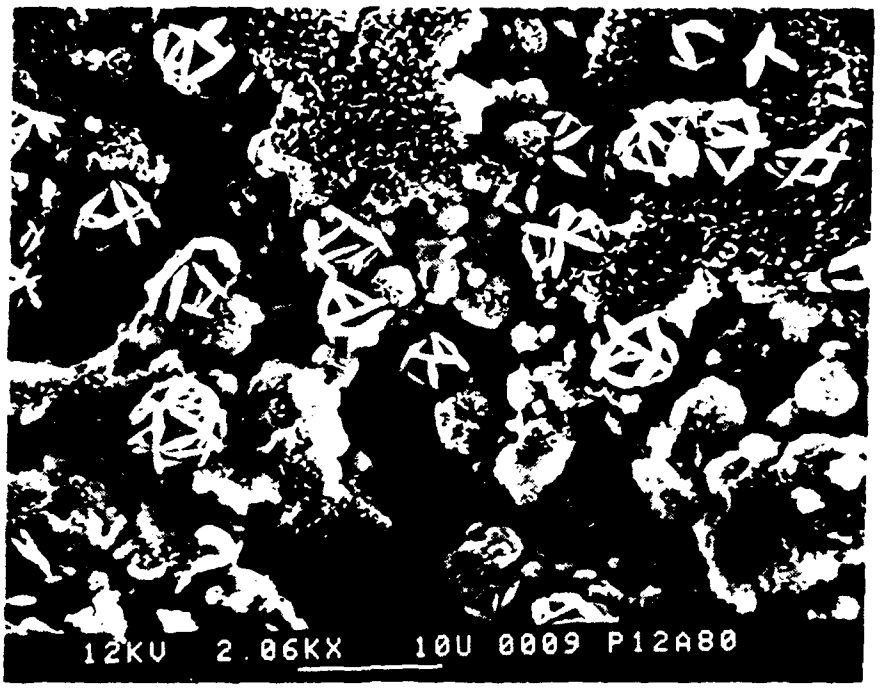

Figure 54. SEM photomicrograph of P12A80 (80% B92, 20% cement, w/s = 0.40, 5M NaOH) cured at 80°C for six days. Phases: B92, chabazite, C-S-H and an unidentified phase.

(a)

(b)

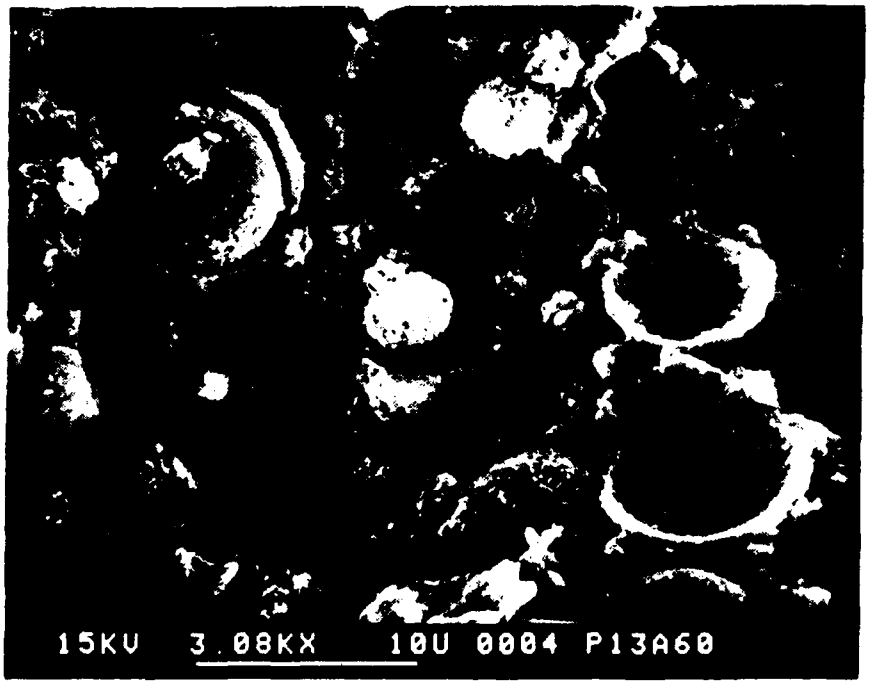

Figure 55. SEM photomicrographs of Paste 13 (80% B92, 20% cement, w/s = 0.40, 5M NaOH). (a) P13A38 cured at 38°C in a humidity chamber for six days; phases: B92, C-S-H and an unidentified phase. (b) P13A60 cured at 60°C for six days; phases: B92, chabazite, C-S-H and an undetermined phase.

hydrated aluminum hydroxide, depicts a paste with little accompanying crystallinity but instead contains a variety of thin, sheet-like structures.

Figure 51 (A-C) contains photomicrographs of the three samples of Paste 8 hydrated at room temperature (RT), 78° and 90°C. Like Paste 2 (Figure 49), Paste 8 contains 80% B92 fly ash and 20% cement; however, Paste 8 was made with a 5M NaOH solution at w/s of 0.8 compared to a 2.8M solution and w/s of 0.4 for paste 2. Micron-sized crystallites have grown on the fly ash surfaces in the RT sample (Figure 51A). However, the morphology of the 78°C (Figure 51B) and 90°C (Figure 51C) microstructures is very different from the RT sample. These figures contain bundles of cross-shaped particles. Using x-ray diffraction analysis, both chabazite and Linde B1 have been identified in these samples.

Photomicrographs of Pastes P1079 and P1179 are presented in Figures 52 and 53, respectively. These samples contain a larger percentage of cement than the samples presented earlier in Figures 49-51; Paste 10 contains 50% cement and Paste 11, 80% cement. Figure 53 shows the abundance of C-S-H in P1179. Round nodules have formed on the fly ash surfaces of P1079 (Figure 52) reminiscent of the blocky nodules found on P8ART (Figure 51A).

Figure 54 illustrates yet another morphology which developed in the cement pastes. This sample, P12A80, contains clusters of intersecting disks (similar to those seen previously in B92NAL, Figure 46). This phase could be chabazite which, according to the x-ray diffraction pattern, is present in the sample. Figures 55A and B show the morphology developed in P13A38 and P13A60, which have the same composition as P12A80 (i.e., 80% B92 fly ash and 20% cement in 5M NaOH at w/s of 0.4), but were cured at lower temperatures (38° and 60°C). Chabazite occurred in P13A60 and could be the micron-sized crystallites seen in Figure 55B (having a different morphology, perhaps, compared to P12A80, Figure 54).

The zeolites Linde B1 (0.95 Na_2O-Al_2O_3-3.35SiO_2) and chabazite ($Ca_2Al_4Si_8O_{24}$-$12H_2O$) have been identified in several of the pastes. Linde B1 occurred in P8A78, P8A90, and P1090 (although not in P1079). A high NaOH concentration and w/s seem to favor its nucleation and growth. Chabazite occurred in P8A78, P8A90, P8B78, P8B90, P12A78 (bar sample),

P12A80, P13A60, and P16A60. Conditions favoring the nucleation and growth of chabazite included: a high percentage of B92 of at least 65%, 5M NaOH solution, and curing temperature of at least 60°C.

It is evident that there are several variables that influence the microstructure of these pastes, namely: amount and type of starting material, w/s ratio, concentration of hydroxide solution, and curing temperature. In an effort to isolate the effects of each variable, Pastes 13-18 were produced. After identifying all of the phases present in each sample, it will be possible to determine which factors promote or inhibit the nucleation and growth of specific zeolites. At this time, it is difficult to draw such specific conclusions because not all of the samples have been characterized. However, it is beneficial to at least examine some of the x-ray diffraction patterns of the samples described in Table 4, noting differences or trends in the patterns as a certain factor is varied.

Figure 56 compares the x-ray diffraction patterns of P8A78 (20% cement, 80% B92 fly ash), P1079 (50% cement, 50% B92), and P1179 (80% cement, 20% B92). Each of these samples has the same w/s ratio, concentration of NaOH, and curing temperature. As stated above, Linde B1 and chabazite are the major phases found in P8A78 (Figure 51A). In P1079 (Figure 52), C-S-H is the major known phase although an unknown crystalline phase is also present. The pattern for P1179 appears more amorphous, and the micrograph (Figure 53) clearly shows the abundance of C-S-H.

Figure 57 depicts the effect of temperature on paste 8 (Figures 51A-C) which contains 20 wt. % portland cement and 80 wt. % B92 fly ash. Both the 78° and 90°C samples contained zeolites while the room temperature sample did not.

Figure 58 compares pastes which were formulated with varying amounts of NaOH but the same compositions and curing temperatures. P0278 (20% cement, 80% B92, w/s=0.4, 2.8M NaOH) has the smallest NaOH content of the three, and it does not contain a zeolitic phase. P12A80 (w/s=0.4, 5M NaOH) has almost twice the amount of NaOH, and chabazite has formed.

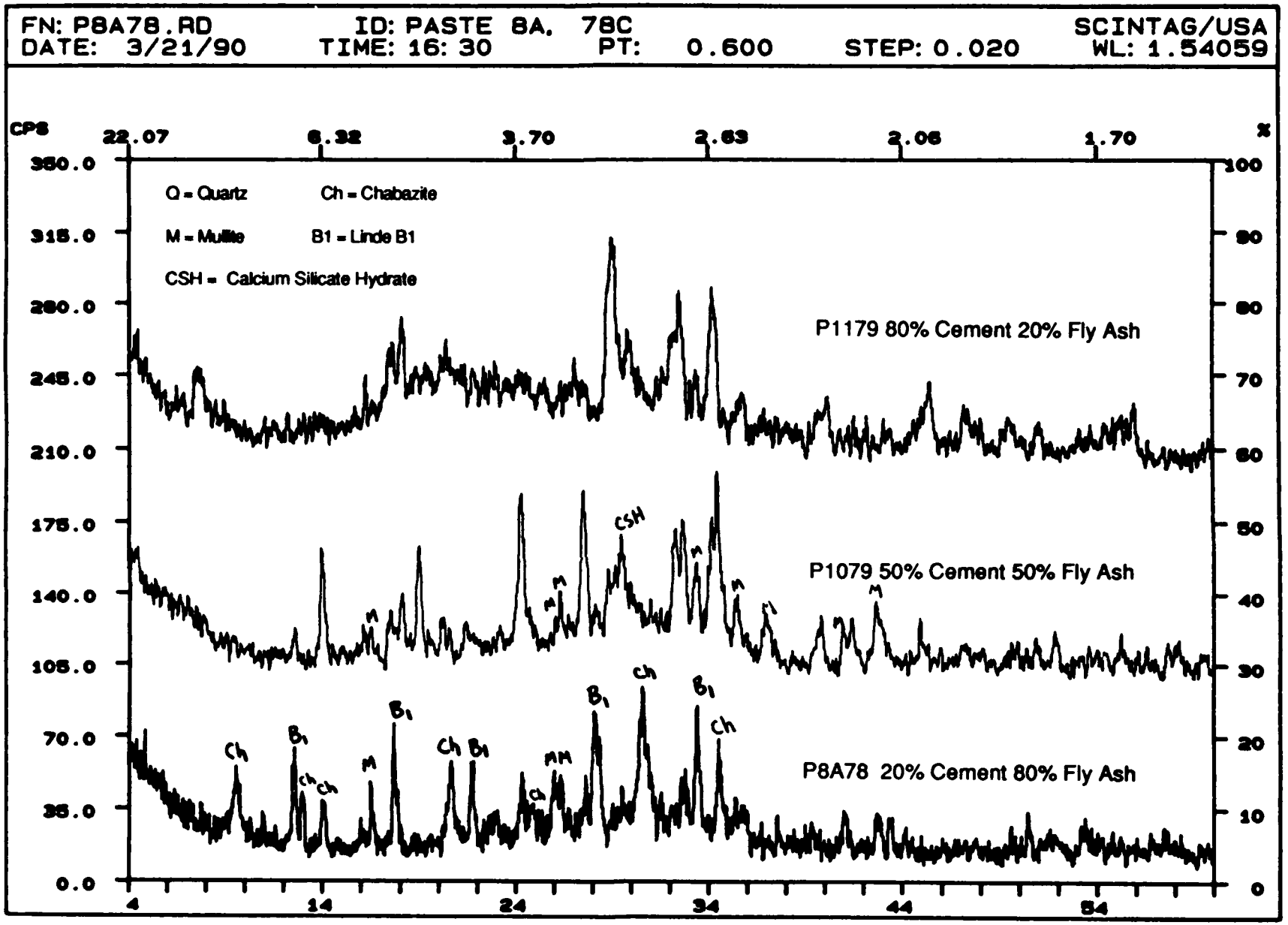

Figure 56. A comparison of x-ray diffraction patterns of pastes with varying amounts of cement (but all with w/s = 0.80, 5M NaOH, and curing temperature of ~80°C) shows that a higher percentage of fly ash favors the formation of zeolites.

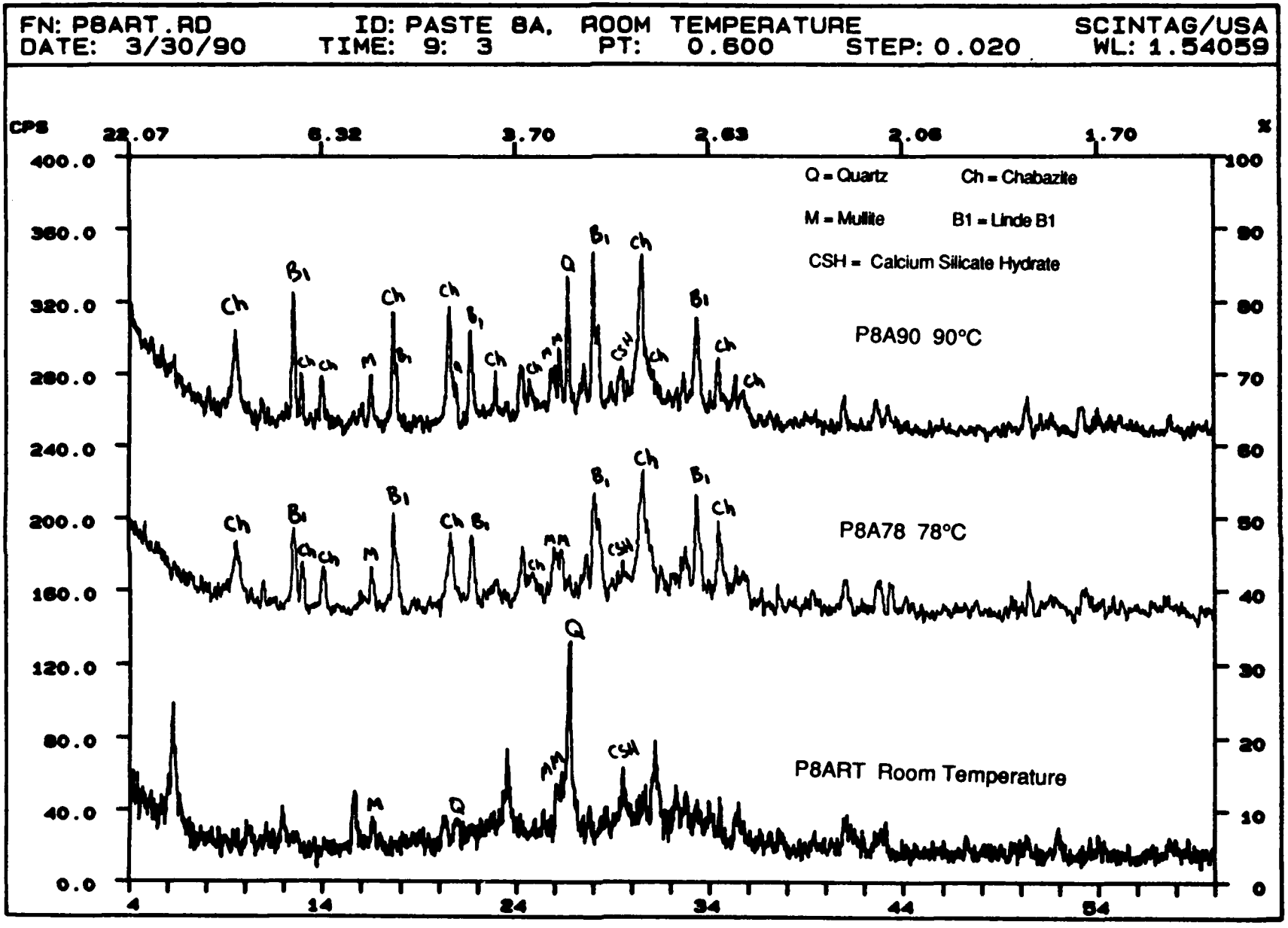

Figure 57. A comparison of Paste 8 x-ray diffraction patterns shows the effect of curing temperature. Higher temperatures favor the formation of zeolites.

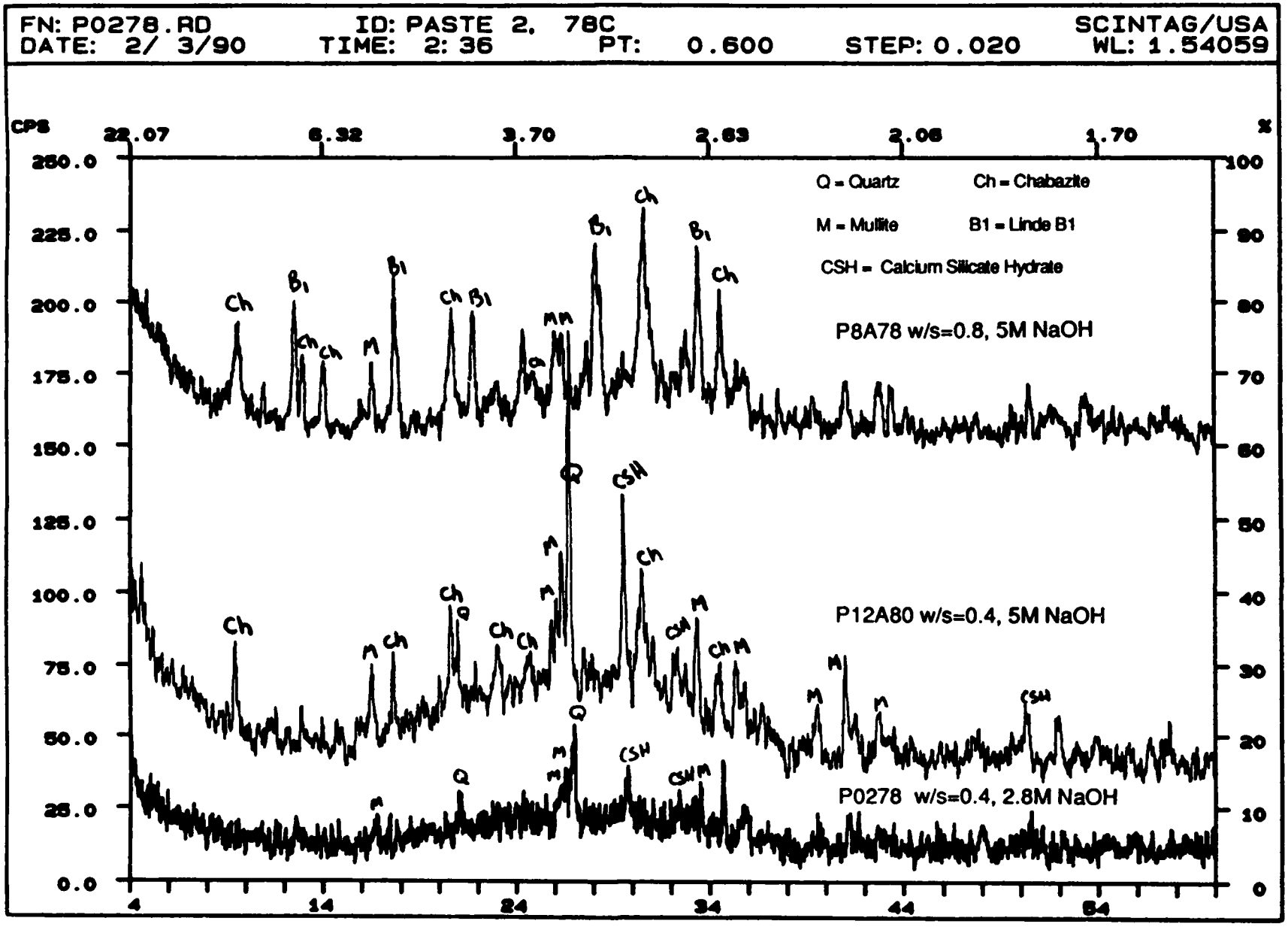

Figure 58. A comparison of x-ray diffraction patterns of pastes with different amounts of NaOH (all were 80% B92, 20% cement and cured at ~80°C) shows that the type of zeolite formed is dependent on the NaOH content.

Both Linde B1 and chabazite have grown in P8A78 (w/s=0.8, 5M NaOH) which has twice the amount of NaOH as P12A80.

Whether the presence of Linde B1 and chabazite in P8A78 is due only to a high fly ash content, a high curing temperature, a large amount of NaOH, or some combination of these needs to be determined, but will become evident as more work is completed.

Of the cement pastes given in Table 4, those with the most promising physical properties include P13ART, 38, and 60, P14A38, P16A38, P17A38, and P18A38. The strength data for these mixtures is being collected and will be reported in the near future.

In the third phase of the experimental program, natural zeolites were added to pastes in an attempt to seed the material and thus promote zeolite growth. A series of natural zeolites were obtained from Minerals Research, NY, and included clinoptilolite, chabazite, erionite, mordenite, and phillipsite. The zeolite/cement pastes were processed similarly to the previous cement pastes. Table 5 lists the composition for each paste. A 2.8M NaOH solution was added to the powders such that the w/s = 0.5. After setting at room temperature for two days, part of each paste was placed on a tray in a glass container which was partially filled with water. The samples were not immersed since the tray rested above the level of the water. The glass container was covered and placed in a 60°C oven for six days while the rest of the samples were left at room temperature to cure.

X-ray diffraction patterns and micrographs have been obtained for all of the samples listed in Table 5. A comparison of the diffraction patterns of Z02RT and Z0260 (which contain 75% B92 fly ash, 20% cement, and 5% clinoptilolite) is given in Figure 59. In all six pastes, the C-S-H peak in the RT sample is more intense and narrower than that in the 60°C sample. Figure 59 is a typical example of this phenomenon.

The microstructure of Z0260 (Figure 60) consists of crystallites in the midst of C-S-H foils. Particles resembling the intersecting disks found in B92NAL (Figure 46) and P12A80 (Figure 54) are also evident and were commonly seen throughout this sample.

Table 5. Cement pastes made with zeolite additions.

Sample	wt.% solids	w/s	solution	Curing temperatures (°C)
Z01	75 B92, 20 PC, 5 clinoptilolite (Castle Creek, IL)	0.5	2.8M NaOH	23, 60
Z02	75 B92, 20 PC, 5 clinoptilolite (Hector, CA)	0.5	2.8M NaOH	23, 60
Z03	75 B92, 20 PC, 5 chabazite	0.5	2.8M NaOH	23, 60
Z04	75 B92, 20 PC, 5 erionite	0.5	2.8M NaOH	23, 60
Z05	75 B92, 20 PC, 5 mordenite	0.5	2.8M NaOH	23, 60
Z06	75 B92, 20 PC, 5 phillipsite	0.5	2.8M NaOH	23, 60

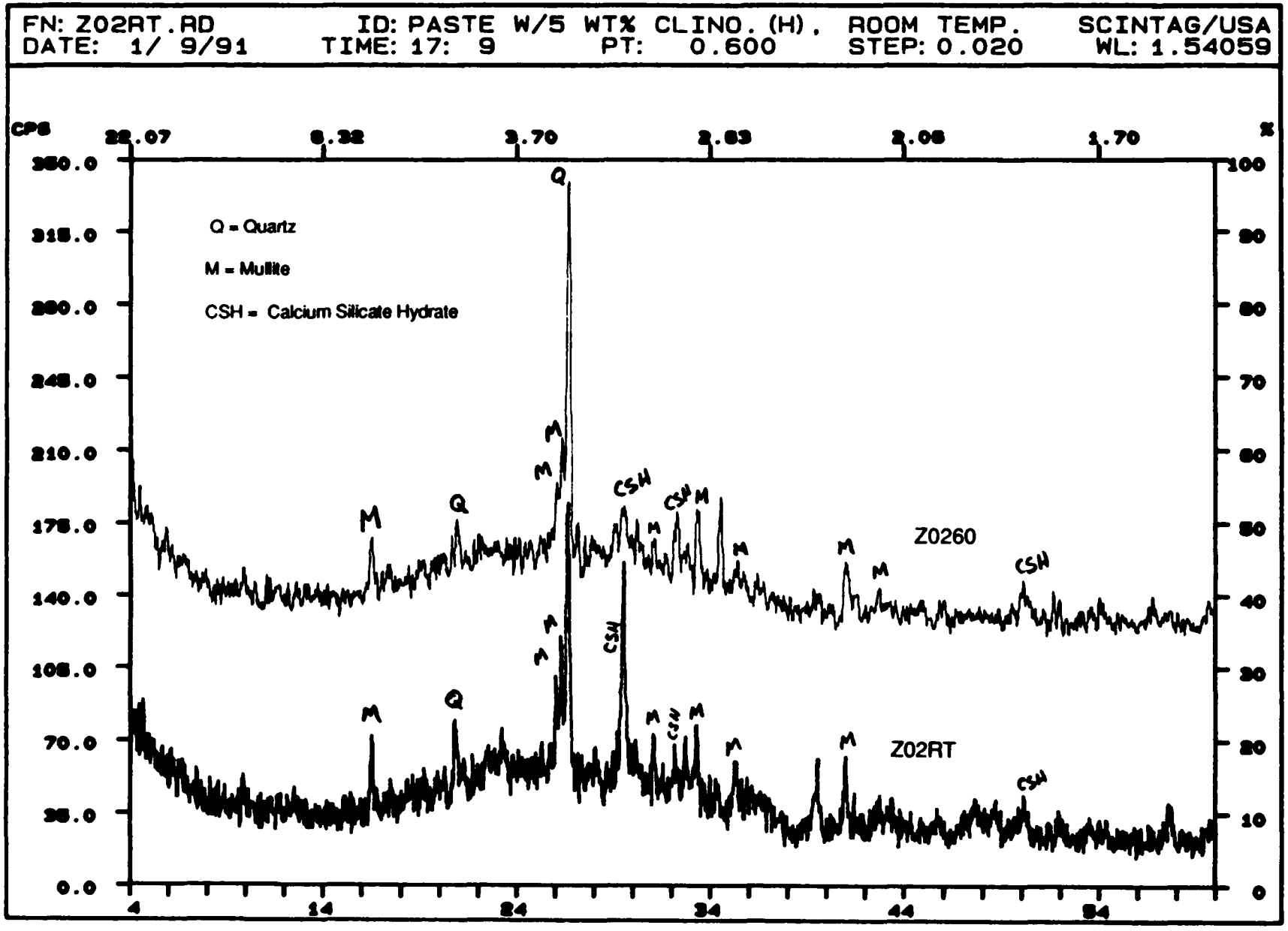

Figure 59. The diffraction patterns of Z02RT and Z0260 (75% B92, 20% cement and 5% clinoptilolite) depict a significant change in the C-S-H peak which occurred in all samples Z01 through Z06.

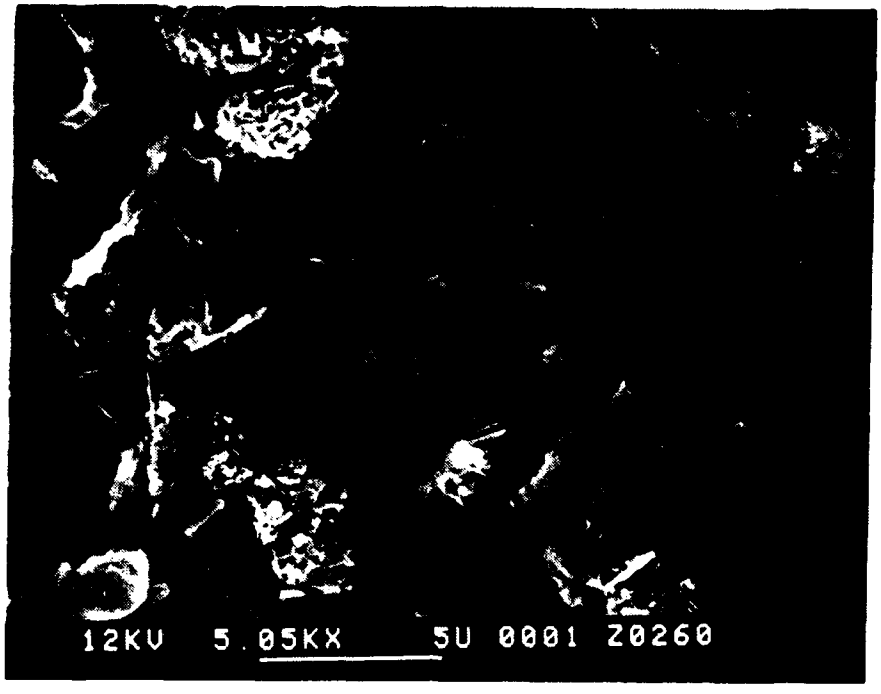

Figure 60. SEM photomicrograph of zeolite paste Z0260 [75% B92, 20% cement, 5% clinoptilolite (Hector, CA)] cured at 60°C for six days.

Comparisons of the diffraction patterns of as-received mordenite and Z0560 (75% B92, 20% cement, 5% mordenite) and of as-received phillipsite and Z0660 (75% B92, 20% cement, 5% phillipsite) are presented in Figures 61 and 62, respectively. In the case of Z0560, it appears that the mordenite has reacted and may no longer be present in the paste. Figure 63 depicts Z0560 which has round nodules covering the fly ash particles similar to P1079 (Figure 52).

In contrast to Z0560, phillipsite was not consumed in paste Z0660 as evidenced by the presence of the major phillipsite peaks in the Z0660 diffraction pattern. Figure 64 shows the microstructure which is dominated by reticulated C-S-H but also contains some of the clusters of intersecting-disks mentioned earlier.

As can be seen from the above work, zeolites are relatively easy to synthesize. In addition, under certain circumstances zeolites can coexist with C-S-H which is a cementing phase. Thus it should be feasible to produce a zeolite-cement composite from fly ash-enriched materials which is not only strong but is also toughened by the presence of the cogenerated zeolites. If this is true, these findings could lead to the development of entirely new technologies.

Summary and Conclusions

The work described in this report deals with a large number of issues ranging from the structure of C-S-H to the production of self-generating zeolite-cement composites.

Data collected for mixtures along isoalumina joins through the system CaO-Al_2O_3-SiO_2-H_2O have been used to construct an internally consistent "phase diagram" for room temperature phase relations in the system. The two C-S-H gels identified and characterized in Part I of the report, were also identified in the Part II kinetic studies of the hydration of C_3S as a function of pH. In both cases, a phase change seems to occur in the molecular structure somewhere in the vicinity of pH 11.5. In cement mixtures enriched with aluminosilicates such as fly ash, the addition of alkali hydroxides promotes the formation of zeolitic materials. Although the presence of zeolites is predicted by phase equilibrium work (Part I), their presence along isoalumina joins has not yet been verified (Part II). However, microstructural evidence gathered in Part III of the

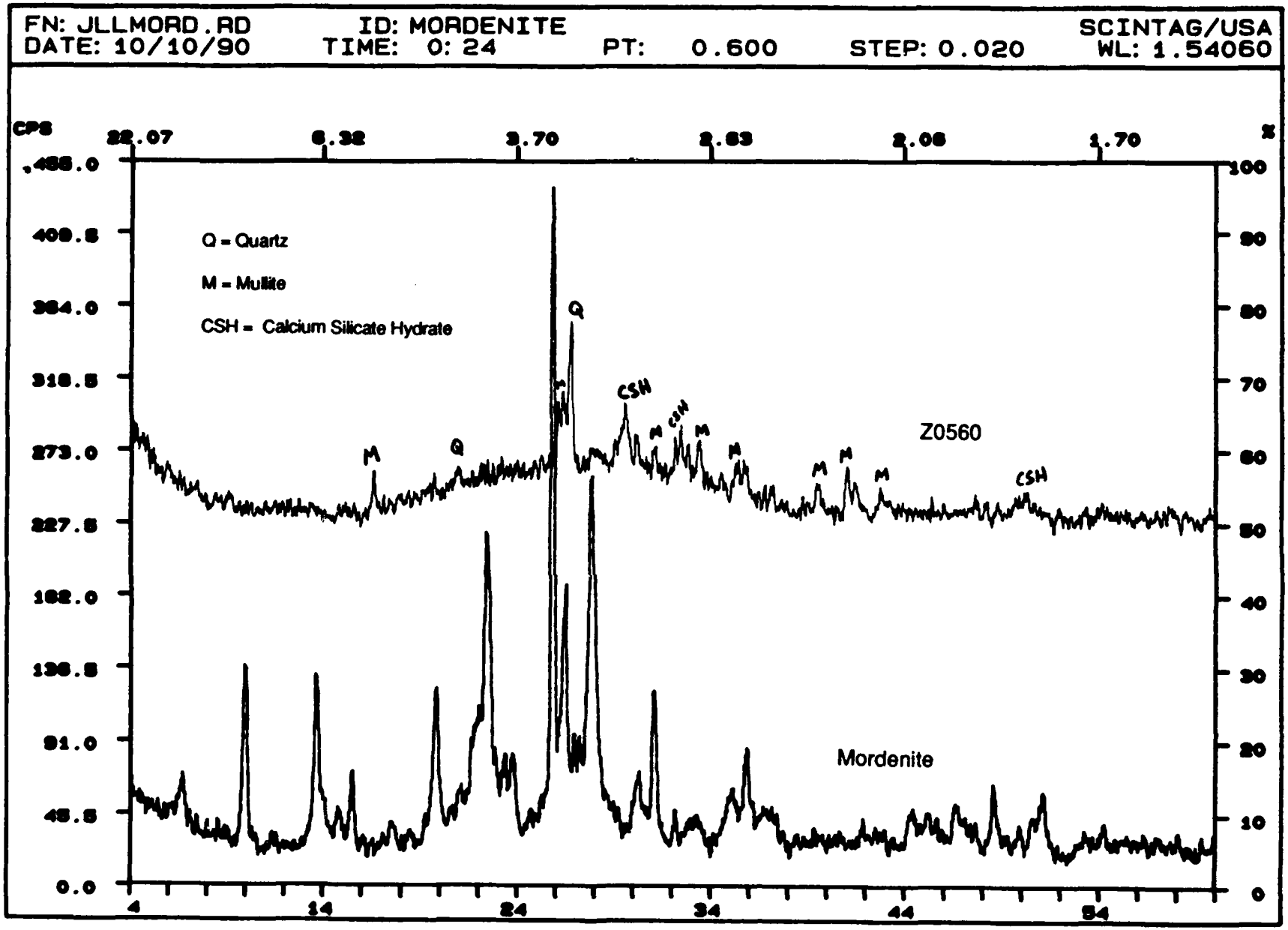

Figure 61. A comparison of the x-ray diffraction patterns of mordenite and Z0560 (5% mordenite, 75% fly ash, 20% cement) suggests that mordenite is not present in the Z0560 paste.

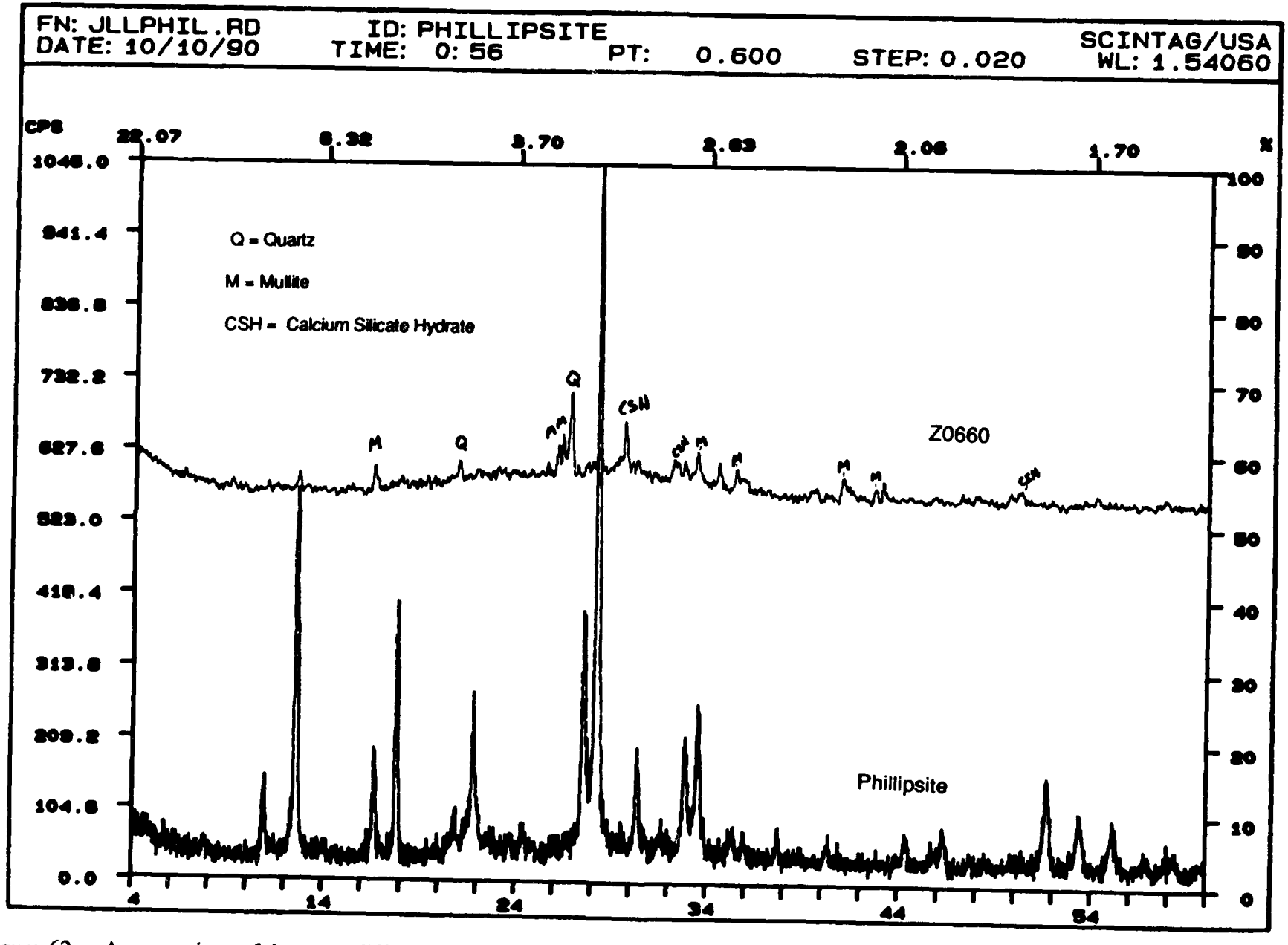

Figure 62. A comparison of the x-ray diffraction patterns of phillipsite and Z0660 (5% phillipsite, 75% B92, 20% cement) shows that phillipsite is still present in the Z0660 paste.

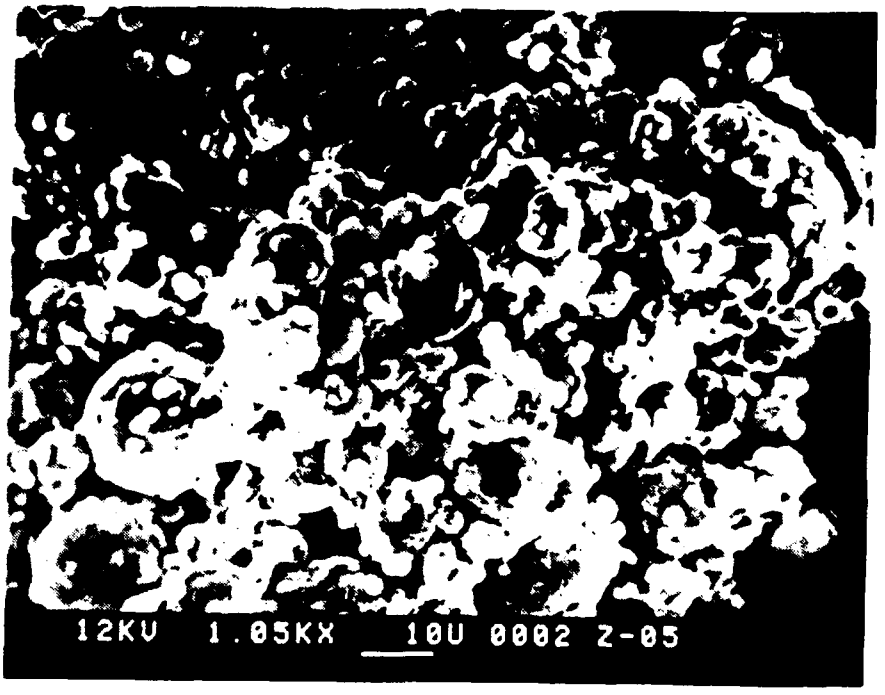

Figure 63. SEM photomicrograph of zeolite paste Z0560 (75% B92, 20% cement, 5% mordenite) cured at 60°C for six days.

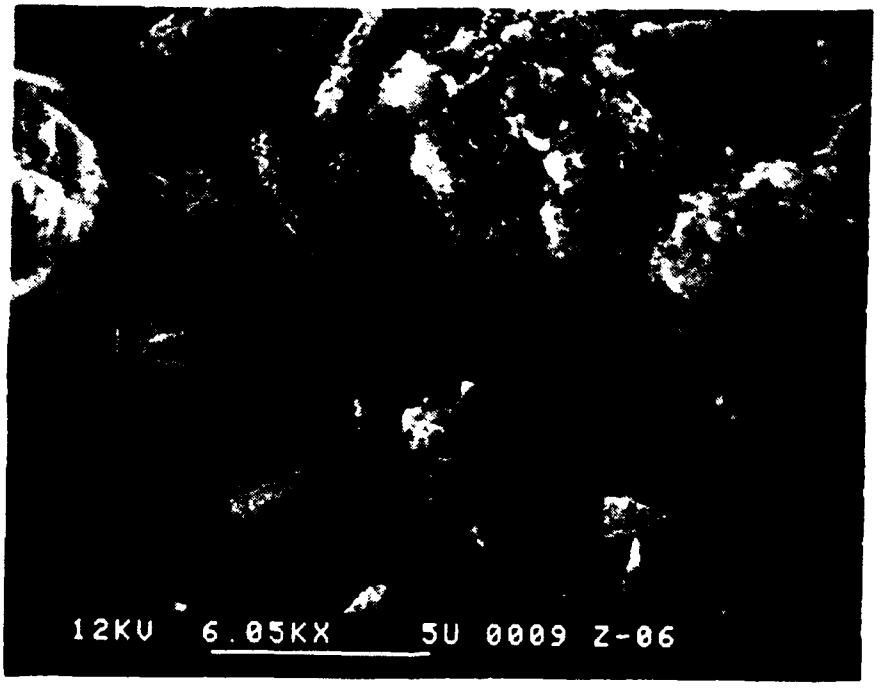

Figure 64. SEM photomicrograph of zeolite paste Z0660 (75% B92, 20% cement, 5% phillipsite) cured at 60°C for six days.

report, suggests that zeolites do indeed coexist with a C-S-H gel, and therefore it should be feasible to produce a zeolite-cement composite.

Although significant progress has been made, many questions still remain. More work is needed. For example, what is the effect of ionic strength on C_3S hydration; will hydration in NaCl differ from that in H_2O? What causes the acceleration of C_3S reaction rates at pH 11.5 and 12; is it $CaCl_2$ formation as HCl neutralizes $Ca(OH)_2$ in solution? Why are zeolites (Q_3Q_4 peaks) absent from the solution/sol mixed system? What are structures of gels occurring in the system Al_2O_3-SiO_2-H_2O and what bearing do they have on gel formation in the larger system containing lime (CaO-Al_2O_3-SiO_2-H_2O)? Hopefully, these questions as well as a host of others will be answered in the near future.

References

1. Ramachandran, A.R. and M.W. Grutzeck, "Hydration of Tricalcium Silicate at Fixed pH," 8th Intl. Congr. Chem. Cement, Rio de Janeiro, Vol. III, pp. 225-230 (1986).

2. Ramachandran, A.R. and M.W. Grutzeck, "Microstructural Development During Suspension Hydration of Tricalcium Silicate Under 'Floating' and Fixed pH Conditions," in Microstructural Development During the Hydration of Cement, Eds. C. Struble and P. Brown, Mat. Res. Soc. Symp. Proc. 85, Mat. Res. Soc., Pittsburgh, PA (1986).

3. Flint, E.P. and L.S. Wells, "Study of the System CaO-SiO_2-H_2O at 30°C and the Reaction of Water on the Anhydrous Calcium Silicates," J. Res. Natl. Bur. Standards 12, 751 (1934).

4. Roller, P.S. and G. Ervin, "The System Calcium Oxide-Silica-Water at 30°C. The Association of Silicate Ion in Dilute Alkaline Solution," J. Am. Chem. Soc. 62, 461 (1940).

5. Taylor, H.F.W., "Hydrated Calcium Silicates, Part I. Compound Formation at Ordinary Temperatures," J. Chem. Soc. 3682 (1950).

6. Grutzeck, M.W., A. Benesi and B. Fanning, "^{29}Si Magic Angle Spinning Nuclear Magnetic Resonance Study of Calcium Silicate Hydrate," J. Am. Ceram. Soc. 72, 665-668 (1989).

7. Ramachandran, A.R., Hydration of Tricalcium Silicate, M.S. Thesis, The Pennsylvania State University (1986).

8. Grutzeck, M.W. and A.R. Ramachandran, "An Integration of Tricalcium Silicate Hydration Models in Light of Recent Data," Cem. Concr. Res. 17, 164-170 (1987).

9. Diamond, S., J. Am. Ceram. Soc. 66 (1983).

10. Hoyle, S.L. and M.W. Grutzeck, "Incorporation of Cesium by Hydrating Calcium Aluminosilicates," J. Am. Ceram. Soc. 72, 1938-1947 (1989).

11. Sand, L.B. and F.A. Mumpton, Natural Zeolites, 546 pp., Pergamon Press, NY (1978).

12. Gottardi, G. and E. Galli, Natural Zeolites, 409 pp., Springer-Verlag, Berlin (1985).

13. Mumpton, F.A., "Utilization of Natural Zeolites" in Mineralogy and Geology of Natural Zeolites, Vol. 4, Reviews in Mineralogy Series, pp. 172-204, F.A. Mumpton (Ed.), Mineralogical Society of America (1977).

14. Jacobs, P.A. and J.A. Martens, Synthesis of High-Silica Aluminosilicate Zeolites, 390 pp., Elsevier, NY (1987).

15. Ottana, R., L.M. Saija, N. Burriesci and N. Giordano, "Hydrothermal Synthesis of Zeolites from Pumice in Alkaline and Saline Environment," Zeolites 2, pp. 295-298 (1982).

16. Burriesce, N., M. Liusa Crisafulli, N. Giordano, J.C.J. Bart and G. Polizzotti, "Hydrothermal Synthesis of Zeolites from Low-cost Natural Silica-alumina Sources," Zeolites 6, pp. 467-473 (1986).

17. Yoshida, Akira and Kouzou Inoue, "Formation of Faujasite-type Zeolite from Ground Shirasu Volcanic Glass,∏ Zeolites 6, pp. 467-473 (1986).

18. Hawkins, D.B., R.A. Sheppard and A.J. Gude, "Hydrothermal Synthesis of Clinoptilolite and Comments on the Assemblage of Phillipsite-clinoptilolite-mordenite," Pergamon Press, Oxford and New York, pp. 337-343 (1978).

19. Kuhl, Natural Zeolites, Springer-Verlag, Berlin Heidelberg, Germany (1985).

20. Barrier, Natural Zeolites, Springer-Verlag, Berlin Heidelberg, Germany (1985).

21. Fiedler, F.J., H.H. Lohse and K. Schurmann, "Synthesis of Zeolites in the System Na_2O-Al_2O_3-SiO_2-H_2O," N. Jb. Miner. Mh., pp. 358-364 (1983).

22. Davidovits, J., Geopolymer '88, Vol. 2, Universite de Technologie, Compiegne, France (1988).

23. Wu, X., W. Jiang and D.M. Roy, "Early Activation and Properties of Slag Cement," Cem. Concr. Res. 20, pp. 961-974.

24. Silsbee, M. and D.M. Roy, personal communication (1990).

25. Locher, F.W., "Hydraulic Properties and Hydration of Glasses of the System CaO-Al_2O_3-SiO_2," in Proc. Fourth Intl. Symp. Chemistry of Cement, Vol. I, pp. 267-276 (1960).

26. MacDowell, J.F., "Hydrogarnet-Gehlenite Hydrate Cements from CaO-Al_2O_3-SiO_2 Glases," in Proc. Eighth Intl. Symp. Chemistry of Cement, Vol. IV, pp. 423-428, Rio de Janeiro (1986).

27. Hoyle, S. and M.W. Grutzeck, "Effect of Pore Solution Composition on Cesium Leachability of Cement-Based Waste Forms," in Scientific Basis for Nuclear Waste Management X, Mat. Res. Soc. Symp. Proc. 84, pp. 309-317, J.K. Bates and W.B. Seefeldt (Eds.), Mat. Res. Soc., Pittsburgh, PA (1987).

28. Hoyle, S. and M.W. Grutzeck, "Effects of Phase Composition on the Cesium Leachability of Cement-Based Waste Forms," in Waste Management '86, Proc. Waste Isolation, Tech. Prog. Public Ed. 3, pp. 491-496, University of Arizona, Tucson, AZ (1986).

29. Bozich, S., Synthesis of Zeolites by Activation of Calcium Aluminosilicate Glasses, B.S. Thesis, Ceramic Science and Engineering, The Pennsylvania State University (1990).

Publications from AFOSR Grant No. 87-0395 (Partial and Fully Supported)

Hoyle, Susan Q., Ph.D. Thesis in Solid State Science, "Cesium and Strontium Partitioning During Hydration of Calcium Aluminosilicates," The Pennsylvania State University (1988). *Partial support.*

Hoyle, S. and M.W. Grutzeck, "Incorporation of Cesium by Hydrating Calcium Aluminosilicate," J. Am. Ceram. Soc. 72 (10):1938-1947 (1989). *Partial support.*

Grutzeck, M.W., A. Benesi and B. Fanning, "Silicon 29 Magic Angle Spinning Nuclear Magnetic Resonance Study of Calcium Silicate Hydrates," J. Am. Ceram. Soc. 72 (4):665-668 (1989). *Partial support.*

Kwan, S. and M.W. Grutzeck, "C-S-H Structure Types Formed from Mixtures of Lime-Alumina-Silica-Water," work in progress, to be submitted to J. Am. Ceram. Soc. (Part I of this report). Abstract accepted by ACS, Cincinnati, OH (1991). *Fully supported.*

Kwan, S. and M.W. Grutzeck, "C-S-H Structure Types Formed from C_3S at pH 11.5 and 12," work in progress, to be submitted to J. Am. Ceram. Soc. (Part II of this report). Incorporated in abstract mentioned above. *Fully supported.*

LaRosa, J. and M.W. Grutzeck, "Zeolite-Cement Composites," work in progress, to be submitted to J. Am. Ceram. Soc. (when additional funding is found and work is completed) (Part III of this report). Abstract accepted by ACS, Cincinnati, OH (1991). *Fully supported.*

Bozich, S., B.S. Thesis in Ceramic Science and Engineering, "Synthesis of Zeolites by Activation of Calcium Aluminosilicate Glasses," The Pennsylvania State University (1990).

Personnel Supported by AFOSR Grant No. 87-0395 (15 September 1987 to 14 December 1990)

Susan Q. Hoyle got her Ph.D. and is presently working as a research associate at Materials Research Laboratory. She was supported by AFOSR early in the program.

Avijit DasGupta received one year of support but, as a result of academic deficiencies, was unable to complete his work.

Stephen Kwan is currently making satisfactory progress towards his Ph.D. He has passed his candidacy, and is primarily working on his Ph.D. thesis work. Parts I and II of this report on NMR investigation of C-S-H are descriptions of his work to date. Stephen's degree will be in Solid State Science, an interdisciplinary program in materials at Penn State.

Judy LaRosa joined us late in the project. She has been with us for about one year. Her work on zeolite synthesis (Part III) suggests that it should be possible to synthesize a one-step zeolite-cement composite material. She has an M.S. in Ceramic Engineering from Ohio State University and has just recently passed her candidacy for the Ph.D. degree in Ceramic Science and Engineering.

Shari Bozich did her undergraduate thesis in ceramic science and engineering. She is presently looking for a job/applying to graduate school.

Reprints

journal

Reprinted from the Journal of the American Ceramic Society, Vol. 72, No. 4, April 1989

J. Am. Ceram. Soc., 72 [4] 665-68 (1989)

Silicon-29 Magic Angle Spinning Nuclear Magnetic Resonance Study of Calcium Silicate Hydrates

Michael Grutzeck,* Alan Benesi,* and Barry Fanning

Materials Research Laboratory and Department of Chemistry, The Pennsylvania State University, University Park, Pennsylvania 16802

The reaction products formed in a series of fully "equilibrated," room-temperature-hydrated, fumed colloidal silica plus lime water mixtures were examined using ^{29}Si magic angle spinning nuclear magnetic resonance. The data suggest that two structurally distinct calcium silicate hydrate (C-S-H) phases exist in the system $CaO–SiO_2–H_2O$. The more silica-rich C-S-H (Ca/Si=0.65 to 1.0) consists predominantly of long chains of silica tetrahedra (Q^2 middle units) similar to those found in 1.4-nm tobermorite. The studied more lime-rich C-S-H (Ca/Si=1.1 to 1.3) consists of a mixture of dimer (Q^1) and shorter chains (Q^1 end units and Q^2 middle units) similar to that reported for synthetic jennite. No monomer units (Q^0) were detected. [Key words: cements, calcium, silicates, nuclear magnetic resonance, hydrates.]

CALCIUM SILICATE HYDRATE (C-S-H), which forms during the hydration of the calcium silicates present in portland cement, is an X-ray amorphous material which is difficult to characterize. Although considerable information is available concerning the physical and chemical properties of C-S-H, its structure is still controversial. When tricalcium silicate is mixed with water, the C-S-H which forms consists of nanometer-thick, micrometer-sized foils which intergrow and densify during hydration.[1] It is generally accepted that the silicate anions (tetrahedra) present in C-S-H are polymerized and that their degree of polymerization increases with time.[2-4] Taylor[5] has suggested that C-S-H consists of disordered layers of short-range order materials with structures similar to those of jennite and 1.4-nm tobermorite.

Recently, Lippmaa *et al.*[6] demonstrated that ^{29}Si magic angle spinning nuclear magnetic resonance (MAS NMR) could be used to study the connectivity of the silica tetrahedra found in crystalline silicates. With this technique, "normal" 1.4-nm tobermorite was found to consist predominantly of middle units (Q^2) representative of chains of silica tetrahedra,[7-9] and jennite synthesized at 80°C by Hara and Inoue was found to contain both dimer and/or end units (Q^1) as well as middle units (Q^2).[9]

Since MAS NMR deals with structure on the angstrom scale, the technique is equally well suited to monitor the development of amorphous C-S-H during the hydration of tricalcium silicate. Barnes *et al.*[10] have shown that hydration begins with the production of the relatively simple monomeric hydrate (Q^0), which tends to persist, followed at later stages by a combination of dimer and/or end units (Q^1), and middle units (Q^2) which become increasingly abundant with time of hydration. An earlier study by Lippmaa *et al.*[11] and a more recent work by Young[12] also using MAS NMR to follow the kinetics of hydration of tricalcium silicate have shown that no significant monomer develops during the hydration reaction. Both of these studies show an early development of dimer (Q^1) followed by the development of middle units (Q^2) after approximately 15 h of reaction.

Stade and Wieker[13] studied solution-precipitated C-S-H using both molybdate and MAS NMR. They found that C-S-H (Ca/Si=1.3) precipitated at 0°C consisted primarily of monomer which quickly condensed to disilicate anions (Q^1) with lesser amounts of polysilicate anions (Q^2) forming with time. In companion papers[14,15] describing both 80° and 150°C material, Stade and his co-workers suggested that the structure of C-S-H with Ca/Si>1.1 consisted of a fixed ratio (1.2) of polysilicate (Q^2) to disilicate anions (Q^1), while materials with a Ca/Si ratio ≤1.0 tended to be richer in polysilicate (Q^2).

In related studies, Hara and Inoue[16,17] described the nature of the phases which formed when fumed colloidal silica was allowed to react with 80°C $Ca(OH)_2$ solutions. They observed that 1.4-nm tobermorite formed at Ca/Si≤0.9 and jennite at Ca/Si=1.1 to 1.5. Similarly, Wu and Young[18] observed that, in the presence of excess colloidal silica, a very low Ca/Si ratio (1.0), highly polymerized, C-S-H formed. Both studies reinforce Stade and co-workers' observation of a structural change at Ca/Si≈1.0.

The objective of the present study was to use MAS NMR to systematically investigate the structure of the various hydrated phases present at equilibrium in the system $CaO–SiO_2–H_2O$. The study was carried out in part to verify whether silica-sol-$Ca(OH)_2$-derived C-S-H consisted of a single phase or possibly two phases, and in part to determine whether structural data obtained for fully "equilibrated" C-S-H could be used to interpret existing ^{29}Si MAS NMR data. Our results suggest that two structurally distinct C-S-H phases exist in the system $CaO–SiO_2–H_2O$.

Experimental Method

Samples were prepared by combining varying amounts of fumed colloidal silica,[†] freshly calcined reagent-grade $CaCO_3$, and freshly boiled deionized water. The compositions that were studied are given in Table I. Mixtures A1 to A11, having a water/solid (W/S) ratio of 11.25 by weight, were allowed to hydrate at room temperature in sealed polyethylene bottles. They were monitored periodically for changes in pH[‡] for 2 years. After approximately 1 year, the A mixtures became highly viscous with time, making the measurement of pH difficult; therefore, to facilitate the measurement, a second set of mixtures were formulated (mixtures B1 to B15) having a W/S ratio of 200. pH was measured for two reasons: first, to track the mixtures' approach to equilibrium and, second, to delineate phase fields in the system $CaO–SiO_2–H_2O$. The measurement of pH as a function of time suggested that the mixtures approached equilibrium relatively rapidly since the pH values did not change to any appreciable extent (±0.1) after a month of hydration. Solution analyses were carried out using conventional emission spectroscopy.

Solid material for the MAS NMR study was separated from the solutions by centrifuging them for approximately 10 min. The liquid over all samples except mixture A1 was perfectly clear and easily decanted from the hydrated phases. After a small portion of each of the wet solids was saved for SEM examination, the remainder of the solid was freeze-dried.

MAS NMR spectra of the freeze-dried

J. F. Young — contributing editor

Manuscript No. 199111. Received May 27, 1988. Approved September 19, 1988.

Support for M. G. provided by National Science Foundation under Grant No. MSM-8304076 and Air Force Office for Scientific Research under Grant No. 87-0395.

*Member, American Ceramic Society.

*Department of Chemistry.

[†]Cab-O-Sil fumed silica, Cabot Corp., Tuscola, IL.

[‡]Ross pH electrode, Orion 611 pH meter, Orion Research Inc., Cambridge, MA.

Table I. Composition of Mixtures and Corresponding Fully Equilibrated Solutions

Mixture	CaO (mol%)*	Ca/Si†	pH	Ca (mmol·L⁻¹)	Si (mmol·L⁻¹)
A1	0.0	0	4.53		
A2	1.0	0.01	9.30		
A3	2.1	0.02	9.80		
A4	3.2	0.03	9.96		
A5	4.3	0.04	9.98		
A6	5.3	0.06	9.99		
A7	10.6	0.12	9.98		
A8	21.1	0.27	9.97		
A9	31.5	0.46	9.98		
A10	41.7	0.71	10.21		
A11	51.7	1.07	10.21		
B1	46.7	0.88	11.15	1.20	0.82
B2	47.7	0.91	11.44	1.48	0.39
B3	48.7	0.95	11.63	1.90	0.27
B4	49.7	0.99	11.81	2.84	0.19
B5	50.2	1.01	11.82	2.91	0.20
B6	50.7	1.03	11.95	3.89	0.16
B7	51.2	1.05	11.91	3.59	0.17
B8	51.7	1.07	11.90	3.51	0.17
B9	52.2	1.09	12.00	4.49	0.15
B10	52.7	1.12	12.04	4.86	0.14
B11	53.6	1.14	12.06	5.16	0.14
B12	53.7	1.16	12.11	5.98	0.13
B13	54.7	1.21	12.13	5.98	0.13
B14	55.7	1.26	12.20	6.73	0.12
B15	56.7	1.31	12.26	8.23	0.11

*Anhydrous basis. †Molar ratio of solid(s).

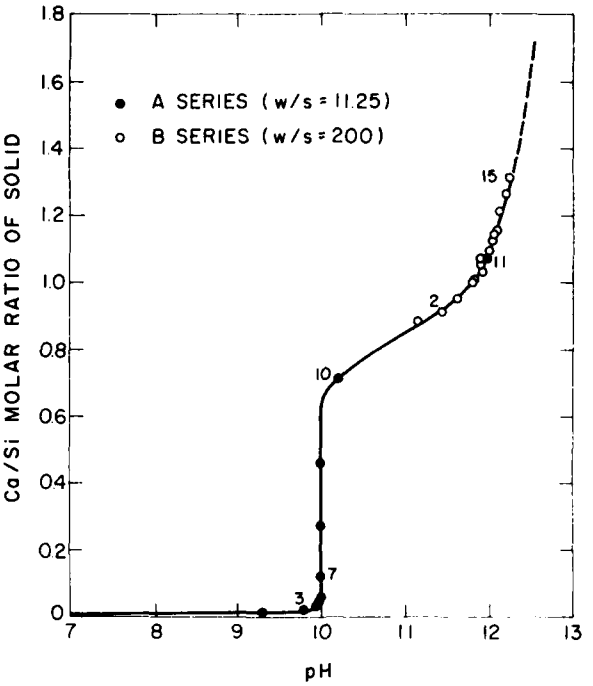

Fig. 1. Ca/Si molar ratio of the solid plotted as a function of the pH of the coexisting solution phase. Two invariances exist in the system, one at pH 9.9 and possibly one at 11.9, as indicated in the text.

samples were obtained at ambient temperature without decoupling or cross polarization on a spectrometer[§] operating at 59.17 MHz for ^{29}Si. Samples were spun at ~3 kHz. Chemical shifts were obtained relative to tetramethylsilane (TMS) by setting the transmitter frequency on-resonance for a separate sample of TMS, and then measuring offsets relative to this frequency. All spectra were obtained with a pulse width of 4 μs (~75° pulse), a relaxation delay of 11 s, and four dummy pulses to achieve steady-state magnetization. The number of transients collected was typically 1000 to 9000.

A scanning electron microscope[¶] was used to examine the microstructure of the hydrated phases and to check for carbonation. No trace of calcite was observed in any of the A mixtures. The B mixtures were not examined.

Results

The bulk compositions of the mixtures fall in various phase fields consisting of hydrated solid(s) and coexisting solution. Since the system is ternary and temperature and pressure are fixed, whenever two solid phases coexist with liquid, the system is by definition invariant. The two invariant triangles commonly associated with the system contain hydrous silica + C-S-H + solution, and C-S-H + $Ca(OH)_2$ + solution.[19] Compositions falling within the boundaries of these triangles consist of various proportions of the end-member phases whose compositions are fixed. Therefore, the systematic measurement of a solution variable such as pH as a function of the Ca/Si molar ratio of the solid (Ca/Si) would necessarily delineate the position of these invariances.

A plot of Ca/Si of the solid versus pH obtained for the A and B series of mixtures (Table I) is given in Fig. 1. An invariance is indicated by the vertical portion of the curve at pH 9.9 which extends from Ca/Si approximately 0.05 to 0.65. Over this interval, phases coexisting with solution are hydrous silica containing a few mole percent calcium oxide and C-S-H with a Ca/Si ratio of approximately 0.65. As the system becomes richer in calcium, i.e., Ca/Si>0.65, only the single solid phase, C-S-H, coexists with solution, the system is no longer invariant, and the pH is seen to rise. The curve is similar in form to the many equilibrium Ca/Si solid versus C_{CaO} curves in the literature, e.g., Steinour.[19] In fact, chemical analyses of the B mixture solutions after 9 weeks (Table I) showed that they fell on these same curves, indicating that equilibrium had indeed been achieved.

However, if two C-S-H phases were to coexist, the system would once again become invariant. The curve for C-S-H which is given in Fig. 1 may in fact contain such a small two-phase region at pH 11.9 where two C-S-H phases having Ca/Si ratios of 1.0 and 1.1 could coexist with solution.

The measured ^{29}Si MAS NMR chemical shifts for six key samples (numbered samples in Fig. 1) as a function of their Ca/Si ratio are given in Table II. To aid the discussion, the spectrum for each sample has also been plotted, and these are shown with the MAS NMR spectra for tobermorite and jennite (see Fig. 2). The spectrum for hydrous silica (Ca/Si=0.02) is similar to those given in the literature.[20] The peaks at −100.7 and −114.5 ppm are attributed to $HOSi(OSi)_3$ and $Si(OSi)_4$, respectively, which are characteristic of tertiary (Q^3) and quaternary (Q^4) networks of silica tetrahedra[6] found in silica gel. Apparently the addition of 2 mol% CaO to silica gel does not alter its structure to any significant extent. The spectrum of the invariant sample with Ca/Si=0.12 (hydrous silica + C-S-H + solution) consists of peaks representing the same silica gel (−100.7, −114.7 ppm) and an additional peak at −85.0 ppm. The new peak is characteristic of secondary (Q^2) unbranched chains of silica tetrahedra.[6] The spectra for mixtures with Ca/Si=0.71 and 0.91 (single-phase C-S-H) contain similar Q^2 peaks at −85.0 and −86.8 ppm, respectively. Although the chains are relatively long, there is a suggestion that they become shorter with increasing Ca content of the mixtures since a small shoulder attributable to end groups (Q^1) can be seen in the Ca/Si=0.91 sample. The spectrum for the sample with Ca/Si=1.07, which has a pH of approximately 12, contains two peaks: a peak at −85.8 ppm, which is again attributed to Q^2 middle units, and an additional peak at −79.2 ppm. This new peak corresponds to dimer and/or end-unit

[§]Chemagnetics CMC-300A, Chemagnetics Inc., Ft. Collins, CO.
[¶]ISI DS-130, International Scientific Instruments Inc., Milpitas, CA.

silica tetrahedra (Q^1).[6] The final sample (Ca/Si=1.31), whose spectrum matches that of the Ca/Si=1.07 sample, also contains Q^1 and Q^2 peaks at −86.6 and −80.4 ppm, respectively.

In addition to the MAS NMR data given above, which indicate structural differences in the C-S-H, the consistency of the A-series sample with Ca/Si=1.07 was noticeably "thicker" and the microstructure more "foillike" than the most silica-rich companion sample with Ca/Si=0.71 and, unlike samples having Ca/Si ratios of 0.02, 0.12, and 0.71, contained no standing water. Finally, X-ray diffraction patterns of the two C-S-H phases, which reflect longer-range order, tended to show no such differences; both patterns resembled Taylor's C-S-H (I).[5]

Discussion

The reported MAS NMR spectra, as well as the shape of the C-S-H portion of the Ca/Si versus pH curve obtained during the present study, are compatible with the hypothesis that, at equilibrium, two structurally distinct C-S-H phases exist in the system $CaO–SiO_2–H_2O$. Figure 3 shows a "not impossible" schematic representation of the proposed two C-S-H system. The figure contains the usual two three-phase invariant triangles mentioned earlier, viz., silica gel+C-S-H+solution and C-S-H+$Ca(OH)_2$+solution, as well as a third, suggested by the present study, representing the coexisting phases C-S-H (Ca/Si=1.0), C-S-H (Ca/Si=1.1), and solution (pH 11.9).

The spectra of the more silica-rich C-S-H (Ca/Si=0.65 to 1.0) given in Fig. 2 are dominated by a single Q^2 peak which represents chains of silica tetrahedra similar to those found in "normal" 1.4-nm tobermorite.[7,9] The observations parallel the findings of Stade and his co-workers,[13-15] Hara and Inoue,[16,17] as well as Wu and Young,[18] who observed an increasing tendency to form polysilicate and/or tobermorite in their low Ca/Si ratio C-S-H precipitates.

The spectra of the more lime-rich C-S-H (Ca/Si=1.1 to 1.3) obtained during the present study consist of two peaks having, what appears to be, a fixed Q^2/Q^1 peak height ratio of 0.7. These results suggest that the more lime-rich C-S-H is dominated by dimer and/or end groups (Q^1) and to a lesser extent chains of silica tetrahedra (Q^2) and that the structure of this C-S-H is relatively insensitive to changes in composition. The spectra for the lime-rich C-S-H recorded during this study are similar to that reported for 80°C synthetic jennite,[9] although jennite's Q^2/Q^1 ratio of 1.5 is significantly larger. Once again, these results parallel those reported by Stade and his co-workers[14,15] inasmuch as they also report a similar tendency of their lime-rich C-S-H to contain both polysilicate and disilicate anions having a fixed ratio of 1.2. Finally, Hara and Inoue[16,17] successfully synthesized jennite only when their Ca/Si ratio exceeded 1.1.

Table II. Observed ^{29}Si Chemical Shifts (ppm) as a Function of C/S Ratio of Solids

Mixture	C/S	Q^1	Q^2	Q^3	Q^4
A3	0.02			−100.7	−114.5
A7	0.12		−85.0	−100.7	−114.7
A10	0.71		−85.0		
B2	0.91		−86.8		
A11	1.07	−79.2	−85.8		
B15	1.31	−80.4	−86.6		

The suggestion that two structurally distinct C-S-H phases exist in this system is strengthened by the fact that the observed transition from the "one-peak" to the "two-peak" situation is abrupt (<4 mol% CaO separate the spectra) rather than gradual, which might be expected if changes were attributable to adsorption or variation in a solid-solution series. In addition, the Ca/Si versus pH curves, taken as a function of time, have repeatedly contained a noticeable inflection at a pH of approximately 11.9, signifying the presence of the invariant phase assemblage C-S-H (C/S=1.0)+CSH (C/S=1.1)+solution. Finally, the existence of two C-S-H phases in the system $CaO–SiO_2–H_2O$ tends to confirm earlier suggestions of invariance found in the works of Roller and Irvin,[21] Flint and Wells[22] (see Fig. 4), and Ramachandran[23] which occur at a pH of approximately 11.5.

In toto, the work suggests that two gellike materials having different short-range order can coexist at equilibrium; i.e., gel immiscibility may in fact exist on the nanometer scale in X-ray amorphous materials. However, the nature of the phase separation is still under study. Clearly, the more silica-rich C-S-H has a tobermorite-like structure consisting of relatively long chains of silica tetrahedra with little or no contribution from end groups (Q^1) except perhaps at its upper stability limit (Ca/Si=1.0). The structure of the lime-rich C-S-H is more problematic. Since the Q^2/Q^1 ratio of these materials is very sensitive to synthesis temperature,[15] at this point one can only infer that it consists of a mixture of dimer and shorter chains of silica tetrahedra similar to that reported in jennite.[9] In ad-

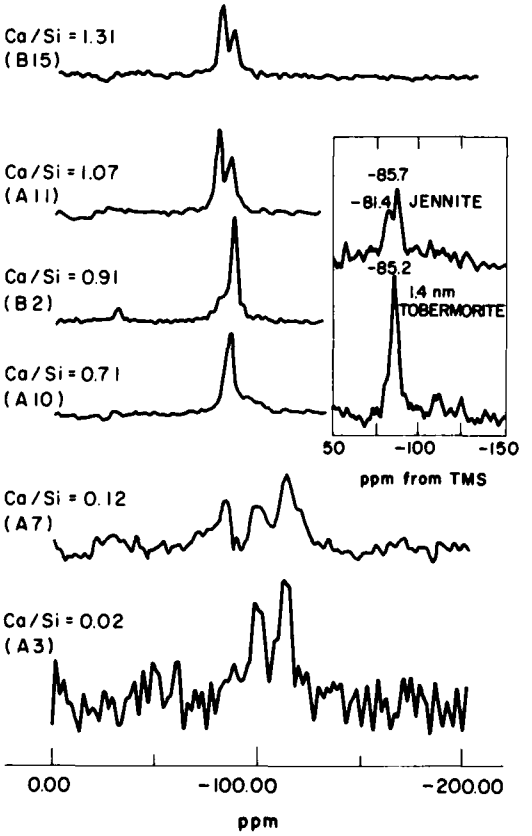

Fig. 2. ^{29}Si MAS NMR spectra of mixtures in the system $CaO–SiO_2–H_2O$. Chemical shifts are reported relative to TMS. The insert has been adapted from Komarneni *et al.*[9]

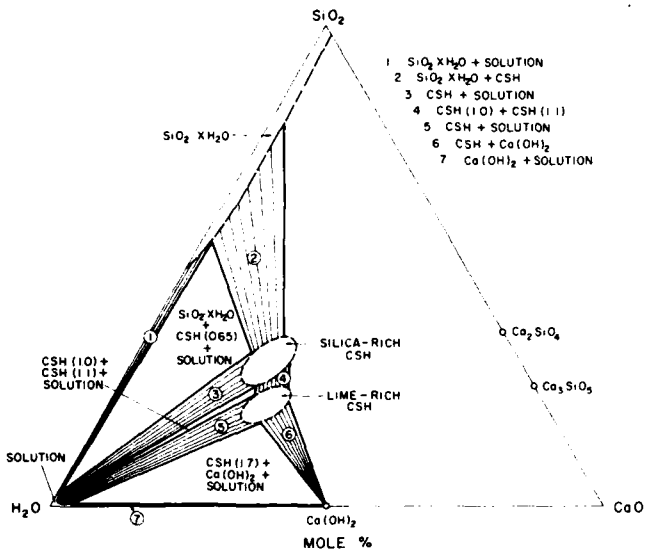

Fig. 3. Schematic representation of proposed room-temperature phase relations in the system $CaO-SiO_2-H_2O$. The compositions of the hydrated solids are based on present experimental data and previously reported H_2O/Ca ratios for C-S-H (2.5 saturated, 1.4 "dry").[5] For sake of representation of the overall phase relations, the solution data[19] have been exaggerated in order to show the bounding two-phase areas (numbered 1 to 7) for the three-phase triangles. Each of the triangles represents an invariant situation. Thus mixtures falling within the boundaries of these triangles will consist of varying proportions of the phases represented by the corners of the triangle; i.e., the compositions of the end-member phases (solids and solution) remain constant, whereas the overall bulk composition of the mixtures will vary.

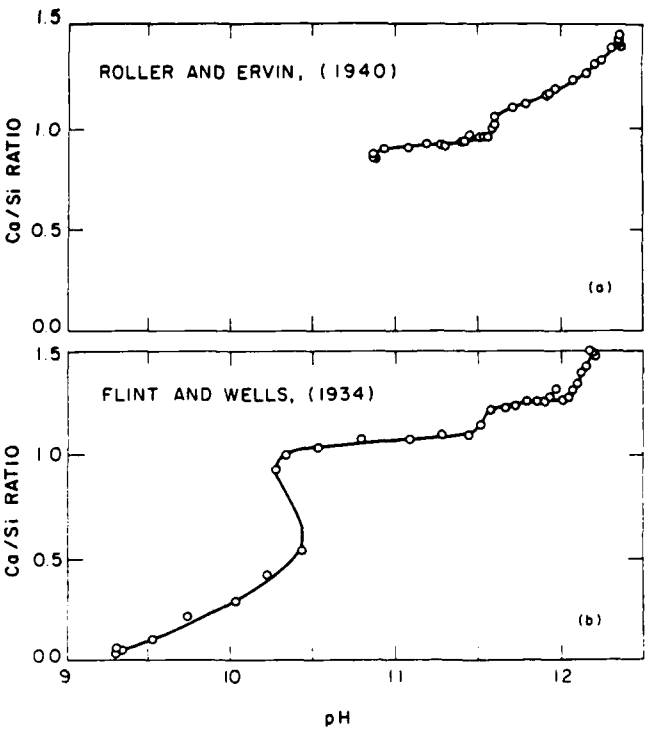

Fig. 4. Ca/Si molar ratio of the solid versus calculated pH of the coexisting solution phase. The original data of Roller and Irvin[21] and Flint and Wells[22] have been reworked by Ramachandran,[23] from which this figure is taken.

dition, if the more lime-rich C-S-H has a fixed Q^2/Q^1 ratio, this would imply that the anionic silicate structure remains constant as the Ca/Si ratio changes, which further reinforces the concept of discrete phase formation. Stade *et al.*[15] have suggested the following mechanism to maintain charge balance in such a situation:

$$\equiv SiOH + OH^- \longrightarrow SiO^- + H_2O$$

Although it is often "dangerous" to speculate as to the relevance of these results to paste-hydration studies, it is at least interesting to note that the MAS NMR spectra obtained for the more lime-rich mixtures (Ca/Si=1.07 and 1.31) look identical to similar spectra obtained for long-duration, room-temperature, paste-hydrated samples of tricalcium silicate and water.[11,12] Finally, the absence of monomer (Q^0) in the equilibrium mixtures studied suggests that monomer formation may be confined to the very early surface attack of tricalcium silicate by water.

Acknowledgments

We thank C. Schauer and R. Gallager for their help in preparing the mixtures and monitoring pH and G. W. Wagner for help with the MAS NMR measurements. Helpful discussions with H. F. W. Taylor and S. Komarneni are appreciated.

References

[1]H. M. Jennings, B. J. Dalgleish, and P. L. Pratt, "Morphological Development of Hydrating Calcium Silicate as Examined by Electron Microscopy Techniques," *J. Am. Ceram. Soc.*, **64** [10] 567-72 (1981).

[2]F. D. Tamás, A. K. Sarkar, and D. M. Roy, "Effect of Variables Upon the Silylation Products of Hydrated Cements"; pp. 55-72 in Hydraulic Cement Pastes: Their Structure and Properties. Cement Concrete Association, Slough, U.K., 1976.

[3]L. S. Dent-Glasser, E. E. Lachowski, K. Mohan, and H. F. W. Taylor, "A Multi-Method Study of C_3S Hydration," *Cem. Concr. Res.*, **8**, 733-39 (1978).

[4]J. Hirljac, Z.-Q. Wu, and J. F. Young, "Silicate Polymerization During the Hydration of Alite," *Cem. Concr. Res.*, **13**, 877-86 (1983).

[5]H. F. W. Taylor, "Proposed Structure for Calcium Silicate Hydrate Gel," *J. Am. Ceram. Soc.*, **69** [6] 464-67 (1986).

[6]E. Lippmaa, M. Mägi, A. Samoson, G. Engelhardt, and A.-R. Grimmer, "Structural Studies of Silicates by Solid-State High-Resolution ^{29}Si NMR," *J. Am. Chem. Soc.*, **102**, 4889-93 (1980).

[7]W. Wieker, A.-R. Grimmer, A. Winkler, M. Magi, M. Tarmak, and E. Lippmaa, "Solid-State High-Resolution ^{29}Si NMR Spectroscopy of Synthetic 14 Å, 11 Å, and 9 Å Tobermorite," *Cem. Concr. Res.*, **12**, 333-39 (1982).

[8]S. Komarneni, R. Roy, D. M. Roy, C. A. Fyfe, G. J. Kennedy, A. A. Bothner-By, J. Dadok, and A. S. Chesnick, "^{27}Al and ^{29}Si Magic Angle Spinning Nuclear Magnetic Resonance Spectroscopy of Al-Substituted Tobermorites," *J. Mater. Sci.*, **20**, 4209-12 (1985).

[9]S. Komarneni, D. M. Roy, C. A. Fyfe, and G. J. Kennedy, "Naturally Occurring 1.4 nm Tobermorite and Synthetic Jennite: Characterization by ^{27}Al and ^{29}Si MASNMR Spectroscopy and Cation Exchange Properties," *Cem. Concr. Res.*, **17**, 891-95 (1987).

[10]J. R. Barnes, A. D. H. Clague, N. J. Clayden, C. M. Dobson, C. J. Hayes, G. W. Groves, and S. A. Rodger, "Hydration of Portland Cement Followed by ^{29}Si Solid-State NMR Spectroscopy," *J. Mater. Sci. Lett.*, **4**, 1293-95 (1985).

[11]E. Lippmaa, M. Magi, and M. Tamak, "A High Resolution ^{29}Si NMR Study of the Hydration of Tricalcium Silicate," *Cem. Concr. Res.*, **12**, 597-602 (1982).

[12]J. F. Young, "Investigations of Calcium Silicate Hydrate Structure Using Silicon-29 Nuclear Magnetic Resonance Spectroscopy," *J. Am. Ceram. Soc.*, **71** [3] C-118-C-120 (1988).

[13]H. Stade and W. Wieker, "Structure of 111-Crystallized Calcium Hydrogen Silicates. I. Formation and Properties of an 111-Crystallized Calcium Hydrogen Disilicate Phase" (in Ger.), *Z. Anorg. Allg. Chem.*, **466**, 55-70 (1980).

[14]H. Stadę, "Structure of 111-Crystallized Calcium Hydrogen Silicates. II. A Phase Consisting of Poly- and Disilicate" (in Ger.), *Z. Anorg. Allg. Chem.*, **470**, 69-83 (1980).

[15]H. Stade, A.-R. Grimmer, G. Engelhardt, M. Magi, and E. Lippmaa, "Structure of 111-Crystallized Calcium Hydrogen Silicates. VII. Solid State Silicon-29 NMR Studies on C-S-H (Di, Poly)" (in Ger.), *Z. Anorg. Allg. Chem.*, **528**, 147-51 (1985).

[16]N. Hara and N. Inoue, "Formation of Jennite from Fumed Silica," *Cem. Concr. Res.*, **10**, 677-82 (1980).

[17]N. Hara and N. Inoue, "Formation of Jennite and Its Thermal Behavior"; pp. 840-58 in Proceedings of the 1st International Symposium on Hydrothermal Reactions, 1982. Edited by S. Somiya. Tokyo Institute of Technology, Tokyo, Japan, 1983.

[18]Z.-Q. Wu and J. F. Young, "The Hydration of Tricalcium Silicate in the Presence of Colloidal Silica," *J. Mater. Sci.*, **19**, 3477-86 (1984).

[19]H. H. Steinour, "The Reactions and Thermochemistry of Cement Hydration at Ordinary Temperatures"; pp. 261-89 in the 3d International Symposium on the Chemistry of Cement, London, 1952. Cement Concrete Association, London, U.K., 1954.

[20]G. E. Maciel and D. W. Sindorf, "Silicon-29 Nuclear Magnetic Resonance Study of the Surface of Silica Gel by Cross Polarization and Magic Angle Spinning," *J. Am. Chem. Soc.*, **102**, 7606-607 (1980).

[21]P. S. Roller and G. Ervin, "The System Calcium Oxide-Silica-Water at 30°C. The Association of Silicate Ion in Dilute Alkaline Solution," *J. Am. Chem. Soc.*, **62**, 461-71 (1940).

[22]E. P. Flint and L. S. Wells, "Study of the System $CaO-SiO_2-H_2O$ at 30°C and the Reaction of Water on the Anhydrous Calcium Silicates," *J. Res. Natl. Bur. Stand. (U.S.)*, **12**, 751-83 (1934).

[23]A. R. Ramachandran, "Hydration of Tricalcium Silicate"; M.S. Thesis, Pennsylvania State University, University Park, PA, 1986. □

Reprinted from the Journal of the American Ceramic Society, Vol. 72, No. 10, October 1989

journal

J. Am. Ceram. Soc., 72 [10] 1938–47 (1989)

Incorporation of Cesium by Hydrating Calcium Aluminosilicates

Susan L. Hoyle and Michael W. Grutzeck*

Materials Research Laboratory, The Pennsylvania State University, University Park, Pennsylvania 16802

The leach behavior of cesium from a series of cement-based waste forms has been modeled in terms of pore solution concentration and phase formation data. Cement-based materials enriched in alumina and silica, and compositionally related glasses, were hydrated in the presence of cesium hydroxide to gauge the degree of partitioning of cesium by the developing hydrates. The compositions of the pore solutions extracted from the cement-based waste forms were compared with corresponding leach data for companion samples. In both pore solution and leachates, the retention of cesium was found to be directly related to the bulk composition of the waste form; the degree of partitioning of cesium by the hydrated phases increased as more alumina and/or silica were added to the formulation, suggesting that cesium-containing phases were forming. Additionally, the leachate concentration of cesium for any given composition was also found to be related to the pore solution concentration. This observation led to the development of a leaching model for cement-based waste forms in which the concentration of cesium in the leachate could be described in terms of pore solution concentration, diffusion, dissolution, and development of cesium host phases. Using this model, effective diffusion coefficients for cesium were calculated to be $\approx 2 \times 10^{-7}$ cm$^2 \cdot$ s^{-1}. Pollucite and cesium-substituted herschelite were identified as two of the hydration products of the studied glasses. The ability of these zeolites to strongly partition cesium suggests that small quantities of zeolitic phases may also be forming in the cement-based waste forms, thus explaining their compositionally related leach behavior. [Key words: cements, aluminosilicates, nuclear materials, cesium, leaching.]

I. Introduction

PORTLAND cement is commonly used to solidify and isolate low-level radioactive waste because it is a readily available, inexpensive, easy-to-use binder material which is adaptable to a variety of waste streams. Although portland cement is widely used in this role, certain elements such as cesium have always been more difficult to isolate than others. Recently, it has been demonstrated that blending of the portland cement binder with colloidal silica,[1] fly ash,[2] clays,[3] and/or zeolites[4] led to significant improvements in cesium leach rates. Although it is evident that improvements are compositionally related, the underlying mechanisms responsible for the improvements are still poorly understood.

Part of the difficulty in understanding the leaching behavior of cement-based waste forms is related to the fact that they are simultaneously multiphasic and porous. The majority of the solid phases are poorly crystalline calcium silicate hydrates which coexist with a liquid phase residing in the pore space. During hydration, ions in the waste stream are partitioned between the hydrating solid phases and the remaining pore solution, the partitioning driven by equilibrium considerations. During leaching, both the solid phase and the pore solution are able to interact with the leachate in a variety of ways. The diffusion, dissolution and/or precipitation reactions, which occur as the system (waste form and leachate) tries to reestablish the status quo, are collectively known as the leaching behavior of the waste form. Thus, for a waste form to have a relatively low leach rate, it must also have a high/solid liquid partitioning ratio which, in turn, would further imply the existence of a crystal chemically suitable host phase for the ion in question.

Although many investigators have studied the leaching behavior of cement-based materials, relatively few have investigated changes in pore solution composition of the waste form in order to understand the leaching process. The objective of the present study was twofold: first, to determine the effect of bulk composition on the leach behavior of a series of cesium hydroxide-doped cement-based waste forms, and second, to relate the observed leach behavior of the waste forms to the corresponding pore solution and phase data for the same or related samples. The observation of a direct relationship between the leach behavior and the cesium concentration of the pore solution, along with the identification of zeolitic host phases, has led to the development of a model in which the leaching behavior of the waste form can be described in terms of pore solution concentration, diffusion, dissolution, and development of cesium host phases.

II. Experimental Procedure

Two sets of samples were prepared (see Fig. 1). The cement-based waste forms, mixtures 1 to 5, were formulated from commercially available cements and colloidal silica. Because the hydrates which formed were usually poorly crystalline and thus X-ray amorphous, this set of samples was primarily used to determine leaching behavior and pore solution composition. Because portland cement and calcium aluminate cement are multiphasic, early hydration reactions are often controlled by the rates of reaction of the individual anhydrous phases rather than by bulk chemical equilibrium. To minimize this complication and to enhance development of possible cesium-containing phases, four calcium aluminosilicates, glasses 6 to 9, were prepared and hydrated in CsOH solution. Details of the sample preparation are given below.

(1) Cement-Based Waste Forms

The cement-based mixtures were formulated from portland cement, calcium aluminate cement, and condensed silica fume (see Table I for the analysis of the starting materials). Each of the starting materials is composed of varying amounts of CaO, Al_2O_3, and SiO_2. The other major components (MgO and Fe_2O_3) behave in a similar chemical fashion to CaO and Al_2O_3, respectively; thus the bulk compositions of the starting materials were normalized to 100% by adding the percentages of MgO to CaO, Fe_2O_3 to Al_2O_3, and combining these with SiO_2. Using these normalized values, compositions of the five cement mixtures were formulated such that the ratio of two of the components was kept constant while the third was varied. This concept is illustrated by the dashed lines in Fig. 1. For example, mixtures 3, 4, and 5 all have the same CaO/SiO_2 ratio but vary in Al_2O_3 content.

C. M. Jantzen — contributing editor

Manuscript No. 198845. Received September 30, 1988; approved March 21, 1989.
Supported by the Basic Energy Sciences Division, U.S. Department of Energy, under Grant No. DE-FG02-84ER45145.
*Member, American Ceramic Society.

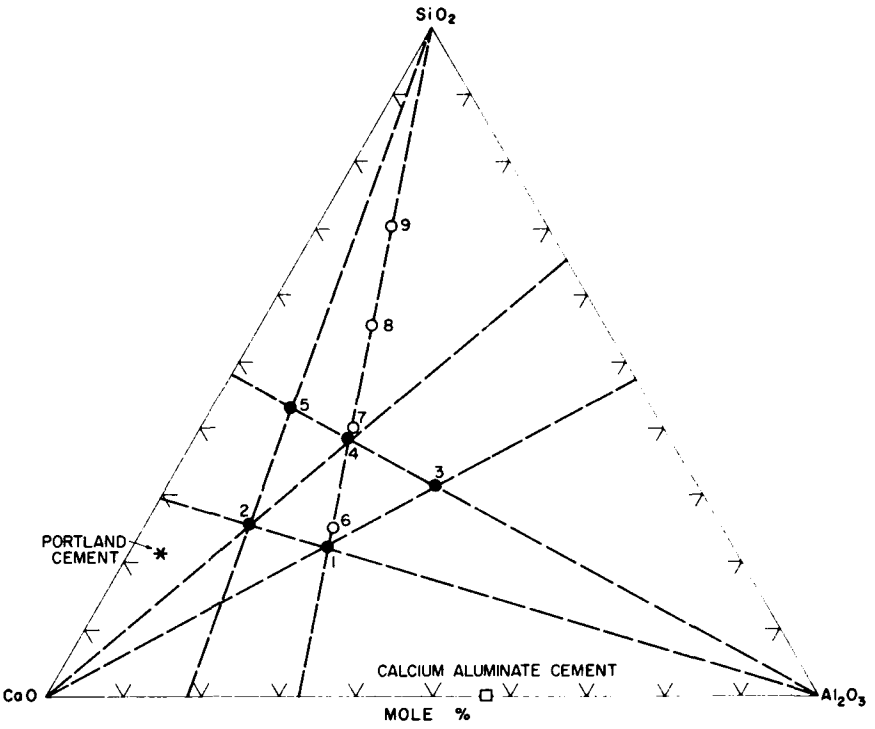

Fig. 1. Compositional diagram illustrating the relative position and relationships of the studied mixtures. Solid circles (1 to 5) represent compositions of cement-based waste forms, open circles (6 to 9) represent compositions of glasses, and the asterisk and box, respectively, represent the normalized composition of portland and calcium aluminate cement used as starting materials.

Appropriate amounts of portland cement, calcium aluminate cement, and silica fume were dry mixed and then blended with a solution containing deionized (DI) water, CsOH, and superplasticizer (Table II) according to ASTM[5] procedures. In the leaching experiments, the mixing solution contained 5 g of CsOH per 100 g of DI water ($\approx 0.33M$), and the formulations had a solution-to-solid (W/S) ratio of 0.6 by weight. The samples to be leached (LT-series) were cured for 28 d at 38°C and 98% relative humidity, then cut and leached using a modified MCC-1[6] static leach test. The MCC-1 procedure was modified by increasing the surface-area-to-volume (SA/V) ratio from 1.0×10^{-2} to 1.2×10^{-2} mm^{-1}, by using triplicate samples for each of the time periods and by using only DI water as leachant. Leachate solutions were analyzed at 3, 7, 14, 28, 56, and 90 d for Ca, Al, Si, Na, and K using dc-plasma emission spectrometry. Cesium was analyzed using atomic absorption spectroscopy. The leached pellets were examined using conventional X-ray diffraction (XRD) and scanning electron microscopy (SEM) techniques.

Pastes with the same compositions were also prepared with a higher W/S ratio of 1.0 to aid in the collection of pore solutions (PS-series). However, the amount of CsOH in the mixing water was reduced to 3 g of CsOH to 100 g of DI water ($\sim 0.20M$) for the pore expression samples in order to maintain the same Cs-to-cement ratio established for the leachate experiments. These samples were also cured at 38°C and the pore solutions were expressed under pressure (44 MPa) in a stainless steel die similar to that described by Barneyback and Diamond[7] at 3, 7, 14, 28, 56, and 90 d. Pore solutions were similarly analyzed for Ca, Al, Si, Na, K, and Cs.

(2) Calcium Aluminosilicate Glasses

Glasses 6 to 9 were formulated with a constant CaO/Al_2O_3 molar ratio and increasing SiO_2 content (see Fig. 1). The amounts of the starting materials (reagent-grade $CaCO_3$,* high-purity gibbsite,† and fumed colloidal silica‡) used to formulate the glasses are given in Table III. After these components were milled with methyl alcohol and alumina media for 24 h, the media were separated from the suspension and the suspension was dried at 90°C for an additional 24 h. The resultant powder was calcined at 800°C for 12 h prior to melting at ~1625°C for 2 h. The molten glasses were water quenched and ground to powders having specific surface areas ranging from 0.29 to 0.84 m^2/g (see Table III). The powders were examined with optical and transmission electron microscopy and were found to be free of crystals.

In order to study phase formation during hydration, 10 g of glass powder was added to 100 g of the $\sim 0.33M$ CsOH solution. In this case the relative proportions of cesium to solid phase was increased to enhance the formation of cesium-containing crystalline materials. The glass samples were hydrated at 38° and also 90°C to determine the effect of temperature on phase formation. The solution in contact with the glass powder was sampled at 15, 28, 56, and 90 d and analyzed for Ca, Al, Si, and Cs using the spectroscopic techniques discussed earlier. Some solid was also removed at these times and analyzed by SEM and XRD.

Table I. Chemical Analysis of Starting Materials

Oxide	Composition (wt%)		
	Type I portland cement	Calcium aluminate cement	Condensed silica fume
SiO_2	20.84	0.68	95.32
Al_2O_3	4.10	71.3	0.02
TiO_2	0.27	0.01	<0.01
Fe_2O_3	2.90	0.09	0.08
MgO	4.05	0.46	0.19
CaO	63.84	26.80	0.38
MnO	0.21	<0.01	<0.01
SrO	0.05	0.02	<0.01
BaO	0.02	0.01	<0.01
Na_2O	0.07	0.37	0.08
K_2O	0.74	0.02	0.55
Rb_2O	<0.01	<0.01	<0.01
Cs_2O	<0.01	<0.01	<0.01
P_2O_5	0.21	0.05	0.06
SO_3	2.67	0.04	0.24
LOI*	1.32	0.70	3.05

*Loss on ignition.

*Fisher Scientific, Pittsburgh, PA.
†Alcoa, Bauxite, AR.
‡Cabot Corp., Tuscola, IL.

Table II. Amounts of Starting Materials Used to Formulate Cement-Base Waste Forms

Mixture*	Starting material (g)					
	PC[†]	CAC[‡]	CSF[§]	DI-H_2O[¶]	CsOH	Mighty RD-1P**
LT1	174.78	193.58	38.01	243.87	12.17	15.93
LT2	280.41	92.83	34.02	244.88	12.21	15.83
LT3	43.65	266.37	95.20	243.15	12.17	15.97
LT4	141.23	156.37	110.44	244.78	12.23	15.93
LT5	215.57	71.58	122.03	245.51	12.23	15.98
PS1	349.65	387.19	75.96	811.91	24.40	7.09
PS2	560.74	183.56	67.98	812.38	24.36	6.84
PS3	87.18	532.83	190.42	810.45	24.38	6.98
PS4	282.42	312.82	220.80	816.00	24.46	7.02
PS5	431.22	143.17	243.99	818.43	24.54	7.04

*LT1–LT5 are the samples used for leach testing and PS1–PS5 are the samples used for pore expression analysis. †Portland cement. ‡Calcium aluminate cement. §Condensed silica fume. ¶Deionized water. **Superplastizer used to increase the workability of the cement pastes.

Table III. Amounts of Starting Materials Used to Formulate Glasses and Their BET Surface Areas After Grinding

Glass	$Al(OH)_3$ (g)	$CaCO_3$ (g)	SiO_2 (g)	Surface area (m^2/g)
6	113.89	146.13	43.87	0.29
7	93.61	120.11	72.11	0.52
8	71.77	92.08	100.95	0.79
9	49.93	63.06	132.80	0.84

III. Results

(1) Leaching Behavior of Cement-Based Waste Forms

The cesium content of the leachate ($mmol \cdot L^{-1}$) as a function of time is given in Fig. 2. Mixture 2, the closest in composition to pure portland cement, had significantly higher cesium leachate concentration than the other mixtures. Comparison of mixtures falling along dashed lines in Fig. 1 graphically illustrates the effect of varying bulk composition of the waste form on its leach behavior. For example, the concentration of cesium in the leachate (>28 d) decreases as the alumina content of the formulation increases (Cs in solution for mixture 5 > 4 > 3 and mixture 2 > 1). Similarly, as the silica content increases, the Cs in solution decreases (mixture 1 > 4 and mixture 2 > 5). The overall effect is apparently related to the lime content of the formulation (Cs in solution for mixture 1 > 3 and mixture 2 > 4). The leachate data for mixtures 1 and 3 include a maximum in the cesium concentration–time curves of these mixtures prior to 3 d, suggesting that a cesium-containing phase was forming at that time.

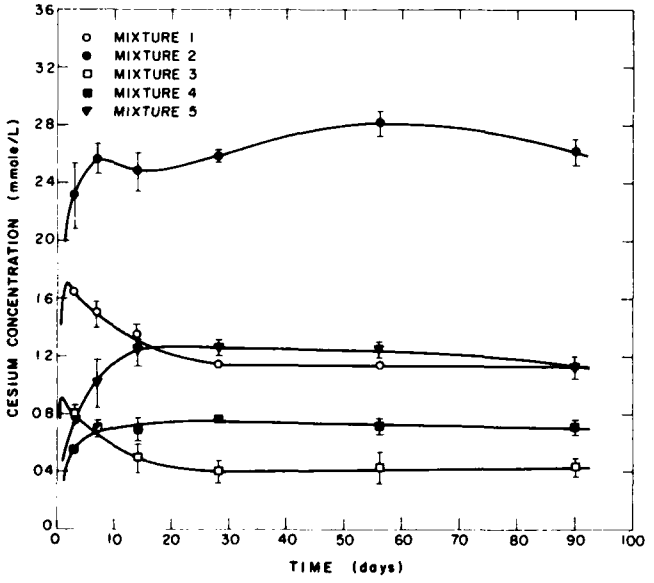

Fig. 2. Cesium leachate concentration for mixtures LT1 through LT5, as function of leaching time. Error bars represent ±1 standard deviation of triplicate samples. When no error bars are present, the standard deviation is less than size of symbol.

The phase composition of each of the studied mixtures as determined by XRD is given in Table IV. In addition to hydrogarnet, strätlingite, gibbsite, and unreacted cement, mixtures 1 and 3 also contained a trace of an unknown phase which was not found in the other mixtures.

(2) Pore Solution Composition of Cement-Based Waste Forms

The cesium concentration found in the pore solution, as a function of curing time, is given in Fig. 3. The initial cesium content of the mixing solution was ~160 $mmol \cdot L^{-1}$. In all cases, the cesium content decreases with time, indicating that cesium is being partitioned into the hydrating cement paste; otherwise the cesium concentration would increase as water was preferentially assimilated by the developing hydrates. Mixtures 1 and 5 exhibit relatively early and significant uptake of cesium occurring before the 3-d samples were taken. Mixtures 3, 4, and 5 exhibit a continuous decrease in cesium concentration after 3 d, whereas mixtures 1 and 2 exhibit a sudden decrease in cesium content after 28 and 7 d, respectively. The initial 3-d decrease in the more silica-rich mixtures (mixtures 3, 4, and 5) could be interpreted as sorption of cesium onto the silica fume[1,2] or to its incorporation in an Al-rich calcium silicate hydrate (C–S–H),[8] but the later drop in cesium concentration for mixtures 1 and 2 after 28 and 7 d, respectively, and the continued decrease in cesium concentration for the remaining mixtures suggest the formation of a cesium host phase. By 56 d of curing, the concentration of cesium in the pore solution of mixtures 1, 3, and 4 have decreased to values below 5 $mmol \cdot L^{-1}$ and remain low throughout 90 d.

The effect of bulk composition on the cesium pore solution concentration may be seen by comparing the results given in this figure with the compositions presented in Fig. 1. After 90 d, the concentration of cesium in the pore solution (mixture 5 > 4 > 3 and mixture 2 > 1) suggests that an increase in alumina content of the formulation promotes the uptake of cesium from the pore solution. Conversely, a decrease in the lime content of the formulation appears to enhance the cesium removal (Cs in solution for mixture 2 > 4). As a group, mixtures 1, 3, 4, and 5 exhibit a relatively strong tendency to partition cesium into the developing hydrated phases, whereas mixture 2 does not, paralleling leach behavior observed earlier.

(3) Phase Formation

The cesium concentration of the coexisting solution for each of the hydrated glasses as a function of time and temperature is

Table IV. 56-d X-ray Diffraction Data

Phases	Mixture* 1	2	3	4	5
Hydrogarnet	X	X	X	X	X
Strätlingite	X	X	X	X	Tr
C–S–H†		Tr			X
Gibbsite	X		X	Tr	
Unreacted cement‡	X	X	Tr	X	X
Unknown	Tr		Tr		
Amorphous phase	Tr	Tr	Tr	Tr	X

*X = significant. Tr = trace. †Calcium silicate hydrate. ‡Unreacted cement is not a single phase, but is composed of many phases.

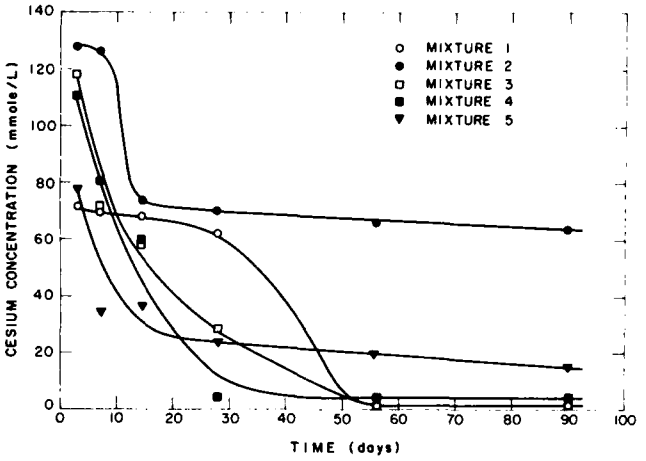

Fig. 3. Cesium concentration in pore solution of mixtures PS1 through PS5, as a function of curing time. Usually only a single sample was analyzed; therefore, no error bars are given.

given in Fig. 4. The initial concentration of the CsOH solution was ~300 mmol · L^{-1}. At both 38° and 90°C, the hydration products of glasses 6 and 7 show little uptake of cesium from the solution. Therefore, strätlingite, hydrogarnet, and wairakite (identified to be present by XRD and examined with EDX) were concluded not to be cesium hosts. In contrast, glass 8 hydrated at 38° and 90°C and glass 9 hydrated at 90°C show significant uptake of cesium when hydrated with the CsOH solution. The cesium concentration of the glass 8 solution drops to approximately one-half of the initial cesium concentration when reacted at both 38° and 90°C. The 90°C glass 9 solution exhibits an even more dramatic reduction in cesium concentration, dropping to ~5 mmol · L^{-1}.

Figure 5 shows representative SEM photomicrographs of glass 8, 90°C hydration products, after more than 90 d of hydration. At least three phases are present: a blocky phase (view (A)) which comprises most of the sample, one or more prismatic phases (view (B)), and a reticulated gellike phase (view (C)) that may be poorly crystalline calcium silicate hydrate (C–S–H). The blocky phase displays well-defined crystal faces and the EDX spectrum (view (D)) indicates the presence of large amounts of cesium. The corresponding bulk XRD patterns of the hydrated glass 8 material is given in Fig. 6. The XRD pattern closely resembles that of herschelite ($NaAlSi_2O_6 \cdot 3H_2O$), also plotted in the figure.[9] Herschelite is a zeolite in the chabazite ($CaAl_2Si_4O_{12} \cdot 6H_2O$) family. Comparison of the patterns given in Fig. 6 reveals slight differences that may be attributable to the incorporation of cesium rather than sodium, the differences in peak intensity due to the greater scattering potential of cesium and the differences in peak location due to the larger ionic radius of cesium. Therefore, the ubiquitous blocky phase is probably a cesium-substituted herschelite ($CsAlSi_2O_6 \cdot 3H_2O$) similar to an ion-exchanged chabazite reported by Calligaris *et al.*[10]

Representative SEM photomicrographs of glass 9 hydration products after more than 90 d of hydration at 90°C are given in Fig. 7. Two phases are present. Icosahedra (views (A), (B), (C)) are very prominent at the surface of the sample where they are cemented together with a reticulated gellike phase (view (B)), probably C–S–H, the major cementing phase found in portland cement. The icosahedral morphology suggests a cubic or pseudocubic phase that may be related to analcime ($NaAlSi_2O_6 \cdot H_2O$)[11] or garnet ($Ca_3Al_2Si_4O_{12}$).[12] The EDX spectrum (view (D)) of the icosahedra and the gellike region indicate that the cesium is concentrated in the icosohedra. The XRD pattern for the

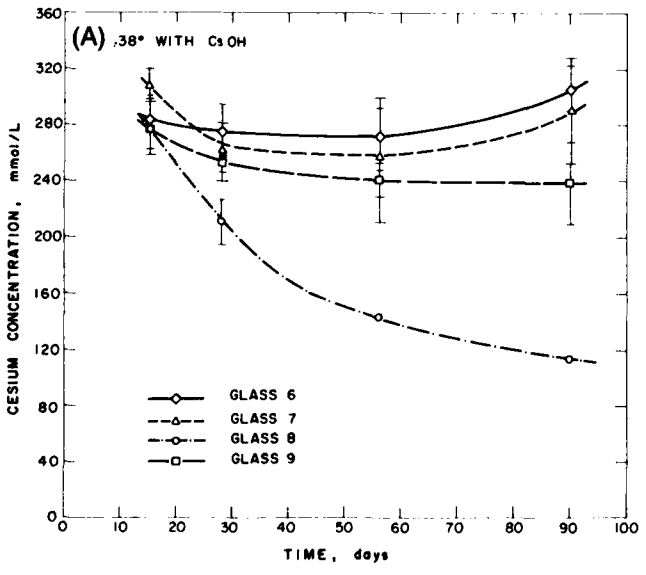

Fig. 4. Cesium concentration of solutions in contact with glasses 6 to 9 as a function of time and temperature (38°, 90°C). Error bars represent ±1 standard deviation of two samples. When no error bars are present, the standard deviation is less than size of symbol. When present, a cross signifies a single data point, because the companion run failed after 28 d.

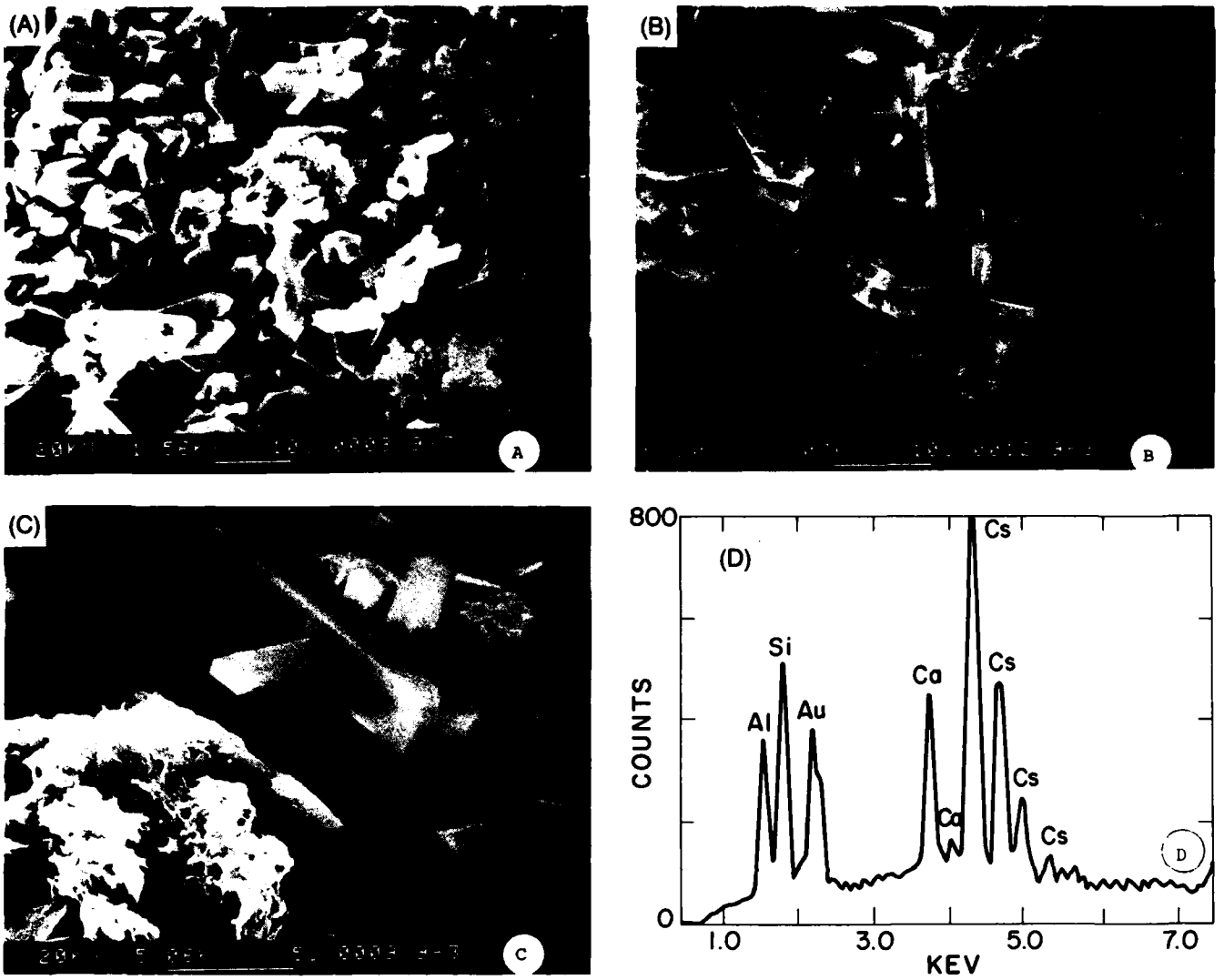

Fig. 5. SEM photomicrographs (A–C) and EDX spectra (D) of glass 8 hydrated with CsOH solution at 90°C for more than 90 d. The blocky phase is Cs-herschelite, the reticulated phase is C–S–H, and the other phases are zeolitic phases which exist in insufficient quantities to identify by XRD. Scale markers are 10, 10, and 5 μm long, respectively.

hydrated glass 9 material is given in Fig. 8 along with a matching pattern for pollucite ($CsAlSi_2O_6 \cdot xH_2O$).[9] Pollucite is a member of the analcime family. Yoshida and Inoue[13] reported the development of analcime from volcanic glasses hydrated with NaOH. The analcime structure may also incorporate calcium.[11] Therefore, the calcium identified by EDX may be present in both the icosahedra and the gellike phase. Some geologists do not consider members of the analcime family to be zeolites because its channels are smaller than those normally found in zeolites and are not interconnected as in most zeolites. Consequently, the cesium in pollucite is less exchangeable with other cations than in other zeolitic structures used in low-level waste disposal,[14] which explains why pollucite has been proposed for isolation of radioactive cesium.[15-19]

IV. Discussion

Figure 9 is a composite of 90-d leach and pore solution data. Current values have been used to plot the approximate location of isocompositional contours on the figures. As such, the figure clearly demonstrates the direct relationship between the observed leach behavior and pore solution composition of a given waste form. In addition, the sequence of cesium leachate concentrations (mixture 2 > 1 > 3 > 5 > 4) at 3 d (Fig. 2) is identical to the sequence of the cesium concentration in the pore solution at 28 d (Fig. 3—NB: the leach samples were cured 28 d prior to leaching). Additionally, the decrease in cesium leachate concentration of mixtures 1 and 3 after going through a maximum (Fig. 2) corresponds to the observed continuing decrease in cesium pore solution content after 28 d (Fig. 3). These results suggest that continued and/or new phase development are responsible for the observed maximum in the leachate concentration–time curves of these mixtures. Such maxima suggest that these samples had not reached maturity prior to leaching and that longer curing would have improved the performance of these waste forms. McDaniel *et al.*[20] similarly observed that longer curing led to improved strontium leachability from cement grouts.

The above observations have led to the development of a conceptual model in which early leaching behavior in a static system is directly related to the mixing of the pore solution with the leachant. This early mixing is followed by continuing diffusion, sample dissolution, and competing reactions such as the development of cesium-containing phases. Eventually a steady state or equilibrium is reached in which the cesium concentration in the leachate approaches the pore solution concentration the waste form would have had, had it not been leached, i.e., the concen-

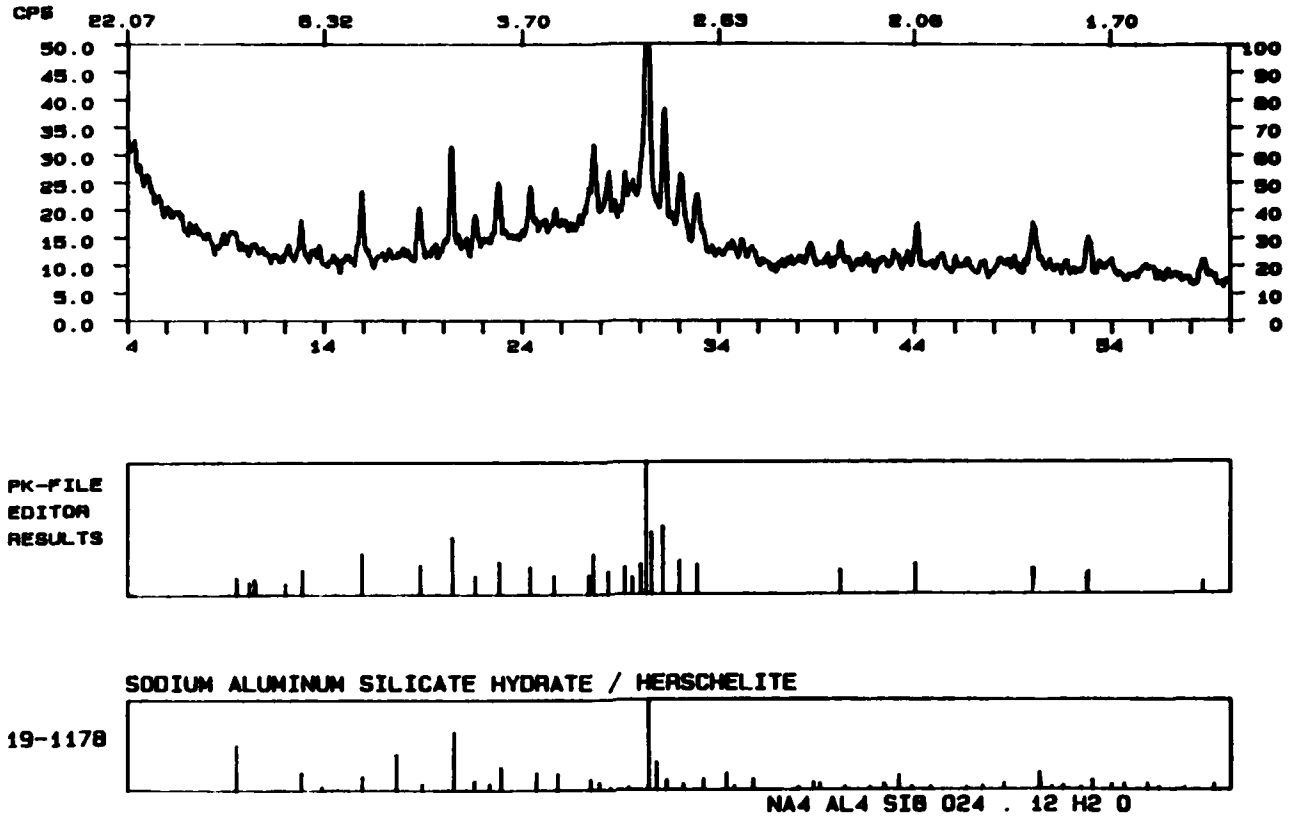

Fig. 6. X-ray diffraction pattern for glass 8 hydrated with CsOH solution at 90°C with a W/S ratio of 10/1 for more than 90 d. The stick figures are computer-generated patterns obtained from a peakfind routine, and JCPDS files (herschelite).[9]

tration of an equivalent unleached sample with approximately the same age. The comparison of 90-d leachate and pore solution data (Table V) demonstrates that the proposed model holds for mixtures 1, 3, and 4. Mixtures 2 and 5 did not contain enough cesium to reestablish the relatively high concentration of cesium in the pore solution; therefore, the cesium is completely leached, making mixtures 2 and 5 relatively poor waste forms. Conversely, samples demonstrating a high degree of cesium partitioning by the solid phase also had the lowest leach rates.

Using the conceptual model, it was possible to curve-fit the leaching of cesium from the cement-based waste forms and calculate rate constants and diffusion coefficients. The mathematical approach was based on one originally proposed by Lerman *et al.*[21] and Lerman[22] and used by them to describe the behavior of dissolving silicates having a maximum in their concentration versus time plots. The equation combines parabolic and first-order rate terms as follows:

$$\frac{dc}{dt} = k_p t^{-1/2} + k(C_s - C) \tag{1}$$

where C is the cesium concentration of the leachate, C_s is the equilibrium/steady-state concentration of cesium, k_p is a combined rate constant for parabolic dissolution and diffusion, and k is the rate constant for first-order dissolution/precipitation of developing phases. Integrating and rearranging terms leads to the following equation, which we have used to curve-fit the leaching data:

$$[C] = (1 - e^{-kt})C_s + \frac{2k_p}{k^{1/2}}\mathrm{Di}[(kt)^{1/2}] \tag{2}$$

Di is Dawson's integral

$$\mathrm{Di}(x) = e^{-x^2}\int_0^x e^{y^2}\,dy \tag{3}$$

which was computed from a series approximation. By substituting experimentally determined values into Eq. (2) (C = leach data, C_s = 90-d pore solution concentration (assumed to be the equilibrium/steady-state value), and time), it was possible to duplicate the shapes of the leachate curves of mixtures 1 and 3 (see Fig. 10). The best fit to the curve of the leachate data occurred when $k \approx 5 \times 10^{-6}$ to 7×10^{-6} s^{-1} and $k_p \approx 1 \times 10^{-9}$ to 2×10^{-9} mol·cm^{-3}·s$^{-1/2}$. Using the relationship

$$k_{ps} = k_p V/S \tag{4}$$

where k_{ps} is a parabolic rate constant independent of the solid/solution volume and V/S is the volume of solution to surface area of the leached pellet (8.3 cm (see Ref. 23)), k_{ps} was calculated as $\approx 1 \times 10^{-8}$ to 2×10^{-8} mol·cm^{-2}·s$^{-1/2}$. Using this value, the effective diffusion coefficient (D) was calculated using another relationship given by Lerman[22]

$$D = 2(k_{ps})^2(\rho_1 - \rho_2)^{-2} \tag{5}$$

assuming that ρ_1 is the cesium concentration in the sample at the start of leaching (i.e., the concentration of the pore solution at 28 d) and ρ_2 is the initial cesium concentration of the leachate (i.e., 0). The calculated value of D ($\sim 2 \times 10^{-7}$ cm^2·s^{-1}) is comparable to the diffusion coefficient for cesium through portland cement pastes (10^{-8} cm^2·s^{-1}) reported by Crawford *et al.*,[24] and determined experimentally by Kumar *et al.*[25] Transport is apparently limited by diffusion through a semisolid gellike material because the calculated value of D is smaller than the observed D for diffusion through a liquid, but larger than the D for diffusion through a solid.[22] The agreement of calculated and observed rate[22] and diffusion data[24,25] not only confirm the consistency of the data but also validate the conceptual model presented earlier.

The final figure in the paper (Fig. 11) is a highly schematic

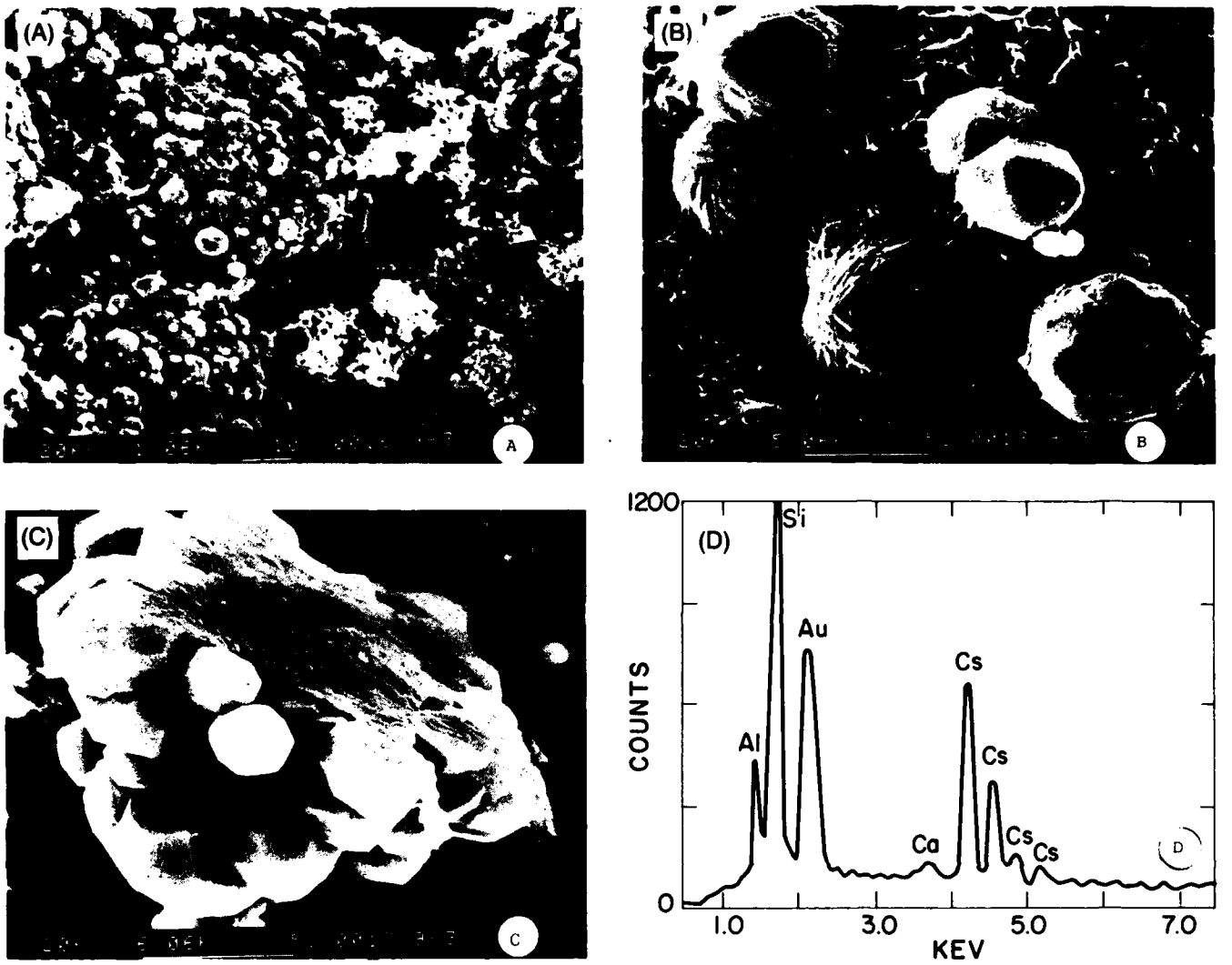

Fig. 7. SEM photomicrographs (A–C) and EDX spectra (D) of glass 9 hydrated with CsOH solution at 90°C for more than 90 d. The polyhedral phase has been identified as pollucite which is coexisting with a reticulated C–S–H phase. The C–S–H phase appears to be cementing the pollucite crystals together. Scale markers are 10, 5, and 5 μm long, respectively.

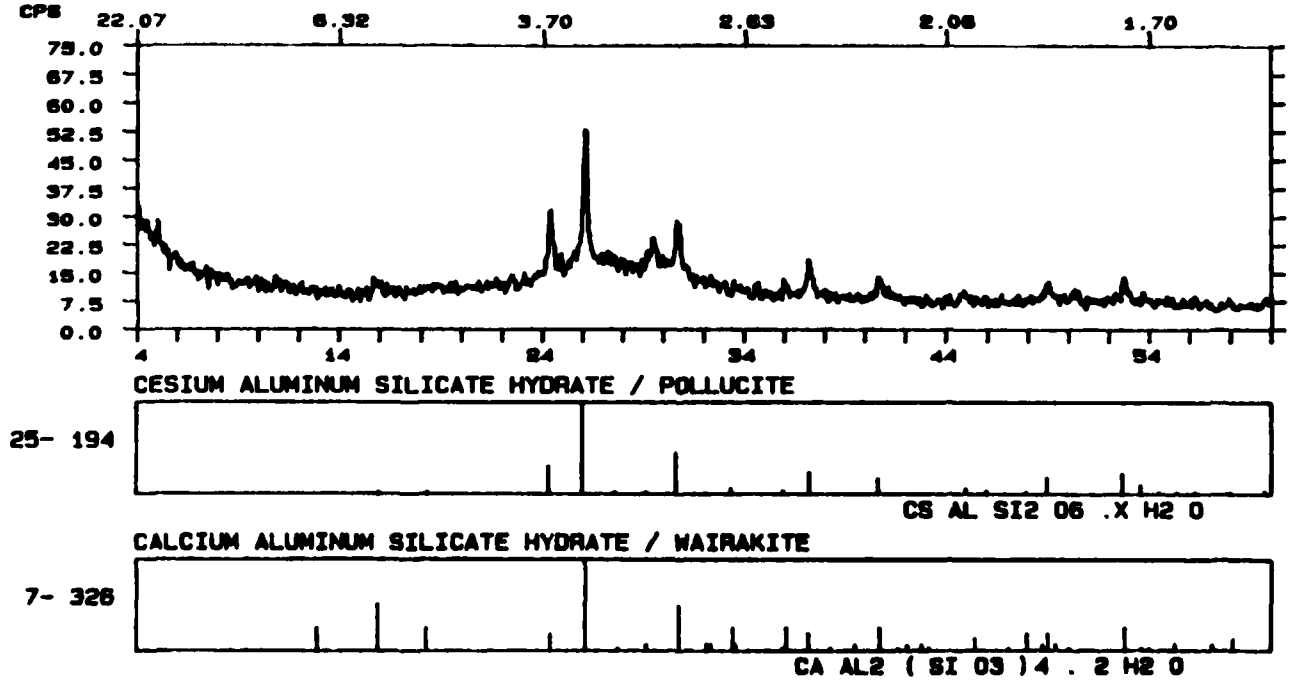

Fig. 8. X-ray diffraction pattern for glass 9 hydrated with CsOH solution at 90°C with a W/S ratio of 10/1 for more than 90 d. The stick figures are computer-generated patterns for pollucite and wairakite obtained from JCPDS files.[9]

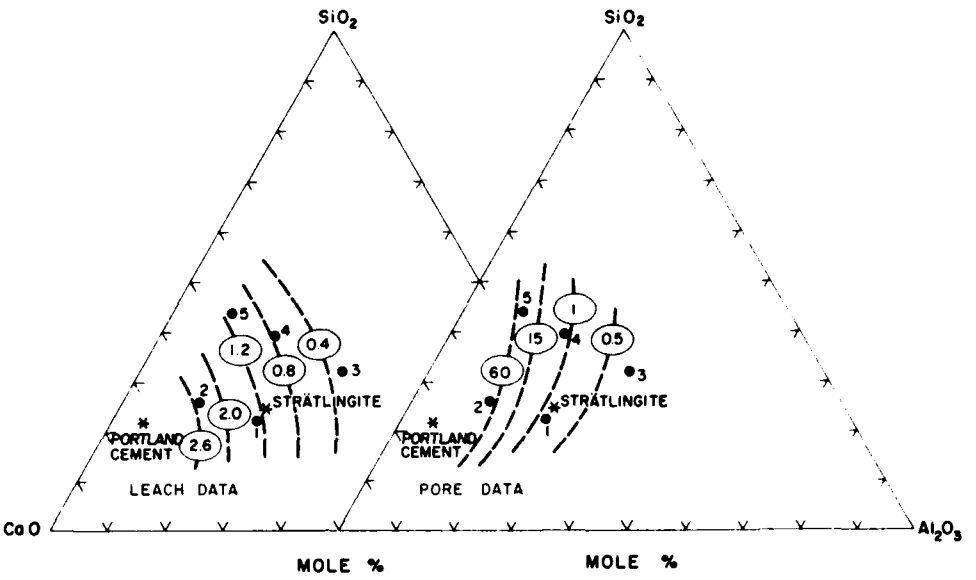

Fig. 9. Comparison of 90-d leach and pore solution data for cesium hydroxide-doped mixtures. Contour lines representing equal concentrations of cesium (mmol·L^{-1}) have been drawn using present data, and as such, clearly illustrate the relationship of bulk composition of the waste form to its observed leach and pore solution behavior.

representation of possible low-temperature phase equilibrium relations for the system $CaO–Al_2O_3–SiO_2–H_2O$. It was developed from existing phase and solubility data presented here and in other publications[23,26-29] and from thermodynamic considerations using methods described by Drever.[30] The compositions of glasses 6 to 9 as well as wairakite and chabazite, the calcium analogues of pollucite and Cs-herschelite, respectively, have been plotted on the figure. Wairakite and chabazite have similar chemical compositions except that wairakite has less water in its structure and is generally considered to be a higher-temperature phase.

Compositions of glasses 8 and 9 lie roughly between the compositions of wairakite/chabazite and C–S–H gel. Therefore, the amount of aluminum present in the unhydrated glasses may in fact determine the zeolite/C–S–H ratio and the maximum amount of Cs-herschelite and pollucite that can form during the hydration of these glasses with CsOH solution. Because the cesium and aluminum molar ratio in both Cs-herschelite ($CsAlSi_2O_6 \cdot 3H_2O$) and pollucite ($CsAlSi_2O_6 \cdot xH_2O$) is unity, the amount of cesium incorporated by either of these zeolites may be nearly the same as the total amount of aluminum available for reaction. For example, in the case of glass 9, 10 g of glass would contain 0.032 mol of aluminum. Figure 4 shows that the cesium concentration in solution at 90°C decreased from ~300 to ~10 mmol·L^{-1}, corresponding to the removal of ~0.029 mol of cesium from solution. This amount is very close to the amount of aluminum available in glass 9, suggesting that approximately 90% of the aluminum has been incorporated in the pollucite. In the case of glass 8, approximately 40% of the aluminum can be accounted for in this manner. The remaining aluminum may be present in the unreacted glass, in the C–S–H gel, or in coexisting phases (see Figs. 5 and 7). Furthermore, the decrease in cesium content of the solution (Fig. 4) as a function of time suggests that the rates of formation of both Cs-herschelite and pollucite are temperature dependent, favored by higher temperatures.

Although both Cs-herschelite and pollucite are richer in silica than the cement-based waste forms studied, these zeolitic phases or their poorly crystalline precursors may still be responsible for the observed decreases in cesium leachate concentrations. The calcium aluminate cement used to formulate the waste forms reacts very quickly with water to form hydrogarnet ($3CaO \cdot Al_2O_3 \cdot 6H_2O$).[23,26] This reaction ties up calcium and aluminum in solution and consequently may shift the bulk composition of the remaining material to more silica-rich regions, where zeolites are stable phases. The results of the glass hydration study suggest that a significant quantity of pollucite is not forming at 38°C, but

Table V. Comparison of 90-d Leach and Pore Solution Concentrations

Mixture	Cesium concentration (mmol·L^{-1})	
	Leach	Pore
1	1.13	0.54
2	2.61*	63.2
3	0.43	0.53
4	0.70	1.54
5	1.13*	14.7

*Insufficient cesium in pellet to reestablish equilibrium.

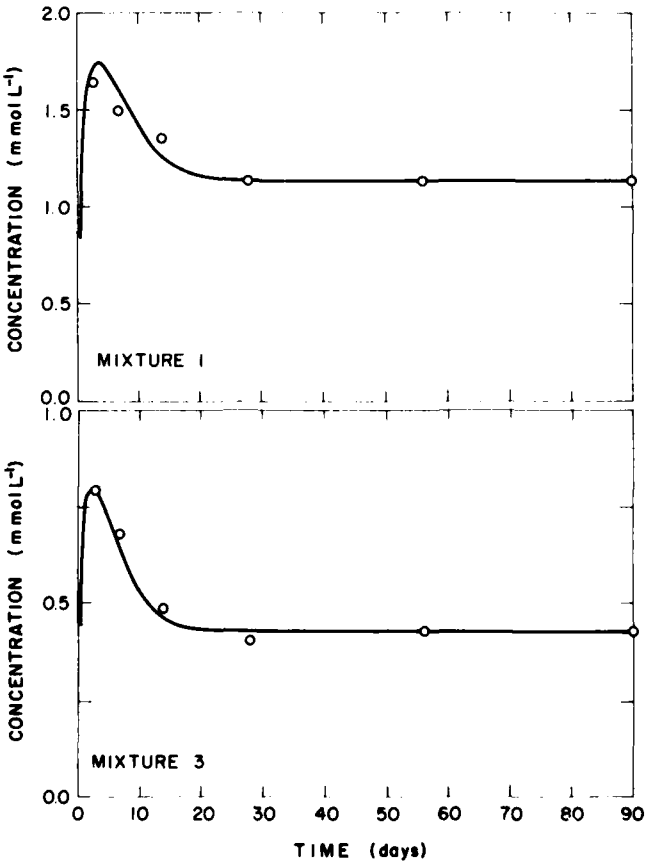

Fig. 10. Calculated curves for experimentally determined leach behavior used to estimate rate constants and effective diffusion coefficients for cesium in cement-based materials.

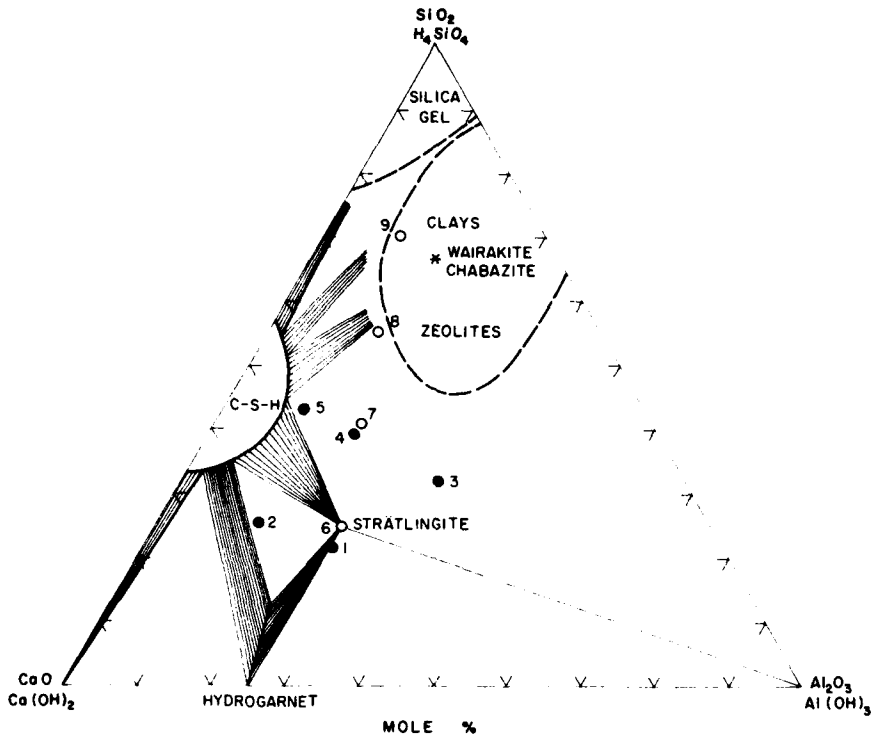

Fig. 11. Schematic representation of low-temperature phase relations in the system $CaO-Al_2O_3-SiO_2-H_2O$ in the presence of excess water, compiled from literature and experimental data. Solid circles represent compositions of cement-based waste forms, and open circles represent compositions of glasses. For ease of discussion, hydrous compositions have been normalized to 100% CaO, Al_2O_3, and SiO_2 and have been plotted on the anhydrous base of this system.

a Cs-herschelite or another zeolitic precursor may be forming instead. Unfortunately, not enough cesium was present in the cement-based waste forms to allow these phases to be identified by XRD.

V. Conclusions

This study demonstrated that the cesium leachability of cement-based waste forms is dependent on bulk composition. The amount of cesium leached from the waste forms decreased as the alumina and/or silica content of the formulations was increased. Examination of the pore solution as a function of time revealed that cesium was being partitioned into the hydrated phases of the cement, and, like the leachability, the incorporation of cesium into the solid phases is also dependent on the bulk composition of the cement paste. The observation of a direct relationship between leach behavior and pore solution concentration led to the development of a conceptual model in which cesium leachability of the cement-based waste form is described in terms of pore solution concentration, diffusion, dissolution, and development of cesium host phases. The identification of pollucite ($CsAlSi_2O_6 \cdot xH_2O$), and cesium herschelite ($CsAlSi_2O_6 \cdot 3H_2O$) suggests that the formation of these or related zeolitic phases and/or their poorly crystalline precursors are responsible for the compositionally related cesium partitioning observed in the present study as well as for the reported general improvement in cesium leach rates of cement-based waste forms when silica fume and/or aluminosilicates are added to the formulation.[1-4]

Acknowledgment: We thank Stephen Kwan for curve-fitting the data.

References

[1]C. E. McCulloch, A. A. Rahman, M. J. Angus, F. P. Glasser, and R. W. Crawford, "Immobilization of Cesium in Cement Containing Reactive Silica and Pozzolans"; pp. 113–28 in Advances in Ceramics, Vol. 8, Nuclear Waste Management. Edited by G. G. Wicks and W. A. Ross. American Ceramic Society, Columbus, OH, 1984.

[2]C. E. McCulloch, M. J. Angus, R. W. Crawford, A. A. Rahman, and F. P. Glasser, "Cements in Radioactive Waste Disposal: Some Mineralogical Considerations," *Mineral. Mag.*, **49**, 211 (1985).

[3]G. Rudolph and R. Köster, "Immobilization of Strontium and Cesium in Intermediate-Level Liquid Wastes by Solidification in Cements"; pp. 467–70 in Scientific Basis for Nuclear Waste Management, Vol. 2. Edited by G. J. McCarthy. Plenum Press, New York, 1979.

[4]A. Dyer and Y. Mikhail, "The Use of Zeolites for the Treatments of Radioactive Waste," *Mineral. Mag.*, **49**, 203–10 (1985).

[5]ASTM Designation C 305. 1979 Annual Book of ASTM Standards, Part 13; pp. 237–39. American Society for Testing and Materials, Philadelphia, PA.

[6]Nuclear Waste Materials Handbook, DOE/TIC-1140, Materials Characterization Center, Pacific Northwest Laboratory, Richland, WA, 1981.

[7]R. S. Barneyback, Jr., and S. Diamond, "Expression and Analysis of Pore Fluids from Hardened Cement Pastes and Mortars," *Cem. Concr. Res.*, **11**, 279–85 (1981).

[8]M. W. Barnes, B. E. Scheetz, and D. M. Roy, "The Effect of Chemically Adjusting Cement Compositions on Leachabilities of Waste Ions"; pp. 313–17 in Advances in Ceramics, Vol. 20, Nuclear Waste Management. Edited by D. E. Clark, W. B. White, and A. J. Machiels. American Ceramic Society, Westerville, OH, 1987.

[9]Joint Committee on Powder Diffraction Standards, Swarthmore, PA, 1987.

[10]M. Calligaris, A. Mezzetti, G. Nardin, and L. Randaccio, "Crystal Structures of the Hydrated and Dehydrated Forms of a Partially Cesium-Exchanged Chabazite," *Zeolites*, **6**, 137–41 (1986).

[11]G. Gottardi and E. Galli, "Zeolites with Singly Connected 4-Ring Chains"; pp. 76–100 in Natural Zeolites. Springer-Verlag, Berlin, FRG, 1985.

[12]B. Mason and L. G. Berry, Elements of Mineralogy; pp. 500–501. W. H. Freeman and Co., San Francisco, CA, 1968.

[13]A. Yoshida and K. Inoue, "Formation of Faujasite-Type Zeolite from Ground Shirasu Volcanic Glass," *Zeolites*, **6**, 467–73 (1986).

[14]T. E. C. Keith, T. M. Thompson, and R. E. Mays, "Selective Concentration of Cesium in Analcime during Hydrothermal Alteration, Yellowstone National Park, Wyoming," *Geochim. Cosmochim. Acta*, **47**, 795–804 (1983).

[15]G. J. McCarthy, S. Komarneni, B. E. Scheetz, and W. B. White, "Hydrothermal Reactivity of Simulated Nuclear Waste Forms and Water-Catalysed Waste-Rock Interactions"; pp. 329–40 in Scientific Basis for Nuclear Waste Management, Vol. 1. Edited by G. J. McCarthy. Plenum Press, New York, 1979.

[16]S. A. Gallager, G. J. McCarthy, and D. K. Smith, "Preparation and X-ray Characterization of $CsAlSiO_4$," *Mater. Res. Bull.*, **12**, 1183–90 (1977).

[17]P. Cerny, "Pollucite and Its Alteration in Geological Occurrences and in Deep-Burial Radioactive Waste Disposal"; pp. 231–36 in Scientific Basis for Nuclear Waste Management, Vol. 1. Edited by G. J. McCarthy. Plenum Press, New York, 1979.

[18]R. Odoj, K. Hilpert, and H. Gerads, "Investigations of the Volatility of Cesium

from Aluminosilicates by Mass Spectrometry"; pp. 227–29 in Scientific Basis for Nuclear Waste Management, Vol. 1. Edited by G. J. McCarthy. Plenum Press, New York, 1979.

[19]D. M. Roy, B. E. Scheetz, and M. W. Barnes, "Preparation of Cement Composite Nuclear Waste Forms and Their Physical and Chemical Properties." Report No. PSU-021, Rockwell Energy Systems Group, Canoga Park, CA, 1981.

[20]E. W. McDaniel, M. T. Morgan, J. G. Moore, H. E. Dwaney, and L. R. Dole, "Strontium Leachability of Hydrofracture Grouts for Sludge Slurries." Report No. IM-8198 Oak Ridge National Laboratories, Oak Ridge, TN, 1982.

[21]A. Lerman, F. T. Mackenzie, and O. P. Bricker, "Rates of Dissolution of Aluminosilicates in Seawater," *Earth Planet. Sci. Lett.*, **25**, 82–88 (1975).

[22]A. Lerman, Geochemical Processes Water and Sediment Environments; pp. 225–56. Wiley, New York, 1979.

[23]S. Q. Hoyle, "The Effect of Phase Composition on the Leach Behavior of Cement-Based Waste Forms"; M.S. Thesis. Pennsylvania State University, University Park, PA, 1986.

[24]R. W. Crawford, F. P. Glasser, A. A. Rahman, M. J. Angus, and C. E. McCulloch, "Diffusion Mechanisms and Factors Affecting Leaching of Cesium-134 from Cement-Based Waste Matrices," *Radioact. Waste Manage. Nucl. Fuel Cycle*, **6**, 177–96 (1985).

[25]A. Kumar, A. Komarneni, and D. M. Roy, "Diffusion of Cs^+ and Cl^- Through Sealing Materials", *Cem. Concr. Res.*, **17**, 153–60 (1987).

[26]S. Q. Hoyle, "Cesium and Strontium Partitioning During Hydration of Calcium Aluminosilicates"; Ph.D. Thesis. Pennsylvania State University, University Park, PA, 1988.

[27]S. Hoyle and M. W. Grutzeck, "Effects of Phase Composition on the Cesium Leachability of Cement-Based Waste Forms"; pp. 491–96 in Waste Management 1986, Proceedings of Waste Isolation; Technical Programs and Public Education, Vol. 3. University of Arizona, Tucson, AZ, 1986.

[28]S. Hoyle and M. W. Grutzeck, "Effect of Pore Solution Composition on Cesium Leachability of Cement-Based Waste Forms"; pp. 309–17 in Scientific Basis for Nuclear Waste Management X, Proceedings of the Materials Research Society Symposium, Vol. 84. Edited by J. K. Bates and W. B. Seefeldt. Materials Research Society, Pittsburgh, PA, 1987.

[29]S. Hoyle and M. W. Grutzeck, "Fixation of Cesium by Calcium Aluminosilicate Hydrates"; pp. 13–21 in Scientific Basis for Nuclear Waste Management XI, Proceedings of the Materials Research Society Symposium, Vol. 112. Edited by M. J. Apted and R. E. Westerman. Materials Research Society, Pittsburgh, PA, 1987.

[30]J. I. Drever, The Geochemistry of Natural Waters; pp. 90–115. Prentice-Hall, Englewood Cliffs, NJ, 1982. □